Functional characterization of miR-96 in the mouse auditory brainstem and identification of new auditory-related microRNAs

Von der Fakultät VI - Medizin und Gesundheitswissenschaften der
Carl von Ossietzky Universität Oldenburg
zur Erlangung des Grades und Titels einer

Doktorin der Naturwissenschaften
(Dr. rer. nat.)

angenommene Dissertation

von Frau Constanze Krohs

geboren am 07.08.1987 in Leer

Table of contents

Table of figures

List of tables

1. Introduction

1.1. The significance of hearing research

"The problems of deafness are deeper and more complex, if not more important than those of blindness. Deafness is a much worse misfortune. For it means the loss of the most vital stimulus – the sound of the voice that brings language, sets thoughts astir, and keeps us in the intellectual company of man." *Helen Keller*

This quotation quite well describes the social factor of our hearing ability. Our society is essentially driven by communication and seen from the perspective of individuals, the hearing sense is required to develop socially important skills like understanding and speaking a language or taking part in social life. It is not only meant to talk and listen to each other, which are absolutely obligatory processes during daily life. This applies also to social activities like watching a film, a concert or visiting the theatre. All this is dependent on a functional hearing sense. Importantly, this sense is not only essential during social interactions with the environment but also in perception of acoustic space: It could save your life to hear the approaching car or train. You normally not only hear it, you also immediately know from where and how fast it is approaching. The importance of our ability to hear and its great benefits is often neglected within our consciousness. This happens because for most people it is absolutely self-evident to hear properly. But in fact, hearing impairment is the most frequent sensory deficit in humans. Around 466 million people worldwide have disabling hearing loss, and 34 million of these are children. It is estimated that by 2050 over 900 million people – or one in every ten people – will have disabling hearing loss (https://www.who.int/news-room/fact-sheets/detail/deafness-and-hearing-loss). The great challenge to perform proper hearing makes the auditory system highly sensitive to any aberrant processes such as mutations in the genome. While investigating the causes of hearing loss, more than 100 genetic loci have been described to contribute to the dysfunction of the inner ear (Brownstein et al., 2012), with a steadily growing list of candidate genes that carry deafness-causing mutations (https://hereditaryhearingloss.org). A better understanding of hearing loss would improve therapeutic approaches to help affected humans. Therefore, detailed in-depth knowledge of genetically induced aberrant developmental processes, that are broadly discussed to contribute to most sensorineural disorders like hearing loss, is required.

1.2.   The central auditory system of mice modeling the human´s

The hearing sense could be characterized by transduction of low-pressure sound waves into electric signals in the inner ear and their subsequent processing in the central auditory structures and pathways. Information about e.g. sound source, loudness and content have to be perceived for proper reaction. The auditory system has evolved to perform this very effectively and efficiently by developing specialized anatomical, cellular and molecular features. Tissues of humans are often only available in a restricted manner and post-mortem, limiting possibilities in research. I will focus on the auditory system of mice because the mouse serves as a model organism for many genetic defects in humans with a very well-studied peripheral and central auditory system resembling in many aspects the human´s auditory system anatomically as well as functionally. Rapid succession of generations, availability of embryonic to adult tissues and broad availability of constitutive and conditional transgenic lines have made the mouse the model of choice for medical research concerning human diseases. **Figure 1** schematically depicts parts of the auditory system of mice as well as their location within the brain. The main focus of my work is the part of the central auditory system situated in the hindbrain.
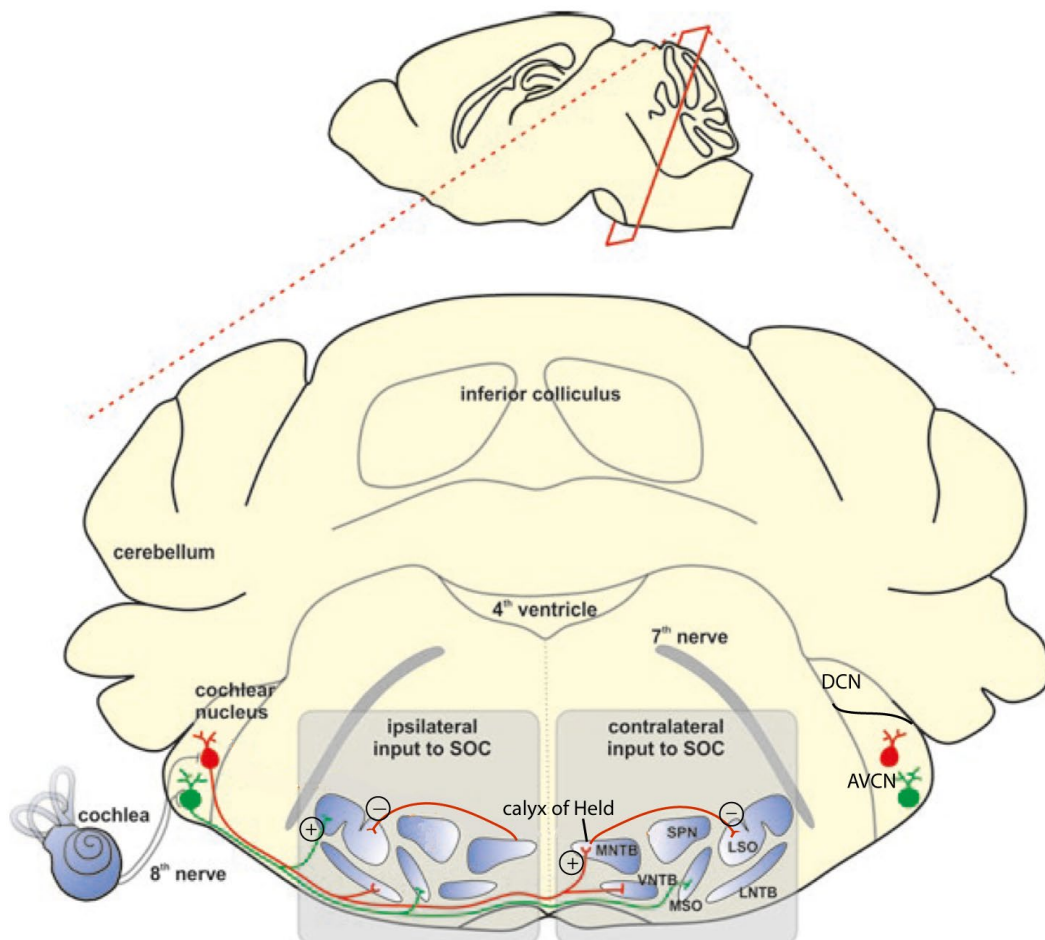
Figure 1: The mouse auditory brainstem and its neuronal pathways.
Schematic drawing of a coronal section through the auditory brainstem region of the mouse brain. The localization of the mouse auditory hindbrain within the brain is shown in the sagittal view with the section plane indicated in the upper part of the picture. The origin of acoustic stimulation is indicated by the cochlea on the lower left side with fibers of the 8th nerve

(auditory nerve) projecting to e.g. bushy cells of the cochlear nucleus. Globular bushy cells (red) and spherical bushy cells (green) of the aVCN projecting to the SOC (gray shaded boxes). The SOC is assembled by the MNTB, VNTB, SPN, MSO, LNTB and LSO. Globular bushy cells project to the ipsilateral LNTB and the contralateral VNTB. Spherical bushy cells project to the ipsilateral LSO and VNTB as well as to the contralateral MSO. Projections from bushy cells are excitatory (indicated by "+"). The MNTB is a relay station receiving contralateral excitatory input at the calyx of Held and projecting to its ipsilateral LSO in an inhibitory manner (indicated by "-"). The LSO therefore receives excitatory input from the ipsilateral VCN and inhibitory input via the contralateral MNTB (shown on the left side). aVCN: anteroventral cochlear nucleus; DCN: dorsal cochlear nucleus; LNTB: lateral nucleus of the trapezoid body; LSO: lateral superior olive; MNTB: medial nucleus of the trapezoid body; MSO: medial superior olive; SOC: superior olivary complex; SPN: superior paraolivary nucleus; VNTB: ventral nucleus of the trapezoid body. Figure modified from Kopp-Scheinpflug and Forsythe (2018).

The central auditory pathways are responsible for processing and integration of binaural auditory input. This is not only computing sound parameters like loudness and source (Carr and Soares, 2002; Grothe et al., 2010), but also sound duration (Kadner et al., 2006), gap detection (Kopp-Scheinpflug et al., 2011) and echo suppression (Pecka et al., 2007). Also aligning acoustic with visual cues belongs to the functions, the central auditory pathways have to perform (Brainard and Knudsen, 1993; Gruters and Groh, 2012). They therefore fulfill manifold tasks for representation of physical auditory space in the brain that could not be fulfilled by the cochlea alone. One cochlea only delivers information like loudness and frequency of the sound. Both cochleae (left and right) and the integration of their inputs are required to properly fulfill all tasks of the auditory system. In this work I will therefore focus on the function of the auditory brainstem nuclei that are mainly responsible for sound source localization.

The auditory hindbrain receives input from both ears via the auditory nerve and is the first place to compute sound source localization by making use of interaural time and level differences (Grothe et al., 2010). It is the assembly of the cochlear nucleus complex (CNC), where the input arrives via the auditory nerve and the superior olivary complex (SOC) where binaural input is integrated. The CNC consists of the dorsal cochlear nucleus (DCN) and the anterior and posterior parts of the ventral cochlear nucleus (aVCN and pVCN respectively) (Cant, 1992). The DCN is a multisensory integrator between auditory, somatosensory, proprioceptive and vestibular sources (Musicant et al., 1990), and has a peripheral granular cell domain (GCD) and an inner layered structure with fusiform cells and giant cells as the principal cell types (Brawer et al., 1974). Major projections from the DCN innervate the contralateral inferior colliculus (IC). The DCN is sensitive to spectral notches and likely plays a role in sound localization in the vertical plane using monaural cues (Spirou and Young, 1991). The VCN consists of two parts, the aVCN and the pVCN. Two main regions can be distinguished within the nucleus: The periphery of the VCN is build up by the GCD which consists of granule cells and small cells (Weedman et al., 1996) and mainly receives somatosensory input. The inner structure (core) of the VCN is called the magnocellular region. Main neuronal cell types are spherical and globular bushy cells (Cant and Morest, 1979; Tolbert and Morest, 1982) and the multipolar cells represented by T and D stellate cells (Doucet and Ryugo, 2006). The VCN (like other auditory hindbrain nuclei) is tonotopically organized with low frequency auditory nerve fibers arriving more ventrally and rostrally and the high frequency fibers more dorsally and caudally (Shepherd, 2004). The VCN mainly innervates the SOC (Moore, 1991), which

mainly consists of the lateral, medial and ventral nuclei of the trapezoid body (LNTB, MNTB and VNTB), the superior paraolivary nucleus (SPN) and the lateral and medial superior olive (LSO and MSO) (Moore, 1991). The spherical bushy cells of the VCN project to the ipsilateral LSO and to the ipsi- and contralateral MSO. MSO neurons consequently can compare the timing of excitatory inputs from the ipsi- and contralateral ear, therefore detecting interaural time differences (ITD) (Grothe, 2003). This mechanism is especially used at low frequencies. For high frequencies, another mechanism is needed, the detection of interaural level differences (ILD) that takes place in the LSO: LSO neurons receive excitatory input only from the ipsilateral ear, getting the contralateral input via the MNTB. The MNTB is the target of the calyx of Held synapse with principal cells receiving one calyx that originates from the globular bushy cells of the VCN. Principal neurons of the MNTB make inhibitory glycinergic projections to the LSO, but also to the MSO and SPN (Banks and Smith, 1992; Sommer et al., 1993). The LSO is the key nucleus of ILD: It integrates precisely timed ipsilateral excitatory input and inhibitory input from the contralateral ear via the MNTB (Tollin, 2003). Amongst other cell types, the LSO contains the principal neurons and the lateral olivocochlear neurons (Helfert and Schwartz, 1986). Summarized, one LSO gets ipsilateral, excitatory input and inhibitory input from the contralateral ear via the MNTB to compute interaural sound intensity differences (Grothe, 2003; Grothe et al., 2010).

1.3.   The calyx of Held, a giant and fast auditory central synapse

In this analysis of the auditory hindbrain in a microRNA knockout mouse model, the focus is set on the calyx of Held, a well-studied giant synapse in the central auditory system (Held, 2011) and this synapse will therefore be described in more detail: The location of this synapse is indicated in **Figure 1**. Because of its size, this synapse is easily recognizable in immunohistochemical tissue sections as well as easily accessible for electrophysiological recordings. Axons of globular bushy cells in the aVCN terminate in the calyx of Held´s huge presynaptic terminals building a large synapse with the somata of contralateral MNTB principal neurons (Thompson and Schofield, 2000). One calyx forms around one postsynaptic cell body like a palm with fingers (Morest, 1968) delivering excitatory glutamatergic input in a fast and precise manner (Forsythe and Barnes-Davies, 1993). The presynaptic terminal contains hundreds of neurotransmitter release sites releasing glutamate on arrival of a single action potential from the globular bushy cell axon (Taschenberger et al., 2002). Excitatory postsynaptic currents (EPSCs) at the calyx are characterized by an amplitude up to 20 nA and their fast kinetics. On the postsynaptic side, the calyx of Held evokes a dual component EPSC with a fast component provided by AMPA (amino-3-hydroxy-5-methyl-4-isoxazole propionic acid) receptors (AMPARs) and a slower component mediated by NMDA (N-methyl-D-aspartate) receptors (NMDARs) (Forsythe and Barnes-Davies, 1993). In mature neurons, decay kinetics of the EPSC are as fast as 0.5 ms for the AMPA component (Koike-Tani et al., 2005) and 15 ms for the NMDA component (Steinert et al., 2010). The AMPARs are composed of glutamate receptor subunits (GluAs), well known for their fast kinetics (Parks, 2000). The

AMPAR subunits GluA1, GluA2/3, GluA4 are all present in auditory nuclei (Petralia and Wenthold, 1992; Geiger et al., 1995). Temporally precise transmission at the postsynaptic MNTB principal neuron requires the expression of a subset of voltage gated potassium channels to make sure that the strong and high frequency EPSCs can reliably and precisely evoke action potentials to transmit temporal information (Dodson et al., 2002). As already stated, the MNTB principal neurons represent a relay station in the auditory system, converting contralaterally originating excitatory input from the calyx of Held to inhibitory input on their ipsilateral principal neurons of the LSO using glycine as a neurotransmitter. But the need for high-speed transmission via the calyx of Held only becomes evident here: the inhibitory signal at the LSO via the contralateral MNTB has to reach the LSO on time with the ipsilateral excitatory signal. This has a much shorter transmission distance and one synapse less to pass. Precisely time-tuned arrival of signals from the ipsi- and contralateral cochlea is essential for the LSO to perform integration of interaural level differences.

1.4.   A partially shared genetic program during development of the peripheral and central auditory system

For proper hearing, the developmental integrity of the individual structures like the peripheral and central auditory systems as well as their connection are essential. Development and function of both, peripheral and central auditory structures are primarily ruled by genetic determinants and therefore peripheral deafness and central auditory dysfunction is often caused by variants in coding and non-coding genes.

The mammalian auditory system is special for its evolution of a three-ossicle tympanic middle ear and its especially high number of auditory brainstem nuclei (Nothwang, 2016). The emergence of the tympanic ear and auditory brainstem nuclei is hypothesized to be orchestrated by a partially shared gene regulatory network (Duncan and Fritzsch, 2012; Willaredt et al., 2014). The shared regulatory program between auditory brainstem neurons and the peripheral auditory system could be summarized as an interaction of transcription factors (TFs), signaling molecules and their receptors. Auditory nuclei are assembled after delamination and migration of neuronal precursor cells from the same rhombomeres (r) sending out the signaling molecules being essential for development of the otic placode, giving rise to the inner ear (**Figure 2**). More detailed, the aVCN originates from r2 and r3, the pVCN from r3 and r4, the DCN from r4 and r5 (Farago et al., 2006). The SOC is derived from r3 and r5 (Farago et al., 2006; Maricich et al., 2009; Marrs et al., 2013). r4 and r5 both giving birth to auditory brainstem structures and are also involved in induction of the otic placode by expression the TF *Hoxa1* (Lufkin et al., 1991; Carpenter et al., 1993). Expression of *Hoxa1* from these rhombomeres and of another TF, *Mafb*, from r5 and r6 are essential for the expression of the signaling molecule *Fgf3* in both rhombomeres (Cordes and Barsh, 1994; McKay et al., 1996). *Fgf3* together with *Fgf10* from the mesoderm is required for the induction of the otic placode (Wright and Mansour, 2003). *Fgf3* also induces the signaling molecule Wnt8a in r4,

which is involved in the specification of the dorsal otic placode (the later vestibular system) (Hatch et al., 2007; Urness et al., 2010; Vendrell et al., 2013).
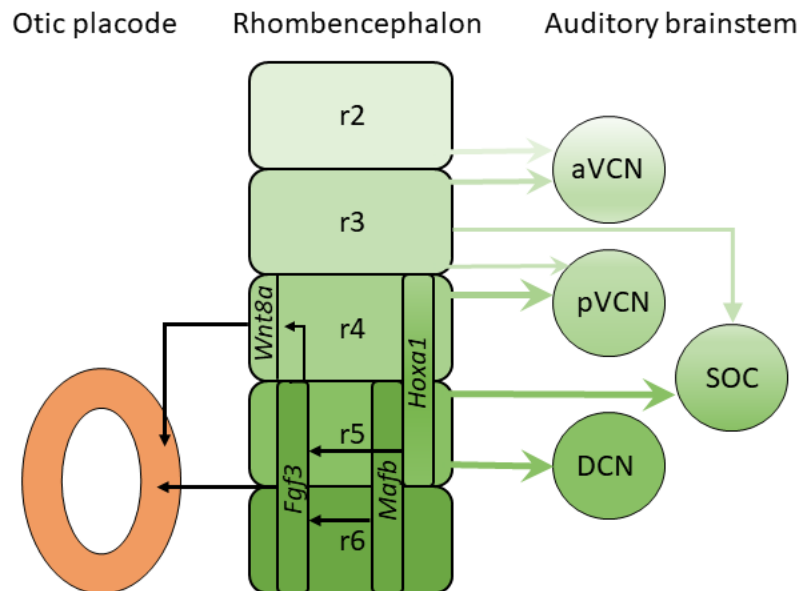
Figure 2: Shared genetic program during development of the peripheral and central auditory system.
The rhombencephalon is schematically depicted from r2-r6. The auditory brainstem nuclei aVCN, pVCN, DCN and the SOC are derived from respective rhombomeres. Signaling pathways including the transcription factors *HoxA1* and *Mafb* are inducing the signaling molecule *Fgf3*. *Fgf3* induces the signaling molecule *Wnt8a*. Together, *Fgf3* and *Wnt8a* are contributing to the development of the otic placode. aVCN: anteroventral cochlear nucleus; DCN: dorsal cochlear nucleus; pVCN: posteroventral cochlear nucleus, SOC: superior olivary complex; r: rhombomere. Figure modified from Willaredt et al. (2014).

Consequently, because of this shared gene regulatory program, mutations in deafness genes might also affect the function of the central auditory system. That would contribute to the frequently observed limited benefit from hearing devices that only substitute inner ear function (Willaredt et al., 2014). Transcriptome analysis of the SOC uncovered a strong general relationship to known deafness genes (Ehmann et al., 2013). The hypothesis of a shared gene regulatory network orchestrating development of the peripheral and central auditory system was further supported by the finding of thirteen deafness genes affecting central auditory processing as well (Willaredt et al., 2014). This list was recently updated with the deafness gene *MIR96* (Michalski and Petit, 2019), a microRNA (miRNA or miR) gene coding for miR-96 (**Table 1**). Importantly, miR-96 was identified to be part of the shared gene regulatory program: Mutations in the seed region of miR-96 causes defects both in the peripheral auditory system of men and mice (Mencía et al., 2009; Soldà et al., 2012; Lewis et al., 2009) and the central auditory system of mice (Schlüter et al., 2018).

Table 1: Gene regulatory network components contributing to cochlear and auditory brainstem function.
ABR: auditory brainste response; CN: cochlear nucleus; DCN: dorsal cochlear nucleus; GRN: gene regulatory network; IC: inferior colliculus; LL: lateral lemniscus; LNTB: lateral nucleus of the trapezoid body; LSO: lateral superior olive; MNTB: medial nucleus of the trapezoid body; MSO: medial superior olive; r: rhombomere; SGN: spiral ganglion neuron; SOC: superior olivary complex; VCN: ventral cochlear nucleus; VNTB: ventral nucleus of the trapezoid body. Adapted from Willaredt et al., 2014 and Michalski and Petit, 2019.

GRN component	Function in the Cochlea	Function in the central auditory system
Transcription factors		
ATOH1	Hair cell differentiation, maturation, and survival	Formation of the VCN, DCN, and a glutamatergic cell type of the MSO and LSO
CHD-7	Early patterning of the inner ear	Early patterning of rhombomeres and IC formation
GATA3	differentiation and maturation of hair cells, and wiring of SGNs	Formation of the efferent olivocochlear system and expression in the auditory brainstem
HOX-A1, -A2, -B1, -B2	Induction of otic placode	Anteroventral rhombomeric patterning
Krox20	indirect effects	r3 and r5 patterning
MAFB	postsynaptic densities in SGNs	r5 and r6 patterning
NEUROD1	SGN differentiation	Formation of the DCN
NEUROG1	SGN differentiation	Expressed in the CN, LL, IC
Signaling molecules		
BMP4 Eph-A7, -B1, -B2, -B3	Wiring of the SGNs	Wiring and tonotopy of all the auditory nuclei
IGF1	Development of the stria vascularis, tectorial membrane, and SGNs	altered ABRs when deleted
WNT1, -3A	Specification dorsal otic placode	Dorsoventral rhombomeric patterning
Miscellaneous proteins		
Bassoon	Anchoring of ribbons to the plasma membrane	Synaptic vesicle replenishment
CAV1.3	Ribbon synapse presynaptic Ca2+ channel	Maturation of auditory brainstem nuclei
KCC2	Expressed in SGNs	Excitability of the LSO inhibitory neurons
KCNQ4	K+ inward rectifier (hair cells and SGNs)	K+ inward rectifier channel expressed from the CN to the IC
NKCC1	Expressed in the stria vascularis	Excitability of the LSO inhibitory neurons
Piccolino and Piccolo	Ribbon morphology	Synaptic vesicle replenishment
Parvalbumin UCN	Ca2+ buffering (hair cells and SGNs)	Ca2+ buffering in CN
VGLUT3	Ribbon synapse vesicular glutamate transporter	Maturation of the MNTB to LSO synapse
micro-RNAs		
MiR-96	Formation and maturation of hair cells and SGNs	Maturation of the CN and SOC

1.5. Biogenesis of miRNAs and posttranscriptional regulation of gene expression

MicroRNAs (miRNAs) have emerged to be a very diverse class of noncoding RNAs of which hundreds have been identified in humans. Each annotated miRNA is characterized by its individual nucleotide sequence. Many of them are evolutionary conserved among species. Their function is posttranscriptional gene regulation of target messenger RNAs (mRNAs). It is estimated that more than 60% of vertebrate protein-coding mRNAs are regulated by miRNAs. In that manner, miRNAs possibly regulate all cellular processes (Friedman et al., 2009b). miRNAs have therefore diverse functional roles in developmental and physiological processes and diseases.

Mature miRNAs are small (20-24 nt) single stranded RNA molecules (Guo et al., 2010). They are mostly encoded in introns of protein coding genes and are therefore dependent on the promotors of those genes (Baskerville and Bartel, 2005). During maturation, they undergo several processing steps beginning in the nucleus of a cell and ending in the cytoplasm where protein biosynthesis takes place (**Figure 3**).
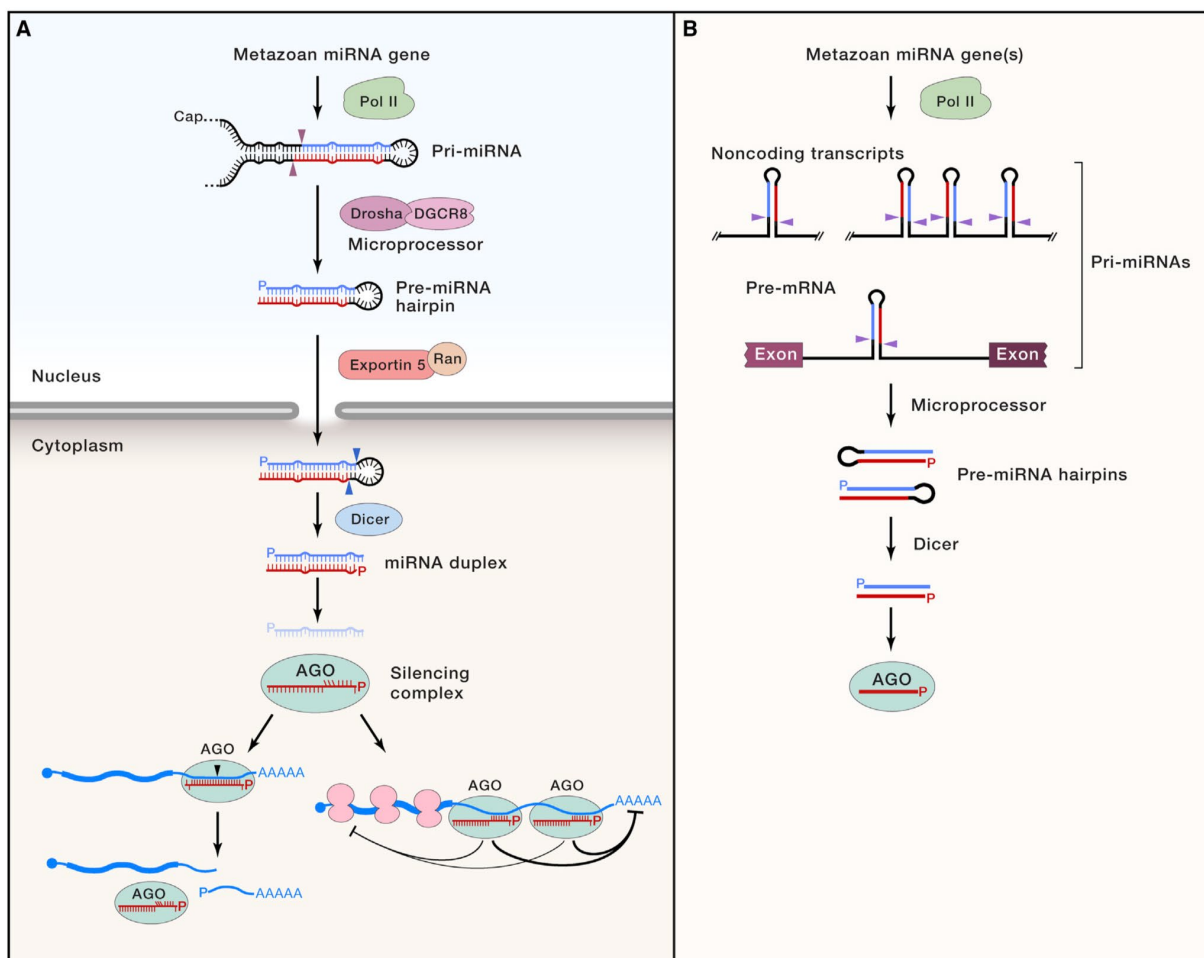
Figure 3: Biogenesis of miRNAs.
A: The canonical biogenesis of a typical miRNA. The pri-miRNA is transcribed from a miRNA gene by a RNa polymerase II. The Drosha/DGCR8 microprocessor processes the pri-miRNA to the pre-miRNA hairpin which is exported out of the nucleus via Exportin5/Ran. The pre-miRNA hairpin ist cleaved by dicer becoming the miRNA duplex. One strand of the miRNA duplex is

incorporated into the Argonaute protein (AGO) building the silencing complex. The silencing complex either leads to mRNA cleavage (to the left) or translational inhibition via action on the poly(A) tail of the mRNA or on ribosomes. **B:** Different sources of noncanonical miRNAs. Pri-miRNA transcripts can either harbor one or several pre-miRNAs before entering the canonical biogenesis to mature miRNAs. Figure from Bartel (2018).

Their biogenesis begins with transcription of a primary miRNA (pri-miRNA) by a RNA polymerase II. The pri-miRNA transcripts have at least one self-complementary region allowing them to fold back on themselves building a hairpin structure (Lee et al., 2004). The pri-miRNAs are processed to approximately 70 nt long precursor miRNAs (pre-miRNAs) by the Drosha ribonuclease III/DGCR8 complex in the nucleus (Zeng et al., 2005). In some cases, one pri-miRNA consists of several miRNA hairpins leading to several pre-miRNAs after Drosha processing (**Figure 3**B). Pre-miRNAs, now consisting of a double stranded "stem-sequence" and a single stranded "loop"-structure, are exported out of the nucleus through the nuclear pore complexes with the help of the Exportin5/Ran-GTP complex (Yi et al., 2003; Bohnsack et al., 2004; Lund et al., 2004). In addition to this canonical biogenesis of pre-miRNAs, there are noncanonical pathways generating miRNAs bypassing the Drosha/DGCR8 microprocessor complex (Okamura et al., 2007; Ruby et al., 2007). In the cytoplasm, pre-miRNAs are cleaved by the Dicer-1 ribonuclease that cuts both strands of the hairpin stem near the loop (Bernstein et al., 2001). The double stranded short RNA now is called miRNA duplex which contains the later biologically active miRNA and its passenger strand. MiRNA duplexes are incorporated into an Argonaute (Ago) protein. Through conformational change, the passenger strand of the miRNA is expulsed from the complex (Kawamata and Tomari, 2010), now consisting of the mature miRNA and the Ago protein forming the RNA-induced silencing complex (RISC). Mature, single stranded miRNAs are conventionally named with the suffix 3-prime (-3p) or 5-prime (-5p) to distinguish the two mature miRNAs arising from one miRNA duplex. Both, the -3p and -5p miRNA can be incorporated into RISC. RISC recognizes sequence specific miRNA target sites on mRNAs by complementary binding of the miRNA´s seed sequence (nucleotides 2-8 of the miRNA) to the target sequences within the 3´UTRs of mRNAs (Bartel, 2009). Ago can either directly slice the mRNA (Hutvágner and Zamore, 2002), leading to degradation by RNases or recruit deadenylase complexes (Jonas and Izaurralde, 2015), shortening the poly(A) tail of mRNAs and therefore shortening their half-lifes (Chen and Shyu, 2011). Recruitment of other protein complexes can also result in translational inhibition of the targeted mRNA (Chu and Rana, 2006; Jonas and Izaurralde, 2015). Using these mechanisms, miRNAs are capable of regulating the translation of many target proteins influencing many signaling pathways with each miRNA possibly contributing to the regulation of hundreds of targeted proteins (Bartel, 2018; Lewis et al., 2016). This makes miRNAs perfect candidates for contribution to gene regulatory networks like the one underlying the development of the peripheral and central auditory system. The emergence of miRNA-96 of being a deafness gene affecting both the peripheral and central auditory structures delivers a perfect miRNA candidate to study its on-site role in the auditory brainstem.

1.6. The miR-183 cluster and its implications for sensory systems

The human miR-96 was the first miRNA of the miR-183 cluster that was identified. It was found while screening for ribosome-interacting small RNAs in the HeLa human cancer cell line (Mourelatos et al., 2002). Two other groups discovered miRs-182 and -183 in 2003: Lim et al. by a bioinformatics approach comparing human and mouse RNAs to the transcriptome of the Japanese pufferfish *Fugu rubripes* (Lim et al., 2003). The other group found these miRNAs as highly expressed in the developing mouse retina and classified them as a miRNA cluster because of their expression pattern in the retina and their close proximity on the human chromosome 7, or on chromosome 6 in mice (Lagos-Quintana et al., 2003). miR-96 was afterwards declared to be part of that cluster because of its chromosomal location between miR-183 and -182 (Weston et al., 2006; Xu et al., 2007). The miR-183 cluster was shown to be highly conserved throughout bilaterian organisms and could be evolutionary traced back 600 million years ago to protostomes and deuterostomes by next generation deep sequencing (Prochnik et al., 2007; Pierce et al., 2008; Benson et al., 2009; Sayers et al., 2018).

The miR-183 cluster is a well-known player regarding the development and function of sensory systems. **Table 2** summarizes the species and neurosensory-related tissues where miR-183 cluster members (or orthologues) have been found. MiR-183 cluster member abundance suggests a role in development and function of most ciliated neurosensory epithelial cell types in vertebrate organs, mediating functions like photoreception, electroreception, chemosensation and mechanosensation (Wienholds et al., 2005; Pierce et al., 2008; Li et al., 2010; Lumayag et al., 2013).

Table 2: Evolutionary conservation of the microRNA-183 cluster.

Species	Tissue	miRNA	Reference
Nematode worm, *Caenorhabditis elegans*	inner/outer labial, cephalic, and amphid sensilla, the posterior deirid, and in phasmid sensilla	cel-miR-228, miR-183 ortholog	Pierce et al. 2008
Fruit fly, D*rosophila melanogaster*	haltere, scolopidia of the Johnston's organ (auditory), and in antennal segment A3	dme-miR-263b, miR-183 ortholog	Pierce et al. 2008
Green sea urchin, S*trongylocentrotus droebachiensis*	tube foot	spu-miR-183-like, spu-miR-96-like	Pierce et al. 2008
Acorn worm, S*accoglossus kowalevskii*	putative sensory epithelial cells	miR-183	Pierce et al. 2008
Atlantic hagfish, M*yxine glutinosa*	ear	miR-183	Pierce et al. 2008
Sea lamprey, P*etromyzon marinus*	ear	miR-183	Pierce et al. 2008

Spotted salamander, *Ambystoma maculatum*	neuromast hair cells, ampillary (electroreceptive) organs	miR-183	Pierce et al. 2008
Zebrafish, *Danio rerio*	nose, ear, retina and cranial and dorsal root ganglions, lateral line neuromasts	miR-183/96/182	Li et al. 2010, Wienholds et al. 2005
Chicken, *Gallus gallus*	inner ear	miR-183/96/182	Zhang et al. 2015
Mouse, *Mus musculus*	retina, ear, olfactory bulb, pineal body	miR-183/96/182	Lagos-Quintana et al. 2003, Sacheli et al. 2009, Lumayag et al. 2013
Human, *Homo sapiens*	cochleovestibular ganglion, neural crest, otic vesicle	miR-183/96/182	Chadley et al. 2018

The expression and function of the miR-183 cluster is well described in the vertebrate retina and inner ear. For the mouse retina it is known that all members of the miR-183 cluster are expressed in the photoreceptors in the outer nuclear layer reaching towards the inner nuclear layer, where the synapses of the photoreceptors are located. A subgroup of ganglion cells in the ganglion cell layer also display expression of miR-183 cluster members. Inactivation of the whole cluster results in early onset progression of synaptic defects at the photoreceptors´ ribbon synapses and in decreased electroretinogram (ERG) amplitudes as well as retinal degeneration (Lumayag et al., 2013). Knockout of only miR-182 resulted in decreased ERG amplitudes as well. Additionally, light induced progressive loss of the outer segments of the photoreceptors has been observed (Wu et al., 2019).

During inner ear development, the miR-183 cluster has been proven to be highly relevant, in Zebrafish (Wienholds et al., 2005; Li et al., 2010) and chicken (Zhang et al., 2015), as well as in mice (Sacheli et al., 2009; Weston et al., 2011): During mouse embryonic development all three members of the miR-183 cluster are expressed in the otic vesicle, the cochlear-vestibular ganglion and in the neural tube. At later embryonic stages the miR-183 cluster members can be found in vestibular hair cells, the spiral ganglion and the whole cochlear duct, predominantly in the hair cell layer. At the day of birth, postnatal (P) day 0, abundance of miRs-183, -96 and -182 is evident only in cochlear and vestibular hair cells and in the spiral ganglion (Sacheli et al., 2009; Weston et al., 2011). Importantly, there´s also miR-96 expression in the central auditory system: miR-96 expression was shown in the mouse brainstem at different timepoints (embryonic day (E)18, P0 and P25) by quantitative PCR (Rosengauer et al., 2012). Additionally, miR-96 expression was visually evident in the mouse P4 and P25 CNC and SOC as well as in central auditory structures of chickens, as shown by *in-situ* hybridization (Pawlik et al., 2016). All these findings suggest a role for miR-183 cluster members in hair cell differentiation and maturation. Expression patterns in the spiral ganglion and in central auditory neuronal structures also implicate a role in development and maintenance of neurons, substantiating the evidence for an on-site role of this miRNA cluster in sensory cells as well as in neuronal populations.

The functional impact of the miR-183 cluster on sensory systems beyond its simple descriptive expression becomes even more evident in a study about several sensory systems in a miR-183 cluster knockout mouse model that led to a broad loss of sensory functions. There was evidence for deficient cone and rod photoreceptor pathways from ERG measurements as well as morphological and molecular changes in cones and rods. In addition to visual defects, a developmental delay and arrest in cochlear and vestibular hair cells was observed (for details see next section). A fourth sensory system was added to the study investigating the olfactory system showing reduced numbers of mature sensory olfactory neurons (Fan et al., 2017).

1.7. MiR-183 cluster member misfunction affects the peripheral and central auditory system

The importance of miRNAs during development of the auditory system in general could be highlighted by one crucial result: auditory brainstem nuclei were missing when Dicer as a key component in miRNA biogenesis was knocked out at early embryonic stages in only rhombomeres 3 and 5, but not when Dicer was knocked out later (Friedman et al., 2009a; Soukup et al., 2009; Rosengauer et al., 2012). These results show miRNAs to be absolutely essential components for the development of the central auditory system. Overexpression of miR-183 cluster members results in an increase of cochlear inner hair cells at P18. Auditory brainstem response (ABR) measurements in those mice show progressive sensorineural hearing loss from P18 to P90 and histological changes in outer hair cells. Both inner and outer hair cells are almost lost at P115 (Weston et al., 2018).

Point mutations in the seed region of miR-96 were linked to nonsyndromic progressive hearing loss in men (Mencía et al., 2009; Soldà et al., 2012), showing the relevance of miR-96 for the human auditory system. A mouse line called *Diminuendo* (*Dmdo*) harboring a point mutation in the seed region of miR-96, was established as a corresponding mouse model (Lewis et al., 2009; Kuhn et al., 2011). *Dmdo* mice display peripheral deafness (Lewis et al., 2009) and an arrest of physiological development of auditory hair cells before differentiation into inner and outer hair cells as well as immature stereocilia bundle (Kuhn et al., 2011) and degeneration of auditory hair cells. These studies in the peripheral auditory system have been complemented with a study in the central auditory system of the *Dmdo* mouse (Schlüter et al., 2018): central auditory nuclei were reduced in volume due to an arrest of cell growth. MNTB neurons displayed an immature electrophysiological phenotype. Importantly, these changes were not observed in a *Claudin14 (Cldn14)* knockout mouse, a peripheral deafness mouse model, suggesting an on-site effect of the miR-96 mutation in the central auditory pathway. The miR-96 *Dmdo* phenotype was accompanied by a morphologically immature calyx of Held, which was shown by cluster analysis of the presynaptic marker protein synaptic vesicle glycoprotein 2 (SV2) immunoreactive signals. SV2 clusters have been described showing immature fenestration of the presynaptic calyceal terminal resulting in missing ring-like structures of the SV2 immunoreactive signal.

Additionally, decreased expression of the potassium channel subunits Kv1.6 and BKβ2 in the LSO and MNTB have been observed and this was discussed to contribute to the immature electrophysiology at the MNTB. The genes coding for these proteins, *KCNA6* and *KCNMB2*, have been predicted to be targets of the mutated miR-96. Thus, it is hypothesized that an important role in the *Dmdo* -phenotype is the gain of function of the mutated form of miR-96. Gain of function results from a gain of novel targets due to the point mutation in the seed region.

Another scenario for the analysis of miR-96 function was delivered by the loss of function case, simulated by knockout of miR-96. Knockout of the whole miR-183 cluster (ko of miR-183, -96 and -182) resulted in profound congenital hearing loss measured by ABRs. At P3, there was no mechanoelectrical transduction at the stereociliary bundles potentially because of missing tip links. These findings were accompanied by defects in cochlear hair cell maturation like no staircase-like arrangement of stereocilia with missing kinocilia (Geng et al., 2018) in cochlear and vestibular hair cells at P0 and P10 (Fan et al., 2017). At P6, the disorganization of inner and outer hair cells within the cochlea became evident with starting loss of hair cells. At P18, hair cell bundles were all lost and cell types were non-specific (Geng et al., 2018). Similar to previous studies, the analysis of the peripheral auditory system of *miR-183/96* ko mice (ko of miRs-183 and -96, leaving miR-182 intact) revealed complete deafness and has severely affected hair cell bundles at four weeks old, but with hair cells still present (unlike *Dmdo* mice, hair cells were gone) (Lewis et al., 2019).

A computational tool for prediction of potential causal regulatory networks, shortly PoPCoRN, was developed for integrating regulators and misregulated genes allowing to explore gene regulatory networks controlled by the miR-183 cluster or any other gene or miRNA (Lewis et al., 2019). The basis was given by datasets of significantly misregulated genes from RNA-seq data from *miR-183/96* ko and *miR-182* ko mice and from microarray and qPCR data from *Dmdo* mice. For the *miR-183/96* ko, PoPCoRN predicts a network consisting of 100 genes with 325 links. For the *Dmdo* mutation, the resulting network includes 231 genes and 869 links, strongly substantiating the gain of function hypothesis. It is also noteworthy that the PoPCoRN prediction for the *miR-182* ko elaborates a very small network including only 6 genes and only 5 links (Lewis et al., 2019). *MiR-182* ko mice only exhibit mild high frequency hearing loss at 2 months of age, with no aberrant phenotype of hair cells (Lewis et al., 2019).

These findings substantiate the essential role of the miR-183 cluster in developmental processes of the peripheral and the central auditory system highlighting the possibly key role of miR-96 that causes general immaturity of both systems only by a single base mutation in its seed sequence. This study focuses on the functional characterization of the loss of function case of miR-96 in the central system of a *miR-183/96* ko mouse model. The SOC of this mouse model will be analyzed on a morphological, electrophysiological and molecular level complementing the already existing loss of function studies in the peripheral auditory system. Results will be compared to those of the analysis of the *Dmdo* mouse in order to discuss gain and loss of function effects of the miR-96 *Dmdo* mutation.

1.8.   Towards the identification of further auditory-related miRNAs

The miR-183 cluster is a well-known player in auditory function by now. However, in the vestibular and auditory system, expression of hundreds of miRNAs has been described, most of them overlapping between vestibular and auditory-related organs (Rudnicki et al., 2014a). Based on the hypothesis of the shared gene regulatory program during development of the central and peripheral auditory structures and the critical role of miR-96 as a representative of the miRNAs, I want to summarize the knowledge about other possibly auditory-related miRNAs here that have been named in the literature so far. Some miRNAs like miR-15a, miR-18a, miR-30b, miR-99a and miR-199a have been selected for expression studies in the mouse inner ear at E16.5, E19.5, P0 and P30 showing differential expression over time. *In-situ* hybridization showed a spatial complementary expression pattern in the P0 inner ear for miR-99a and miR-199a. Targets like *Slc12a2*, *Cldn12* and *Bdnf*, all known for their function in the inner ear have been found to be regulated by miR-15a (Friedman et al., 2009a), adding these miRNAs to the list of possibly auditory-related ones. These are still lacking further functional studies. miR-24-3p, miR-16-5p, miR-185-5p and miR-451a have been found to be upregulated after loud noise exposure (Ding et al., 2016). miR-124 was associated with neuronal differentiation of mouse inner ear neural stem cells (Di Jiang et al., 2016) and was shown to be a regulator of hair cell differentiation by targeting *Sfrp4/5* involved in Wnt signaling (Huyghe et al., 2015). miR-200b was identified to play an important role in inner ear morphogenesis via regulation of the *Zeb1* pathway (Hertzano et al., 2011). miR-210, was also added to the auditory-related miRNAs because its overexpression induced differentiation of auditory hair cells from supporting epithelial cells (Riccardi et al., 2016). miR-34a, miR-29b, miR-299-3p, and miR-431 have been identified to serve as markers of hearing loss in mice (Di Stadio et al., 2018) with evidence for miR-34a to be a hearing loss marker also in humans (Pang et al., 2016). A miRNA sequencing approach comparing patients with sudden sensorineural hearing loss (SSNHL) and a healthy control group uncoverd miR-15a, miR-18b, miR-24-1, miR-34a, miR-99b, miR-190a, miR-210, miR-296, miR-451a, miR-660, miR-1180, miR-3667 and miR-3940, and to be upregulated and miR-1-1, miR-1-2, miR-23a, miR-95, miR-143, miR-548a, miR-1255a, miR-3074, miR-3679 and miR-4742 to be downregulated in SSNHL patients (Li et al., 2017). These results at least show repeatedly hearing related implications for miR-15a, miR-18, miR-24, miR-99, miR-210, miR-451a.

Many validated miRNA gene targets play a key role in the inner ear (**Table 3**, modified after Mahmoudian-sani et al., 2017).

Table 3: Auditory-related miRNAs and their target genes.

miRNA	Target genes	Reference
miR-9	Cartilage-Specific Short Collagen (*Col9a1*)	(Sivakumaran et al., 2006)
miR-15a	*Slc12a2*, *Cldn12* and *Bdnf*	(Friedman et al., 2009a)
miR-124	Secreted frizzled-related protein 4 (*Sfrp-4*) and *Sfrp-5*, two inhibitors of the Wnt pathway	(Huyghe et al., 2015)
miR-135b	SFRS1 interacting protein 1 (Psip-1), a transcriptional co-activator in the inner ear	(Elkan-Miller et al., 2011)
miR-140	Nuclear receptor subfamily 2 group F member 1 (*Nr2f1*)	(Chiang et al., 2013)
miR-182	*Tbx1*, a transcription factor that has been implicated in inner ear development and hair cell fate	(Wang et al., 2012)
miR-183	Thousand and One Amino Acid Protein Kinase 1 (*Taok1*)	(Patel et al., 2013)
miR-200b	Zeb1, pro-mesenchymal fate transcription factor	(Hertzano et al., 2011)
miR-204	*Tmprss3* (transmembrane protease, serine 3) involved in development of SGNs	(Li et al., 2014)
miR-224	Pentraxin 3 (*Ptx3*)	(Rudnicki et al., 2014b)
miR-376	Phosphoribosyl pyrophosphate synthetase 1 (*Prps1*) are associated with a spectrum of non-syndromic to syndromic hearing loss	(Yan et al., 2012)

Despite all these findings of possibly auditory-related miRNAs in the inner ear, information about possibly roles of other miRNAs than miR-96 in the central auditory system is missing. Highly expressed miRNAs from the cochlea seem to represent a good starting point for analysis of miRNAs in the central auditory system, based on the hypothesis of the partially shared gene regulatory network between the auditory periphery and central structures. miRNAs-22, -26a, -27b, -127, -143, -181a, -181b, -181c, -183, -191, -204, and -let-7c have been characterized as being among the most highly expressed miRNAs from cochlear and vestibular epithelia at P0 (Rudnicki et al., 2014a). These miRNAs have been chosen for this thesis to characterize their expression in the SOC using an *in-situ* approach for visualization on SOC tissue.

Furthermore, a comprehensive Next Generation Sequencing (NGS) approach including miRNA and mRNA sequencing of SOC tissue at different time points in development seems promising to illuminate the overall miRNA expression landscape of the SOC. Integration of information about differentially expressed miRNAs and mRNAs during development delivers a tool to find regulated pathways in the central auditory system. It would be of special interest, whether deafness genes described in the auditory periphery also show up among regulated genes in the SOC, and if so, if their regulation could be attributed to certain miRNAs.

1.9.   Main questions and aim of this thesis

Regarding the contribution of the miR-183 cluster to the development of the auditory hindbrain, it remains unclear whether the identified changes in the *Dmdo* mouse reflect a gain or a loss of function of mutated miR-96. A gain of function would be due to recruitment of newly recognized mRNA targets because of the changed seed sequence of miR-96. A loss of function would be explained by original mRNA targets of miR-96 that are not recognized anymore. To answer this fundamental question, a constitutive *miR-183/96* ko mouse model representing the loss of function scenario will be analyzed in this thesis on the anatomical, electrophysiological (in cooperation) and molecular level. Furthermore, the aim of this study is to evaluate the general regulatory landscape of miRNAs during the development of the auditory system. I therefore asked the question, whether the early shared gene regulatory network for development of the otic placode and the auditory hindbrain also applies to miRNAs and whether it does extend to later developmental stages? In order to answer this question, a further aim of my thesis was to analyse the expression pattern of highly abundant miRNAs from cochlear and vestibular epithelia in the auditory brainstem of mice. First, this will be done by visualization of expression of a small subset of selected miRNAs. A more global sequencing approach of miRNAs in the SOC will contribute to elucidate the general miRNA expression landscape. This data will also be used to compare miRNA expression in the SOC with already published data from the cochlea. The last question I try to answer is what other possibly auditory-related miRNAs could be found and in what regulation of genes may they be involved in? Therefore miRNA sequencing data will be integrated to mRNA sequencing data delivering regulatory miRNA candidates in the SOC. This analysis is based on the known function of miRNAs which is downregulation of mRNA levels.

2. Material and Methods

2.1. Material

Table 4: Primer.

Primer	Sequence (5´-´3´)	Application
Cld14-1	GGCTGCATAACCAGGATACTC	Genotyping of Claudin14 mice
Cld14-2	CAGCTCATTCCTCCCACTCATGATC	
Cld14-3	GTACAGGCTGAATGACTACGTG	
GAPDH_for_qRT	AGGTCGGTGTGAACGGATTTG	Reference gene in qRT-PCR
GAPDH_rev_qRT	TGTAGACCATGTAGTTGAGGTCA	
GluA1_for	CCAATTTCCCCAACAATATCC	qRT-PCR of Glutamate receptor subunits GluA1 – GluA4
GluA1_rev	AAAGCTGTCGCTGATGTTCA	
GluA2_for	CAGTTTCGCAGTCACCAATG	
GluA2_rev	ACCCAAAAATCGCATAGACG	
GluA3_for	CCACTTGGATTCCTCCAATAGT	
GluA3_rev	GCATACACCCCTCTGGAGAA	
GluA4_for	CTGCCAACAGTTTTGCTGTG	
GluA4_rev	AAATGGCAAACACCCCTCTA	
kcna6-f	CCTGGATGAGATGCACGTTT	qRT-PCR of potassium channel subunits
kcna6-r	TTACAAGACCCAGGCATGAAAA	
kcnma1_439f	ACTGCGGGGGCAAGACGAAG	
kcnma1_783r	CCACAGCTTATCGTTGGCTGC	
kcnmb2_149f	TGTGGAGGACTACACGGGAT	
kcnmb2_453r	GGTCCCTGATTTTCTGGTAG	
RPL3-819f	GGTTTGCGCAAAGTTGCCTG	Reference gene in qRT-PCR
RPL3-1318r	ACCATCTGCACAAAGTGGTC	
miR-183-96ko_for	TATTGGGATGTGATGGGAAACTCTG	Genotyping of *miR-183/96* ko mice
miR-183-96ko_rev	TAGCAGAAGGCTAGACCCCAAAGAC	
mmu-miR-22_for	GCCAGTTGAAGAACTGTTGCC	amplification of miRNA precursor molecules serving as templates for transcription of miRNA RNA-probes for *in-situ* hybridization
mmu-miR-22_rev	AGACCTTCCCACCCCAGTT	
mmu-miR-26a-1_for	CAAAAGCTGGAGGACCGAGG	
mmu-miR-26a-1_rev	GGAAACTCTGTTGTTGCCGC	
mmu-miR-27b_for	AGCCTTCGAAGATGCTCACC	
mmu-miR-27b_rev	TCTCCTCCTCTGGAGTGACC	
mmu-miR-127_for	TTGCTGCCTGGCTTTCTCTT	
mmu-miR-127_rev	CATACTCAGACCTGGCCGAC	
mmu-miR-143_for	AGACCCGGATAGGAGGCAG	
mmu-miR-143_rev	CCAACACTTACCACGTCCCG	
mmu-miR-181a-1_for	ATCTCTGCCTCACAGGTTGC	

mmu-miR-181a-1_rev	CTGAAGAGGCGGGGGAGAATC	
mmu-miR-181b-1_for	TGAAGACAGAACCGCAAAGC	
mmu-miR-181b-1_rev	GATTGCGACAGCAAAAAGCG	
mmu-miR-181c_for	CCCTGGTTTCTCTCTCGTCC	
mmu-miR-181c_rev	GGTCTACAGGGTGGGGATGG	
mmu-miR-183_for	TGGAGAGTGTGACTCCTGTC	
mmu-miR-183_rev	GTCTAGGCAGAAAGGGGTGAG	
mmu-miR-191_for	TCCTTCCTACTCAGCCCACT	
mmu-miR-191_rev	AAGTGCAGCTGGAATGCTCT	
mmu-miR-204_for	GCAGGAAATGAAGAGGTTGGC	
mmu-miR-204_rev	TCCACGAGTCACATGAAGAAGG	
mmu-let-7c-1_for	TCTACAACCTTGCCAAGCCC	
mmu-let-7c-1_rev	GATGGCTCAAGTGTGCTCCA	
T7	GTAATACGACTCACTATAGGGC	colony-PCR, PCR for amplification of miRNA precursors
M13 -21F	GTAAAACGACGGCCAGT	Sanger sequencing LCG Genomics

Table 5: TaqMan Assays.

TaqMan® Advanced miRNA Assays	Order number
mmu480910_mir / mmu-miR-127-3p	A25576
mmu482604_mir / mmu-miR-181c-5p	A25576
001973 U6 snRNA	4427975

Table 6: Kits.

Kits	Manufacturer / Order number
High Pure Plasmid Isolation Kit	Roche Cat. No. 11 754 777 001
innuPREP Micro RNA Kit	Analytik Jena Cat. No. 845-KS-2030010
innuPREP RNA Mini Kit	Analytik Jena Cat. No. 845-KS-2040050
LightCycler® 480 SYBR Green I Master	Roche Cat. No. 04 707 516 001
pGEM®-T Easy Vector System I: pGEM®-T Easy Vector (50 ng/µl), Control Insert DNA (4 ng/µl), T4 DNA Ligase, 2× Rapid Ligation Buffer	Promega Cat. No. A1360
RevertAid First Strand cDNA Synthesis Kit: RevertAid RT (200 U/µl), RiboLock RNase Inhibitor (20 U/µl), 5× Reaction	Thermo Scientific Cat. No. K1622

Buffer (250 mM Tris-HCl (pH 8.3), 250 mM KCl, 20 mM MgCl$_2$, 50 mM DTT), 10 mM dNTP Mix, 100 µM Oligo(dT)18 Primer, 100 µM Random Hexamer Primer	
TaqMan®Advanced miRNA cDNA Synthesis Kit: 10× Poly(A) Buffer, 10 mM ATP, Poly(A) Enzyme 5U/µl, 5× DNA Ligase Buffer, RNA Ligase 10 U/µl, 50% PEG 8000, 25× Ligation Adaptor, 10× RT Enzyme Mix, 5× RT Buffer, 20× Universal RT Primer, 100 mM dNTP Mix, 20× miR-Amp Primer Mix, 2× miR-Amp Master Mix	Applied Biosystems Cat. No. A28007

Table 7: Antibodies.

Primary Antibodies	Manufacturer / Order number
anti-Bassoon, monoclonal mouse, 1:200	Enzo Cat. No. SAP7F407
anti-DIG-AP, Fab fragments from sheep; 1:1000	Roche Applied Science Cat. No. 11093274910
anti-GluA1, monoclonal mouse, 1:500	Synaptic Systems, Cat.No. 182011
anti-GluR4, polyclonal rabbit, 1:500	Millipore, Cat.No. AB1508
anti-KCNA6, polyclonal rabbit, 1:500	Sigma, Cat.No. HPA014418
anti-KCNMB2, monoclonal mouse, 1:200	abcam, Cat.No. ab94589
anti-Piccolo, polyclonal guinea pig, 1:200	Synaptic Systems Cat. No. 142104
anti-SV2, mouse monoclonal, 1:500	Developmental Studies Hybridoma Bank
Secondary Antibodies	**Manufacturer / Order number**
Alexa Fluor 488 goat anti mouse, 1:1000	Invitrogen Cat. No. A-11001
Alexa Fluor 488 goat anti rabbit, 1:1000	Invitrogen Cat. No. A-11008
Alexa Fluor 647 goat anti guinea pig, 1:1000	Invitrogen Cat. No. A-21450
Alexa Fluor 647 goat anti rabbit 1:1000	Invitrogen Cat. No. A-21244

Table 8: Enzymes.

Enzymes	Manufacturer / Order number
DNaseI	NEB, Cat. No. M0303S
Dream Taq	Thermo Fisher Scientific Cat. No. EP0701
Proteinase K (10 mg/ml)	Carl Roth Cat. No. 7528.2
T7 RNA polymerase	Roche Cat. No. 10881767001

Table 9: Buffers, Solutions and Chemicals.

Buffers, Solutions and other Chemicals	Manufacturer / Compounds
4% Paraformaldehyde (PFA)	4% paraformaldehyde in PBS, pH 7.4
10× Transcription Buffer	Roche Cat. No. 10881767001, 0.4 M Tris-HCl, pH 8.0 (+20°C), 60 mM $MgCl_2$, 100 mM dithiothreitol, 20 mM spermidine
10× Dream Taq Buffer	includes 20 mM $MgCl_2$
10% Blocker (*in-situ* hybridization)	10% Roche blocking reagent (Cat. No. 11096176001) in maleic acid buffer
Ampicillin	100 mg/ml in sterile H_2O
AP-Buffer	100 mM Tris,150 mM NaCl, 5 mM $MgCl_2$, pH 9.5
Blocking solution (Immunohistochemistry)	2% BSA, 0.3% Triton X-100, 10% goat serum in PBS
Blocking Solution (*in-situ* hybridization)	10% Blocker in PBS
Bovine Serum Albumin (BSA)	Carl Roth, Cat. No. 8076.2
Carrier (Immunohistochemistry)	1% BSA, 0.3% Triton X-100, 1% goat serum in PBS
Denaturating solution (RNA extraction)	4 M Guanidinthiocyanat, 25 mM Sodium citrate, 0.5% N-Lauroylsarcosine
DEPC	Carl Roth, Cat. No. K028.1
Digoxigenin-11-UTP 10 mM	Roche 11209256910
DIG-Mix	10 mM each ATP, CTP, GTP, 7.5 mM UTP, 2.5 mM Dig-UTP
Dimethysulfoxide (DMSO)	Carl Roth Cat. No. 4720.1
Ethanol (EtOH)	Sigma Aldrich, Cat. No. 32205
Ethanol (70%)	70% EtOH in H_2O
Gelatin-Chromalaun solution	0,25% Gelatin, 0,025% Chrom(III)-Potassium sulphate in H_2O dest.
gDNA isolation buffer	1% SDS, 0.1 M NaCl, 0.1 M EDTA, 0.05 M Tris pH 8.0
Guanidinthiocyanat	Carl Roth Cat. No. 0017.1
Hybridization Buffer	50% formamide, 5× SSC, 2% blocker (Roche Applied Science), 0.02% SDS, 0.1% N-lauryl-sarcosine
Isopropanol	Sigma Aldrich, Cat. No. 33539
LB agar	1% (w/v) NaCl, 1% (w/v) Trypton, 0,5% (w/v) yeast extract, 2% (w/v) agar in desalted H_2O, autoclaved
LB medium	1% (w/v) NaCl, 1% (w/v) Trypton, 0,5% (w/v) yeast extract in desalted H_2O, autoclaved

20

Maleic acid buffer	0.1 M maleic acid, 0.15 M NaCl, pH 7.5
Moviol + DAPCO + DAPI	Carl Roth Cat. No. 0713.1
N-Lauroylsarcosine	Serva Cat. No. 27570
NBT/BCIP staining solution	Roche Applied Science Cat. No. 11681451001
Phosphate buffered saline (PBS)	136.9 mM NaCl, 2.7 mM KCl, 10.1 mM Na_2HPO_4, 1.8 mM KH_2PO_4, pH 7.4
RNA extraction buffer	20 ml Denaturing Solution, 0.144 ml β-Mercaptoethanol, 2 ml 2 M Sodium acetate pH 4, 22 ml H_2O saturated Phenol
Roti®-Histokitt II	Carl Roth Cat. No. T160.1
Sodium citrate	Carl Roth Cat. No. HN13.2
TaqMan® Fast Advanced Master Mix	Applied Biosystems Cat. No. 4444557
TE buffer	10 mM Tris pH8, 1 mM EDTA
Triton X-100 Serva Cat. No. 37240	
Tissue freezing medium	TBS Durham, North Carolina, USA
Zamboni	15% picric acid saturated H_2O, 2% PFA in PBS

Table 10: Technical equipment and software.

Technical equipment	Manufacturer
Confocal Microscope Leica SP8	Leica Biosystems, Nußloch, Germany
Cryostat Leica AG Protect	Leica Biosystems, Nußloch, Germany
Gene Pulser	BioRad, Hercules, CA, USA
Light Cycler® 96	Roche Applied Science, Penzberg, Germany
Nanophotometer	Implen GmbH, München, Gemrany
Sliding Microtome Microm HM 430	Thermo Scientific, Schwerte, Germany
Slide Scanning Microscope AxioScan Z1	Zeiss, Oberkochen, Germany
Tabletop Centrifuge Eppendorf 5424R	Eppendorf AG, Hamburg, Germany
Thermocycler Biometra Professional	Analytik Jena AG, Jena, Germany
Tissue Homogenizer Miccra D-8	Miccra GmbH, Heitersheim, Germany
Software	**Manufacturer / Version**
GraphPad Prism	GraphPad Software, LLC, Version 8.3.0
Huygens Essential by Scientific Volume Imaging B.V.	Huygens compute engine 18.04.0p2 64b
ImageJ	Wayne Rasband, NIH, USA Version 1.52e
Light Cycler® 96 Software	Roche Diagnostics International Ltd, Version 1.1.0.1320

2.2. Mouse lines

All protocols for animal husbandry and usage were approved by the local animal care and use committee (LAVES, Oldenburg). All experiments were in accordance with the regulations of German federal law on the care and use of laboratory animals and followed the guidelines of the EU Directive 2010/63/EU for animal experiments.

For assessment of miR-96 function in the auditory brainstem, two mouse lines have been investigated: The *Diminuendo* (*Dmdo* or miR-96 *Dmdo*) mouse, harboring a point mutation in the miR-96 seed sequence (Lewis et al., 2009; Schlüter et al., 2018), and the *miR-183/96* knockout (ko) mouse simulating the loss of function of miRNAs-96 and -183. Both mouse lines are deaf (Kuhn et al., 2011; Geng et al., 2018). To analyze on-site effects of *miR-96 Dmdo* in the auditory brainstem, another mouse line was used as a control for effects due to peripheral deafness, the *Claudin14* ko (*Cldn14* ko) mouse (Schlüter et al., 2018). Deafness in this mouse line is caused by the lack of the gap junction protein Claudin14 in the cochlea. This protein is not expressed in the brain, therefore this mouse doesn´t exhibit any *Cldn14* ko related phenotypes there. This thesis focuses on the investigation of the auditory brainstem of the *miR-183/96* ko mouse to compare its phenotype to the already characterized und published miR-96 *Dmdo* phenotype (Schlüter et al., 2018). *miR-183/96* ko animals will therefore be compared to their wildtype (wt) littermates and to the *Cldn14* ko mouse. The following **Table 11** and **Figure 4** sum up the genetic characteristics of these mouse lines.

Table 11: Mouse lines.

Mouse Line	Background Strain	Origin	Reference
miR-96 Dmdo	C3HeB/FeJ	European mouse mutant archive	(Lewis et al., 2009)
miR-183/96 ko	C57BL/6N	Haydn Prosser	(Prosser et al., 2011)
Cldn14 ko	NMRI		(Ben-Yosef et al., 2003)

Figure 4: Mouse models.
Schematic depiction of mouse models used in this study, always showing the transgenic allele. miRNAs of the miR-183 cluster are colour-coded, miR-183 is shown in blue, miR-96 in pink, and miR-182 in orange. For the *miR-96 Dmdo* mouse, miR-96 is illustrated in its mutated form. In the *miR-183/96* ko mouse, miRs 183 and 96 are missing. In the *Cldn14* ko mouse, the miR-183 cluster is intact. *Cldn14* ko is depicted as the non-functional cochlea.

The *miR-183/96* ko mouse was bred in an C57BL/N background. This inbred background strain develops age related hearing loss (AHL) due to a single nucleotide polymorphism in the Cadherin23 allele (*Cdh23*[753A]) (Noben-Trauth et al., 2003). Higher frequencies are affected first by AHL after 4 weeks, lower frequencies are unaffected up to 6 months (Li and Borg, 1991). *miR-183/96* wt mice in the C57BL/N background show good hearing sensitivity at 3-12 kHz up to an age of 6 month (Lewis et al., 2019). I analyzed the auditory brainstem of *miR-183/96* wt and ko mice at the age of 1-2 months. Therefore, AHL should not interfere with discussions about the impact of *miR-183/96* ko on auditory brainstem morphology or physiology.

2.3.   Genotyping

2.3.1.   Isolation of genomic DNA from mouse toe biopsies

In order to assign the right genotype to each individual animal, stable genotyping PCRs are required. Animals are number-coded by toe biopsies at P7-9 and organized in the PyRat animal facility software line/strain database. Tissue from the toe biopsies serve as material for DNA isolation for subsequent PCR. Each animal is genotyped once for the database and gets genotyped again after sacrificing for validation of the right genotype.

Toe biopsies enter genomic (g)DNA isolation to serve as the template DNA in each genotyping PCR. To each toe biopsy 700 µl Tail Buffer and 50 µl 10 mg/ml Proteinase K were added and mixed well, followed by an overnight incubation at 56°C. The mixture was centrifuged for 10 min at 13000 rpm and the supernatant was transferred to a new reaction tube. After adding 500 µl of Isopropanol the mixture was inverted thoroughly and incubated for 2 min at room temperature. This was followed by another centrifugation step for 5 min at 13000 rpm and the supernatant was discarded. 500 µl of 70% Ethanol were added to the DNA-pellet and the reaction tubes were inverted to wash the pellet. The mixture was centrifuged again for 5 min at 13000 pm and the supernatant was discarded. The reactions tubes were centrifuged shortly and the remaining Ethanol was thoroughly removed with a pipette. After air-drying the pellets at 37°C for approximately 10 min the pellets were dissolved in 50 µl nuclease free water and stored at 4°C until the genotyping PCR was performed.

2.3.2.   Genotyping of *miR-183/96* mice

PCR reactions were set up and run according to **Table 12**. After PCR, samples were analyzed on a 2% TBE-agarose gel 60 min at 100 V. Heterozygous animals show two bands, one for the wt allele (841 bp) and one for the ko allele (645 bp). Wildtype animals only show the wt band, knockouts only the ko band.

Table 12: PCR reaction for genotyping of miR-183/96 mice.

Mastermix for 1 PCR reaction (25 µl)	PCR Program
2.5 µl 10× Dream Taq Buffer 0.5 µl dNTPs (10 mM each) 0.5 µl 20 pmol/µl miR-183-96ko_for Primer 0.5 µl 20 pmol/µl miR-183-96ko_rev Primer 0.1 µl Dream Taq 19.9 µl nuclease free H_2O • mix well and add to 1 µl extracted mouse gDNA	Initial denaturation: 95°C → 5 min Cyclic denaturation: 95°C → 30 s Primer annealing: 62°C → 30 s ⎱ 30 cycles DNA polymerization: 72°C → 30 s Final DNA polymerization: 72°C → 5 min Hold: 4°C → ∞

2.3.3. Genotyping of *Cldn14* mice

PCR reactions were set up and run according to **Table 13**. After PCR, samples were analyzed on a 2% TBE-agarose gel 60 min at 100 V. Heterozygous animals show two bands, one for the wt allele (340 bp, Primer 1 and 3) and one for the ko allele (275 bp, Primer 1 and 2). Wildtype animals only show the wt band, knockouts only the ko band.

Table 13: PCR reaction for genotyping of Cldn14 mice.

Mastermix for 1 PCR reaction (25 µl)	PCR Program
2.5 µl 10× Dream Taq Buffer 0.5 µl dNTPs (10 mM each) 0.5 µl 20 pmol/µl Cld14-1 Primer 0.5 µl 20 pmol/µl Cld14-2 Primer 0.5 µl 20 pmol/µl Cld14-3 Primer 1 µl DMSO 0.2 µl Dream Taq 18.3 µl nuclease free H_2O • mix well and add to 1 µl extracted mouse gDNA	Initial denaturation: 95°C → 5 min Cyclic denaturation: 95°C → 30 s Primer annealing: 60°C → 30 s ⎱ 30 cycles DNA polymerization: 72°C → 30 s Final DNA polymerization: 72°C → 5 min Hold: 4°C → ∞

24

2.4. Volume measurements of auditory brainstem nuclei

The auditory hindbrain (as well as any other brain region) consists of a variety of accumulated mixed cell populations that are interconnected with fiber tracts. These accumulations of neurons (and glia) are referred to as nuclei, that can be distinguished by eye due to their location, shape and cell morphology. In order to detect morphological changes in terms of volume, cell number and cell size in auditory brainstem nuclei of *miR-183/96* ko mice compared to their wt littermates, we decided for a morphometric analysis of several auditory and non-auditory brainstem nuclei. The non-auditory nuclei serve as an internal control for effects that maybe interfere with the whole brain(stem) and are therefore not auditory-related. **Figure 5** shows an overview about the anatomy of the brainstem in the region of the auditory-related nuclei, depicting two section planes through the brainstem. It shows the auditory and non-auditory nuclei that were morphologically analyzed as described below.
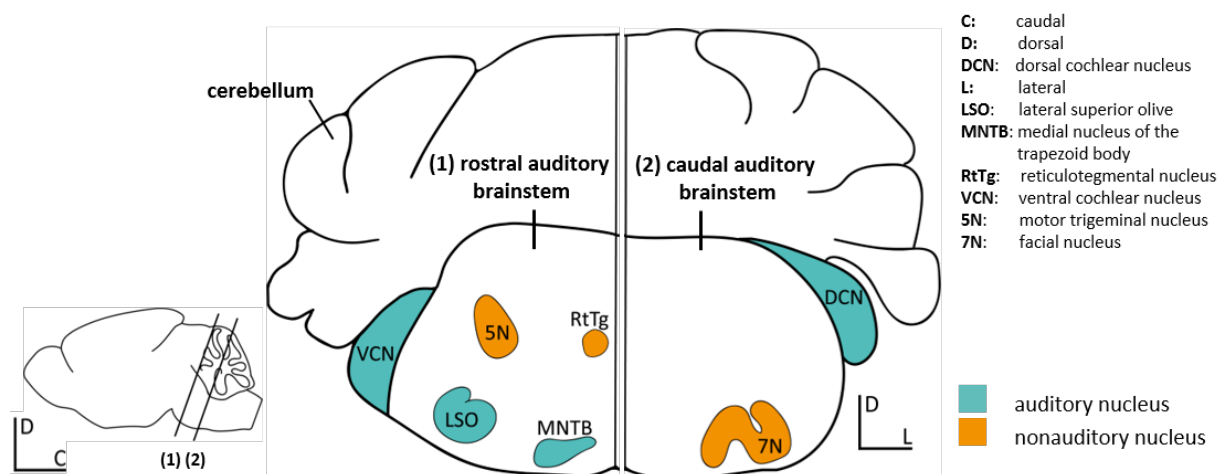
Figure 5: Topology of auditory and non-auditory brainstem nuclei for morphological analysis.
Schematic illustration of auditory and non-auditory structures for morphological analysis and their location in the auditory brainstem of mice. There are two section planes indicated, the more rostral one (1) harboring the VCN, LSO, MNTB, 5N and RtTg, and the more caudal one (2) harboring the DCN and 7N. Auditory nuclei are depicted in blue while non-auditory nuclei are shown in orange.

2.4.1. Tissue preparation

miR-183/96 ko mice and their wt littermates at the age of P60 were injected intraperitoneally with a lethal dose of sodium pentobarbital (Narcoren©, Merial, Lyon, France; 650 mg/kg bodyweight) and perfused transcardially with phosphate buffered saline (PBS) followed by 4% Paraformaldehyde (PFA). Brains were postfixed in 4% PFA overnight and incubated for at least 16 h in 30% Sucrose in PBS for cryoprotection. Brains were embedded in Tissue freezing medium and stored at -80°C until analysis. Coronal serial sections of 30 μm thickness were cut on a cryostat using Gelatin-Chromalaun coated slides and stored at -80°C until used. Only complete series of auditory brainstem sections from the beginning of the dorsal cochlear

nucleus (DCN) to the end of the reticulotegmental nucleus (RtTg) (seen from caudal) have been used for subsequent NISSL staining and analysis of the volume of 4 auditory brainstem nuclei (DCN, LSO, MNTB and VCN) and 3 non-auditory nuclei (5N, 7N, RtTg).

2.4.2. NISSL staining

Selected slide series were air-dried and incubated over-night in Chloroform/Ethanol (1:1) in preparation for NISSL staining, followed by an 1 h incubation in 100% EtOH. Slides were dipped 3 min each in 96%, 96%, 90%, 70%, 50% EtOH and H_2O to slowly hydrate the tissue. Staining of the tissue with Thionin which is specific for DNA and Nissl bodies (primarily ribosomal RNA) was performed by incubation of the slides for 2 min in Thionin-solution. The ascending EtOH series of 3 min each H_2O, 50%, 70%, 90% EtOH, 96% EtOH with acidic acid, 96% EtOH dehydrates the slides again and differentiates the staining with the help of acidic acid that washes away unbound basic Thionin-stain. For organic mounting slides were incubated in Xylol-Terpineol (1:1), Xylol I and Xylol II and afterwards mounted with Roti®-Histokitt II mounting medium and coverslipped. Every section was pictured with the Zeiss AxioScan Z1, an automated slide scanning microscope.

2.4.3. Morphometry of brainstem nuclei

Every section of the left and right DCN, LSO, MNTB, VCN and 5N, 7N and RtTg respectively of three specimen of each genotype (*miR-183/96* ko and wt) was selected and saved as single photographs from these scans. Every second section of each left and right nucleus was analyzed using ImageJ: The nucleus was surrounded with a selection and the area of the selection was calculated by ImageJ according to the known image dimensions. For the missing section between every second analyzed picture the mean was calculated. The volume of the nucleus was calculated by multiplicating its area in each section by 30 µm (the thickness of the cryosections) and building the sum of each section of the nucleus. The values from the left and right nucleus were averaged. Three values for each nucleus of each genotype were statistically compared to detect significantly altered volumes in *miR-183/96* ko mice compared to their wt littermates using multivariate analysis of variance (MANOVA).

Additionally, data about the number of cells of the LSO and MNTB of *miR-183/96* ko mice and their wt littermates have been collected. For that purpose, every second NISSL-stained section of the left and right LSO and MNTB of each specimen was used to count the cells with ImageJ. The mean was built from the data from both left and right sides of each LSO and MNTB. Three values for each nucleus and genotype were statistically compared with a Student´s *t*-test. The analysis of the cross-section area of cells, 120 cells per nucleus (60 cells from the left and right side each) per animal were randomly chosen by an ImageJ algorithm, circled and the area was calculated due to the known image dimensions by ImageJ. 120 values per nucleus and animal were averaged. Statistical differences between groups were analyzed using Student´s *t*-test.

2.5.   Immunohistochemistry

Immunohistochemistry is a method to visualize the localization of proteins. Via specific binding of a primary antibody to a certain epitope of a protein and binding of a secondary fluorescent dye coupled antibody, the protein is labeled with a fluorophore. Using that method, it becomes possible to detect the protein with a fluorescence microscope. The protein expression is relevant, because the abundance of the RNA transcript alone doesn´t necessarily lead to expression of the protein and also contains no information about the subcellular location of the active protein in the cell.

Mice at the age of P30 were injected intraperitoneally with a lethal dose of sodium pentobarbital (Narcoren©, Merial, Lyon, France; 650 mg/kg bodyweight) and perfused transcardially with phosphate buffered saline (PBS) followed by Zamboni solution. Brains were postfixed in Zamboni for 3-4 hours and incubated for at least 16 h in 30% Sucrose in PBS for cryoprotection. 30 µm thick coronal sections of the auditory brainstem were cut on a sliding microtome and stored in PBS at 4°C. Selected slices of the auditory brainstem were transferred to fine meshes and washed 3×5 min in PBS in a 6 well plate, followed by a 30 min blocking step in blocking solution. All washing and incubation steps were carried out on a shaker. The primary antibody was diluted in 500 – 1000 µl carrier solution (for dilutions see **Table 7**), the sections were transferred into the primary antibody solution in a 24 well plate and incubated over night at 4°C. On the next day the sections were again transferred to the fine meshes and washed 3× 5 min in PBS. The secondary antibody was diluted 1:1000 in in 3 ml carrier solution. The meshes with the washed sections were transferred into the secondary antibody solution (in a 6-well plate) and incubated in the dark for 1.5 h at room temperature, followed by 3×5 min washing in PBS in the dark. The free-floating sections were attached to a gelatin-chromalaun coated slide with the help of a fine brush and air-dried. Because of the fluorescence of the secondary antibody, slides were kept in the dark at all times now. Sections on the slides were mounted with Moviol plus DAPI and coverslipped. Confocal Laser Scanning microscopy was carried out soon after performing the Immunohistochemistry to avoid fading of the secondary antibodie´s fluorescence. Quantifications were made on deconvoluted, thresholded, binary images using the respective ImageJ plugins.

2.6.   Electrophysiological recordings

Electrophysiology on acute brainstem slices containing the MNTB was done in cooperation by Dr. Christoph Körber, Institute of Anatomy und Cell Biology, Department of Functional Neuroanatomy, Heidelberg University. *miR-183/96* ko mice and their wt littermates were therefore sent to our cooperation partner. Mice of either genotype were rapidly decapitated at P 25-27. Brains were removed in ice-cold slicing solution containing 125 mM NaCl, 25 mM NaHCO$_3$, 2.5 mM KCl, 1.25 mM NaH2PO4, 3 mM myoinositol, 2 mM Na-pyruvate, 0.4 mM ascorbic acid, 0.1 mM CaCl$_2$, 3 mM MgCl$_2$ and 25 mM glucose aerated with carbogen (5% CO$_2$ in O$_2$). Coronal auditory brainstem slices of 250 µm thickness were prepared on a vibratome (VT1200S, Leica) and stored in artificial cerebrospinal fluid (ASCF) containing 125 mM NaCl, 25 mM NaHCO$_3$, 2.5 mM KCl, 1.25 mM NaH$_2$PO$_4$, 2 mM CaCl$_2$, 1 mM MgCl$_2$ and 25 mM glucose aerated with carbogen (pH 7.3) at 37°C for 45 min and at room temperature (22 ± 1°C) thereafter. Whole-cell patch-clamp recordings from MNTB principal neurons were performed at room temperature in ACSF using an EPC-10/2 amplifier controlled by PatchMaster software (HEKA, Lambrecht, Germany). Pipettes with open tip resistances of 2-4 MΩ were pulled from thick-walled borosilicate glass (Cat. no.: 1807515, Hilgenberg, Malsfeld, Germany) and filled with pipette solution containing 130 mM Cs gluconate, 10 mM CsCl, 10 mM HEPES, 10 mM TEA-Cl, 5 mM Na$_2$-phosphocreatine, 5 mM EGTA, 4 mM Mg-ATP and 0.3 mM GTP (pH 7.2). The membrane potential was set to -70 mV and the series resistance (3-6 MΩ) was compensated by >90%. Currents were digitized at 20-100 kHz and Bessel-filtered (2.9 kHz). Synaptic release from the calyx of Held was evoked by afferent fibre stimulation via a parallel bipolar electrode (FHC, Bowdoin, ME) close to midline (2-6 V stimuli, 70-100 µs duration). In some recordings, ACSF was supplemented with 1 mM kynurenic (Kyn) acid (Abcam). sEPSC amplitudes in ACSF supplemented with 1 mM Kyn were calculated assuming a similar decrease in amplitude for sEPSCs and evoked EPSCs, as described previously (Neher and Sakaba, 2001). This was necessary, since the reduction in sEPSC amplitude may have caused a large fraction of sEPSCs to vanish in the noise, thereby preventing us from accurately measuring them. Data were analysed using custom-written IGOR (Wavemetrics, Lake Oswego, OR) routines.

2.7.   Quantitative Reverse Transcriptase PCR

This technique was applied to detect differences in gene expression between *miR-183/96* ko mice and their wt littermates. RNA from the SOC was used to generate cDNA and relative gene expression of genes of interest was determined compared to the housekeeping gene coding for Ribosomal Protein L3 (*RPL3*). The efficiency of specific primers for genes of interest was tested in advance using a dilution series of cDNA before running the quantitative PCR.

2.6.1. RNA isolation and cDNA synthesis

Mice were killed with CO_2 and decapitated. The brain was immediately removed from the scull and frozen on dry ice. The SOC region of at least 3 *miR-183/96* ko mice or wt littermates respectively per sample has been cut out from freshly frozen cryostat sections. Sections before and after have been collected on slides, postfixed with 4% paraformaldehyde and NISSL stained to control if the SOC region was properly recognized. Total RNA was isolated from collected SOC tissue with the innuPREP RNA Mini Kit. For each genotype 3 biological samples were created. cDNA was synthesized with the RevertAid First Strand cDNA Synthesis Kit. For each sample the exact RNA concentration was determined with the Nanophotometer and the exact volumes of RNA and H_2O were calculated to apply the same amount of RNA for each cDNA synthesis reaction. 170 ng of RNA were mixed with 1 µl of Poly-T primer and added up with nuclease free H_2O to 12 µl. The mixture was incubated for 5 min at 70°C and then 5 min on ice. To each reaction 4 µl 5× reaction buffer, 2 µl dNTPs, 1 µl RNase Inhibitor and 1 µl Reverse Transcriptase was added and mixed with the pipette tip and then incubated for 5 min at 25°C. The cDNA synthesis was performed for 60 min at 42°C. The reaction was stopped at 70°C for 5 min. To reach enough volume of cDNA, 10 µl of each cDNA sample was diluted 1:10 in preparation of the experiment.

2.6.2. Primer efficiency test

Following dilutions of cDNA were prepared with nuclease free water: 1:2, 1:10, 1:25, 1:50, 1:100. For each reaction a volume of 5 µl cDNA was needed to minimize effects caused by pipetting errors. For each primer pair to test, a 150 µl master mix (10 reactions) was prepared containing 0.5 - 1 µM of each Primer per PCR reaction, 100 µl LightCycler® 480 SYBR Green I Master (2× conc.) and nuclease free H_2O ad 150 µl. 15 µl of the master mix were mixed with each 5 µl of cDNA dilution according to below pipetting scheme (**Table 14**) in a Light cycler 96 well plate.

Table 14: cDNA dilutions for primer efficiency tests for qPCR.

	well	1	2	3	4	5	6	7	8	9	10
					cDNA dilution						
primer pair 1	A	1:2	1:10	1:10	1:25	1:25	1:50	1:50	1:100	1:100	neg. contr.
primer pair 2	B	1:2	1:10	1:10	1:25	1:25	1:50	1:50	1:100	1:100	neg. contr.

The PCR program from below table was run by the Roche Light Cycler® 96 instrument measuring the fluorescence of SYBR green after each amplification cycle.

Table 15: Roche Light Cycler 96 settings for primer efficiency tests.

3-step amplification	melting curve
Initial denaturation: 95°C → 10 min Cyclic denaturation: 95°C → 10 s ⎤ Primer annealing: 60°C → 10 s ⎬ 45 cycles DNA polymerization: 72°C → 10 s ⎦	Denaturation: 95°C → 10 s Annealing: 65°C → 60 s Melting: 97°C → 1 s

Quantification cycle (Cq) values for every cDNA dilution were averaged, except the 1:2 dilution where only one value exists (see **Table 14**). Mean Cq values were plotted against the -log of cDNA dilutions resulting in a half logarithmic amplification line of PCR product generated by tested primers. The slope of its regression line was used to calculate the primer efficiency due to following formula (Pfaffl, 2001):

$$primer\ efficiency = \ 10^{[-\frac{1}{slope}]}$$

An ideal value for primer efficiency is 2, meaning doubling of the PCR product in every amplification cycle. Results for primer efficiency tests are shown in the appendix (**Figure 29**, **Table 41**).

2.6.3. Quantitative PCR

For each gene of interest, a 20× master mix was pipetted, containing the positively tested primer concentration (e.g. 0.5 µM), 200 µl LightCycler® 480 SYBR Green I Master 2× conc., ad 300 µl with nuclease free water. 5 µl of cDNA (1:10 dilution) of respective samples was previously pipetted into the Light cycler 96 well plate according to the scheme shown below (**Table 16**). In addition to the three biological replicates (wt 1-3 and ko 1-3), each sample is represented in technical triplicates. 15 µl of respective master mix was added to the cDNA and

mixed with the pipette tip. The 96 well plate was covered with a sticky, transparent foil and inserted into the Roche Light Cycler® 96 instrument.

Table 16: Pipetting scheme for qPCR.

| | well | sample |
		1	2	3	4	5	6	7	8	9	10	11	12
gene 1	A	wt 1	wt 1	wt 1	wt 2	wt 2	wt 2	wt 3	wt 3	wt 3	ko 1	ko 1	ko 1
	B	ko 2	ko 2	ko 2	ko 3	ko 3	ko 3	-RT	H_2O				
gene 2	C	wt 1	wt 1	wt 1	wt 2	wt 2	wt 2	wt 3	wt 3	wt 3	ko 1	ko 1	ko 1
	D	ko 2	ko 2	ko 2	ko 3	ko 3	ko 3	-RT	H_2O				
ref gene	E	wt 1	wt 1	wt 1	wt 2	wt 2	wt 2	wt 3	wt 3	wt 3	ko 1	ko 1	ko 1
	F	ko 2	ko 2	ko 2	ko 3	ko 3	ko 3	-RT	H_2O				

Table 17 shows the PCR program, that was run on the Roche Light Cycler® 96 instrument for quantitative PCR.

Table 17: Roche Light Cycler 96 settings for qPCR.

3-step amplification	melting curve
Initial denaturation: 95°C → 10 min Cyclic denaturation: 95°C → 10 s Primer annealing: 60°C → 10 s ⎬ 45 cycles DNA polymerization: 72°C → 10 s	Denaturation: 95°C → 10 s Annealing of PCR products: 65°C → 60 s Melting: 97°C → 1 s

The result of the quantitative PCR was analyzed using the Light Cycler® 96 Software. A result batch export containing the statistically relevant data was imported into Microsoft Excel. Basically, calculation of the expression ratio of targeted genes (target) and reference gene (ref) was done according to Pfaffl (2001), using following formula:

$$ratio = \frac{(primer\ efficiency_{target})^{\Delta Cq_{target}(wt-ko)}}{(primer\ efficiency_{ref})^{\Delta Cq_{ref}(wt-ko)}}$$

31

2.8.   RNA *in-situ* hybridization

RNA *in-situ* hybridization is a well-established technique to visualize mRNA expression qualitatively directly on the tissue, using Digoxigenin (Dig)-labeled RNA-probes that are complementary to certain target mRNAs expressed in the tissue of interest. An alkaline phosphatase coupled anti-Dig antibody that specifically binds the Dig-labeled RNA probes is then used to catalyze the colour precipitation from a dye via the alkaline phosphatase. The precipitated dye can be detected by bright field microscopy and shows the location of mRNA expression of interest. This method can also be applied to miRNAs, using their precursor transcripts as targets for specifically designed RNA probes. Dig-labeled RNA-probes for mmu-miR-22, -26a, -27b, -127, -143, -181a, -181b, -181c, -183, -191, -204, and -let-7c and had to be generated for visualization of miRNA precursor expression in mouse auditory brainstem sections. For accession numbers of miRNAs and PCR primers see **Table 18**. The workflow consists of RNA isolation and cDNA generation, PCR amplification of miRNA precursors from this cDNA and cloning them into an appropriate vector for in-vitro transcription of RNA probes. Afterwards, these probes have been applied on fixed auditory brainstem tissue.

Table 18: miRNAs´ accession IDs and primers for amplification.

MiRNA	MirBase Accession	NCBI Accession	Forward Primer	Reverse Primer
mmu-miR-22	MI0000570	NC_000077.6	5´-GCCAGTTGAAGAACTGTTGCC-3´	5´-AGACCTTCCCACCCCAGTT-3´
mmu-miR-26a-1	MI0000573	NC_000075.6	5´-CAAAAGCTGGAGGACCGAGG-3´	5´-GGAAACTCTGTTGTTGCCGC-3´
mmu-miR-27b	MI0000142	NC_000079.6	5´-AGCCTTCGAAGATGCTCACC-3´	5´-TCTCCTCCTCTGGAGTGACC-3´
mmu-miR-127	MI0000154	NC_000078.6	5´-TTGCTGCCTGGCTTTCTCTT-3´	5´-CATACTCAGACCTGGCCGAC-3´
mmu-miR-143	MI0000257	NC_000084.6	5´-AGACCCGGATAGGAGGCAG-3´	5´-CCAACACTTACCACGTCCCG-3´
mmu-miR-181a-1	MI0000697	NC_000067.6	5´-ATCTCTGCCTCACAGGTTGC-3´	5´-CTGAAGAGGCGGGGAGAATC-3
mmu-miR-181b-1	MI0000723	NC_000067.6	5´-TGAAGACAGAACCGCAAAGC-3´	5´-GATTGCGACAGCAAAAAGCG-3´
mmu-miR-181c	MI0000724	NC_000074.6	5´-CCCTGGTTTCTCTCTCGTCC-3´	5´-GGTCTACAGGGTGGGGATGG-3´
mmu-miR-183	MI0000225	NC_000072.6	5´-TGGAGAGTGTGACTCCTGTC-3´	5´-GTCTAGGCAGAAAGGGGTGAG-3´
mmu-miR-191	MI0000233	NC_000075.6	5´-TCCTTCCTACTCAGCCCACT-3´	5´-AAGTGCAGCTGGAATGCTCT-3´
mmu-miR-204	MI0000247	NC_000085.6	5´-GCAGGAAATGAAGAGGTTGGC-3´	5´-TCCACGAGTCACATGAAGAAGG-3´
mmu-let-7c-1	MI0000559	NC_000082.6	5´-TCTACAACCTTGCCAAGCCC-3´	5´-GATGGCTCAAGTGTGCTCCA-3´

2.8.1. RNA Isolation and reverse transcription

Total RNA was extracted from unfixed C57BL6/J P4 and P30 mouse brainstem with the guanidine thiocyanate method: One freshly prepared and immediately frozen whole mouse brainstem was homogenized in RNA extraction buffer using the tissue homogenizer. The homogenate was divided into two 1.5 ml reaction tubes for further processing. This protocol describes the procedure for one reaction tube: 150 µl of Chloroform were added and the reaction was mixed by shaking followed by a 15 min incubation on ice. The mixture was centrifuged at 13000 rpm for 15 min at 4°C. The upper phase was carefully collected and transferred into a new 1.5 ml reaction tube. Depending on the volume of the upper phase,

500 µl/ml Isopropanol was added and the solution was mixed by inverting the reaction tube. The reaction was centrifuged at 13000 rpm for 45 min a 4°C to spin down precipitated RNA. After discarding the supernatant, the pellet was washed with 500 µl 70% EtOH followed by another centrifugation step at 13000 rpm for 10 min at 4°C. The supernatant was discarded thoroughly and the pellet was shortly air-dried before dissolving it in 50 µl of nuclease free water. The quality and quantity of RNA was determined by gel electrophoresis and optical density measurements, respectively.

We performed reverse transcription of total brainstem RNA with the RevertAid First Strand cDNA Synthesis Kit. 7.5 µg of either P4 or P30 total RNA was mixed with 1 µl random Hexamer Primer and 1 µl Oligo (dT)18 primer and filled up to 12 µl with nuclease free water in PCR reaction tubes. The reaction was mixed and incubated at 70°C for 5 min. All incubation steps were performed in a Thermocycler. After that, the reaction was immediately chilled on ice for 5 min and 4 µl of the 5× reaction buffer, 2 µl 10 mM dNTP mix and 1 µl 20 U/µl RiboLock RNase Inhibitor were added and the reaction was mixed with a pipette tip. The reaction was allowed to incubate at 25°C for 5min before adding 1 µl 200 U/µl RevertAid M-MuLV Reverse Transcriptase. The mixture was incubated at 42°C for 60 min and after that at 70°C for 10 min to inactivate the reverse transcriptase. 25 µl of nuclease free water have been added to the reaction and cDNA was stored at -80°C until downstream PCR reactions.

2.8.2. Cloning of miRNA precursors

PCR products of chosen miRNAs were generated from a mixture of P4 and P28 brainstem cDNA. See **Table 19** for assembly of the PCR. They are referred to as "insert" in the following steps. Subsequently, they were cloned into the pGEMT-Easy vector containing the RNA polymerase transcription sites SP6 and T7. These are needed for later transcription of DIG-labeled RNA probes for *in-situ* hybridization.

Table 19: PCR reaction generating the insert miRNA for cloning into pGEMT-Easy.

Mastermix for 1 PCR reaction (50 µl)	PCR Program
5 µl 10× Dream Taq Buffer	Initial denaturation: 95°C → 5 min
1 µl dNTPs (10 mM each)	
1 µl 20 pmol/µl miRNA-for Primer	Cyclic denaturation: 95°C → 30 s
1 µl 20 pmol/µl miRNA-rev Primer	Primer annealing: 57°C → 30 s — 30 cycles
1 µl cDNA mixture (P4 and P28)	DNA polymerization: 72°C → 30 s
2 µl Dream Taq	
39 µl nuclease free H_2O	Final DNA polymerization: 72°C → 5 min
	Hold: 4°C → ∞

For each miRNA, two reactions were prepared in order to pool them for later precipitation earning enough yield. 5 µl of each PCR product were analyzed on a 2% agarose gel after electrophoresis at 100 V for 30 min. 4 µl 3M NaAc and 100 µl Isopropanol were added to the PCR reactions for precipitation. The mixture was mixed well and incubated for 5 min and centrifuged for 15 min at 13000 rpm. The supernatant was discarded and 500 µl 70% EtOH were added to wash the pellet. The mixture was again centrifuged for 5 min at 13000 rpm and the supernatant was carefully removed. The pellets were air-dried for 10 min at 37°C and were dissolved in 20 µl nuclease free H_2O. DNA yield and purity were determined with the Nanophotometer.

For cloning the miRNA precursor DNA fragments into pGEMT-Easy, the number of insert molecules should exceed the number of vector molecules by the factor of at least 3. The minimal amount of insert-DNA for the ligation reaction was therefore calculated with following formula:

$$amount\ of\ insert\ [ng] = \frac{(amount\ of\ vector\ [ng] \times length\ of\ insert\ [kb]) \times 3}{length\ of\ vector\ [kb]}$$

For an insert length of 0.2 kb and 50 ng of vector DNA with 3 kb in length the amount of insert was therefore calculated like following example:

$$amount\ of\ insert = \frac{(50\ ng \times 0.2\ kb) \times 3}{3\ kb} = 9.9\ ng$$

The amount of insert-DNA for each precipitated miRNA PCR was adjusted to approximately 10 ng/µl and the ratio of insert / vector was doubled to 6:1 ending up with 2 µl of insert DNA for the ligation reaction. The ligation reaction was set up for covalently connecting the insert to the vector DNA with the help of a T4 DNA ligase according to **Table 20**.

Table 20: Ligation reaction for ligating miRNA inserts to pGEMT-Easy.

ligation reaction (10 µl)	Protocol
5 µl 2× Rapid Ligation Buffer 1 µl 50 ng/µl pGEMT-Easy 2 µl miRNA Insert DNA 1 µl T4 DNA Ligase 1 µl nuclease free H_2O	Ligation: 4°C → over night

In order to amplify the plasmids carrying the miRNA precursors and T7 or SP6 transcription sites, the ligation product was transformed into E.*coli* XL1-blue competent cells. The feature of Ampicillin resistance encoded on pGEMT-Easy served for selection of ligated plasmids on respective Ampicillin containing media.

40 µl of competent cells were stored in 1.5 ml reaction tubes at -80°C and thoroughly thawn on ice. 1 µl of ligation reaction was added to the competent cells and mixed by tapping the reaction tube with the finger. The mixture was transferred to a clean electroporation cuvette and cells were electroporated. 500 µl of pre-warmed to 37°C LB medium were immediately added to electroporated cells and the cells were allowed to shake at 37°C for 1 h. 100 µl of cell suspension was applied to a pre-warmed to 37°C LB agar petri dish containing 100 µg/ml Ampicillin and incubated overnight at 37°C. On the next day, at least 10 colonies were chosen for colony-PCR screening colonies for plasmids containing the miRNA precursors that were ligated with pGEMT-Easy in the right orientation (T7 promotor upstream of miRNA-precursor). Colonies were touched with a sterile toothpick and attached cell material was transferred to 30 µl sterile H_2O. Colony-PCR reactions were set up according to **Table 21**.

Table 21: PCR reaction mixture for colony-PCR.

Mastermix for 10 PCR reactions (à 25 µl)	PCR Program
25 µl 10× Dream Taq Buffer 5 µl dNTPs (10 mM each) 5 µl 20 pmol/µl miRNA-for Primer 5 µl 20 pmol/µl T7 Primer 20 µl Taq Polymerase 140 µl nuclease free H_2O • mix and add 20 µl to 5 µl of colony suspension	Initial denaturation: 95°C → 5 min Cyclic denaturation: 95°C → 30 s Primer annealing: 50°C → 30 s ⎫ 30 cycles DNA polymerization: 72°C → 30 s ⎭ Final DNA polymerization: 72°C → 5 min Hold: 4°C → ∞

Colony-PCR products were analyzed on 2% agarose gels after electrophoresis at 100 V for 30 min. Plasmid clones showing a band at appropriate height relative to a C11 marker were chosen for plasmid preparation and subsequent Sanger-sequencing for verification of the DNA-sequence. Culturing chosen cell clones and mini-plasmid preparation were performed according to the Roche High Pure Plasmid Isolation Kit instruction manual. Quantity of Plasmid DNA was determined with the Nanophotometer. Plasmid DNA was prepared due to LGC Genomics Berlin requirements for Flexi-Run Sanger sequencing service containing at least 100 ng/µl DNA. Sequencing primer was the standard M13-21F primer. Only sequence-verified clones entered the next steps.

2.8.3. *In-vitro* transcription of RNA probes

In-vitro transcription of sequence-verified clones with the T7 polymerase in presence of digoxigenin-11-UTP resulted in digoxigenin-labeled antisense probes encompassing the precursors and partial primary transcripts of miRNAs. Note that sense probes for miRNAs are also complementary to the target to a certain degree because of the self-complementarity of miRNAs in general.

For generation of enough linear and easily accessible template DNA for *in-vitro* transcription, a PCR amplification step was performed in which only the precursor miRNA template together with the T7 RNA polymerase promotor needed for transcription was amplified from the pGEMT-Easy/miRNA vector. For each miRNA clone the specific miRNA forward primer was used together with a T7 primer to amplify the template DNA for transcription of the antisense probe. The PCR reaction was set up according to **Table 22**.

Table 22: PCR reaction for amplification of miRNA precursors prior to transcription.

Mastermix for T7-PCR reaction (250 µl)	PCR Program
25 µl 10× Dream Taq Buffer 5 µl dNTPs (10 mM each) 5 µl 20 pmol/µl T7 Primer 5 µl 20 pmol/µl miRNA forward-Primer 1 µl (50-100 ng) Plasmid DNA 1.5 µl Dream Taq 208 µl nuclease free H$_2$O • divide into 5× 50 µl reactions	Initial denaturation: 95°C → 5 min Cyclic denaturation: 95°C → 30 s ⎤ Primer annealing: 50°C → 30 s ⎬ 30 cycles DNA polymerization: 72°C → 30 s ⎦ Final DNA polymerization: 72°C → 5 min Hold: 4°C → ∞

The success of the PCR was controlled on a 2% agarose gel via gel electrophoresis and the PCR reactions were pooled and the PCR product was precipitated. The reaction was mixed with 1/10 vol 10 M ammoniumacetate and 2.5 vol of Isopropanol and incubated for 1h on ice. The mixture was centrifuged for 20 min at 4°C at 13000 rpm. The pellet was washed with 500 µl 70% EtOH and centrifuged again for 5 min at 4°C at 13000 rpm. The supernatant was thoroughly removed and the pellet was air-dried. The pellet was resolved in 50 µl nuclease free water and the DNA concentration and was determined using the Nanophotometer. DNA was stored at -20°C or immediately used for transcription.

The volume of template DNA was calculated with the help of measured values to apply 1 µg template DNA in each transcription reaction (**Table 23**).

Table 23: Reaction for in-vitro transcription of DIG-labeled RNA probes.

in-vitro transcription (1 reaction à 50 µl)	Protocol
5 µl 10× Transcription Buffer 10 µl DIG-Mix (containing digoxigenin-11-UTP) 1 µg T7-miRNA PCR product 1.5 µl T7 RNA Polymerase Ad 50 µl with nuclease free H_2O	• mix and incubate for 4 h at 37°C • add 2 µl of DNaseI, 15 min at 37°C • add 2 µl 0,5 M EDTA, 65°C for 10 min • check 1 µl of the reaction on 1% agarose gel

The transcribed RNA was precipitated over night at -20°C with 100 µl 4 M Lithium chloride and 500 µl 100% EtOH. The reaction was centrifuged for 20 min at 4°C at 13000 rpm and the pellet was washed with 500 µl of 70% EtOH in DEPC-treated H_2O. After centrifugation for 10 min at 4°C at 13000 rpm the pellet was air-dried and resolved in 50 µl DEPC-treated H_2O. The RNA concentration was determined using the Nanophotometer and the RNA integrity was again checked on a 1% agarose gel. RNA probes were stored at -80°C until they were used in *in-situ* hybridization.

2.8.4. RNA *in-situ* hybridization

Mice were injected intraperitoneally with a lethal dose of sodium pentobarbital (Narcoren©, Merial, Lyon, France; 650 mg/kg bodyweight) and perfused transcardially with PBS followed by 4% PFA. Brains were postfixed in 4% PFA overnight and incubated for at least 16 h in 30% Sucrose in PBS. Brains were embedded in Tissue freezing medium and stored at -80°C until analysis. Coronal alternating serial sections of 20 µm thickness were cut on a cryostat and stored at -80°C until used.

On-slide *in-situ* hybridization was performed according to the following steps: Slices were treated with proteinase K (10 µg/ml) for 8 min and deacetylated for 10 min with 12.5 µl acetic anhydride in 5 ml 0.1 M Triethanolamine and 0.9% NaCl. After that, slices were incubated for 2 h at 50°C in hybridization buffer, followed by an overnight incubation at 50°C in hybridization buffer containing 1 µg/ml RNA probe. After washing for 30 min each at 45°C with 2× SSC, 0.5× SSC and PBS 1% Tween, slices were incubated for 1 h with blocking solution at room temperature (RT) followed up by an 1.5 h incubation with an alkaline phosphatase conjugated Antibody against Digoxigenin (Anti-DIG AP) 1:1000 in blocking solution. Signal detection was performed in presence of NBT/BCIP staining solution 1:50 in AP-Buffer at RT. Results were documented with an AxioScan Z1. *In-situ* hybridization was repeated at least three times for each probe on at least three different animals. Pictures shown are representative results.

2.9. TaqMan® quantitative PCR on miRNAs

Our *in-situ* hybridization approach was designed to detect the precursor molecules of certain miRNAs and not for quantitative but only for qualitative description of miRNA expression. To make a quantitative statement of expression of mature miRNAs we used the quantitative qPCR approach with TaqMan® probes. TaqMan® probes are fluorescently labeled probes that anneal specifically to a complementary sequence between the forward and reverse primer sites during PCR. As long as the probe is intact, a quencher dye suppresses the reporter dye fluorescence. During DNA-polymerization, the DNA polymerase cleaves probes that are hybridized to their target sequence. That process separates the reporter dye from the probe resulting in fluorescence. With every amplification cycle during PCR and therewith increasing amount of PCR product, more TaqMan probes can specifically bind to their target sequence leading to increasing fluorescence in the reaction that is measured by the qPCR thermocycler. This method is especially suitable for detecting the expression of short RNAs like miRNAs, because due to their only 22 nucleotides length it is not possible to amplify them with conventional PCR. The TaqMan system enables amplification of all miRNAs by polymerization of a poly(A) tail at the 3-prime end and ligating an adaptor at the 5-prime end of short RNAs before performing a universal cDNA synthesis for all abundant miRNAs.

The aim of this experiment was to quantify the expression of the mature miR-127-3p and -181c-5p in the SOC and the neocortex of 3 different time points, at E16, P0 and P30. E16 represents a time point when the migration of neurons is completed, at P0 auditory brainstem neurons begin to functionally mature being located within their functional circuits. P30 is a timepoint after hearing onset and represents the adult tissue. All samples from E16, P0 and P30 SOCs and neocortices were processed in biological triplicates.

2.9.1. RNA extraction from the SOC and neocortical tissue

Mice of the strain C57Bl6/J were killed with CO_2 and decapitated at P0 and P30. The brain was immediately prepared out of the skull and frozen on dry ice. For E16 embryos a C-section was performed on an anesthetized pregnant mouse and embryos were decapitated and the heads were frozen on dry ice. The SOC region or the neocortical region respectively were cut out on a cryostat and the tissue of several animals was collected for RNA isolation: For E16 the tissue of 8 individuals per sample, for P0 6-8 individuals per sample and for P30 3 individuals per sample were collected. Total and small RNA was isolated with the innuPrep miRNA Kit and frozen at -80°C. The RNA concentration was determined with the Nanophotometer.

2.9.2. Poly(A) tailing reaction

The poly(A) tailing reaction catalyzes the addition of several adenosine triphosphates to the 3-prime end of small RNAs. This step enables binding of the universal RT primer during cDNA synthesis during the "reverse transcription" step.

18 RNA samples, the samples from the SOC and cortex at E16, P0 and P30 each in biological triplicates, were diluted in RNase free water to a concentration of ≥ 5 ng/μl and then for each sample the amount of diluted RNA and water was calculated to bring the RNA to a concentration of exactly 5 ng/μl. 2 μl (10 ng) of each RNA sample then was prepared in 0.2 ml PCR tubes on ice. The poly(A) tailing reaction mix was then prepared and processed according to below **Table 24**.

Table 24: Poly(A) tailing reaction mixture.

Poly(A) tailing (1 reaction à 5 μl)	Protocol
0.5 μl 10× Poly(A) Buffer 0.5 μl 10 mM ATP 0.3 μl Poly(A) Enzyme 1.7 μl RNase-free water • mix well and add to 2 μl 5 ng/μl RNA	Polyadenylation: 37°C → 45 min Stop reaction: 65°C → 10 min Hold: 4°C → immediately proceed to next step

During the run of the poly(A) tailing reaction, the reaction mixture for the next step, the adaptor ligation reaction was prepared.

2.9.3. Adaptor ligation reaction

The poly(A)-tailed RNAs are now immediately processed in an adaptor ligation reaction that catalyzes ligation of an adaptor molecule to the 5-prime end of the RNA molecules. This adaptor enables binding of the miR-Amp forward primer during the "miRNA amplification" step and therewith universal amplification of all abundant miRNAs. The reaction mixture was prepared and processed according to **Table 25**.

Table 25: Adaptor ligation reaction mixture.

Adaptor ligation (1 reaction à 15 μl)	Protocol
3 μl 5× DNA Ligase Buffer 4.5 μl 50% PEG 8000 0.6 μl 25× Ligation Adaptor 1.5 μl RNA Ligase 0.4 μl RNase-free water • mix well and add to 5 μl poly(A) tailing reaction	Ligation: 16°C → 60 min Hold: 4°C → immediately proceed to next step

During the run of the adaptor ligation reaction the reverse transcription reaction was prepared.

2.9.4. Reverse transcription

During this step cDNA was synthesized by binding of an universal RT primer to the poly(A) tail of the RNAs and a reverse transcriptase that is a RNA dependent DNA polymerase. The reaction mixture was prepared and processed according to **Table 26**.

Table 26: Reverse transcription reaction mixture.

Reverse transcription (1 reaction à 30 µl)	Protocol
6 µl 5× RT Buffer 1.2 µl dNTP Mix (25 mM each) 1.5 µl 20× Universal RT Primer 3 µl 10× RT Enzyme Mix 3.3 µl RNase-free water • mix well and add to 15 µl adaptor ligation reaction	Reverse transcription: 42°C → 15 min Stop reaction: 85°C → 5 min Hold: 4°C → store at -20°C

2.9.5. miRNA amplification

In order to universally increase the number of cDNA molecules, universal forward and reverse primers complementary to the universal RT-primer and the adaptor, are now used in a PCR reaction. 5 µl of each cDNA were prepared in new PCR tubes and the reaction mixture was pipetted and processed according to **Table 27**.

Table 27: miRNA amplification reaction mixture.

miRNA amplification (1 reaction à 50 µl)	Protocol
25 µl 2× miR-Amp Master Mix 2.5 µl 20× miR-Amp Primer Mix 17.5 µl RNase-free water • mix well and add to 5 µl cDNA	Enzyme activation: 95°C → 5 min Cyclic denaturation: 95°C → 3s ⎤ Anneal / Extend: 60°C → 30 s ⎦ 14 cycles Stop reaction: 99°C → 10 mn Hold: 4°C → store at -20°C

2.9.6. quantitative PCR

In preparation of the quantitative PCR a 1:10 dilution of each cDNA from the miRNA amplification reactions was made. 5 µl of these dilutions were pipetted each to respective wells of a 96-well qPCR plate, for each sample in technical duplicates. The PCR reaction mixture was set up according to **Table 28**, using the respective TaqMan® Advanced miRNA Assay for miR-127-3p or -181c-5p respectively. As a reference gene the miRNA Assay for the U6 snRNA was chosen. **Table 28** also shows the settings of the Light Cycler® 96.

Table 28: TaqMan qPCR reaction mixture.

quantitative PCR (1 reaction à 20 µl)	Protocol
10 µl TaqMan® Fast Advanced Master Mix (2×) 1 µl TaqMan® Advanced miRNA Assay (20×) 4 µl RNase-free water • mix well and add to 5 µl diluted miR-amplification reaction	Enzyme activation: 95°C → 20 s Denaturation: 95°C → 3s Anneal / Extend: 60°C → 30 s } 40 cycles

Table 29 shows an overview about the experimental setup during the quantitative PCR for quantifying the expression of two miRNAs in one tissue type at three different timepoints.

Table 29: Pipetting scheme for TaqMan qPCR.

	well	1	2	3	4	5	6	7	8	9	10	11	12
						sample							
miR-127-3p	A	E16 1	E16 1	E16 2	E16 2	E16 3	E16 3	P0 1	P0 1	P0 2	P0 2	P0 3	P0 3
	B	P30 1	P30 1	P30 2	P30 2	P30 3	P30 3	H₂O					
miR-181c-5p	C	E16 1	E16 1	E16 2	E16 2	E16 3	E16 3	P0 1	P0 1	P0 2	P0 2	P0 3	P0 3
	D	P30 1	P30 1	P30 2	P30 2	P30 3	P30 3	H₂O					
U6 snRNA	E	E16 1	E16 1	E16 2	E16 2	E16 3	E16 3	P0 1	P0 1	P0 2	P0 2	P0 3	P0 3
	F	P30 1	P30 1	P30 2	P30 2	P30 3	P30 3	H₂O					

2.10. RNA isolation and RNA sequencing

In order to generate an overview about miRNA expression in the SOC and to detect differential expression of miRNAs between several timepoints, we performed next generation sequencing (NGS) of miRNAs. For integration of mRNA and miRNA data we also performed mRNA sequencing. This was supposed to show active miRNA regulation and the important biological pathways contributing to the development of the auditory system.

Mice of the strain C57Bl6/J were killed with CO_2 and decapitated at P0 and P16. The brain was immediately prepared out of the skull and frozen on dry ice. For E16 embryos a C-section was performed on anesthetized pregnant mice and embryos were decapitated and the heads were frozen on dry ice. The SOC region was cut out on a cryostat and the tissue of several animals was collected for RNA isolation. For E16 the tissue of 8 individuals per sample, for P0 6-8 individuals per sample and for P16 3 individuals per sample were collected RNA was isolated with the innuPrep miRNA Kit (Isolation of miRNAs and total RNA) and frozen at -80°C. **Table 30** gives an overview on ages and tissues that were used for sequencing.

Table 30: Overview of Next Generation Sequencing approaches.

Ages	Tissue	Sequencing
E16	SOC	miRNA and mRNA/lncRNA
P0	SOC	miRNA and mRNA/lncRNA
	cortex	miRNA
P16	SOC	miRNA and mRNA/lncRNA
	cortex	miRNA

The library preparation and next generation sequencing service was done by Macrogen, Korea. For each mRNA/lncRNA sequencing reaction 1 µg of total RNA was sent, for each miRNA sequencing reaction 3 µg of total RNA was required. Each age and tissue were prepared in biological triplicates. **Table 31** sums up the technical requirements for the sequencing reactions:

Table 31: Requirements for Next Generation Sequencing for mRNA/lncRNA and miRNAs.

mRNA/lncRNA	Library type: Illumina transcriptome; library: Illumina TruSeq Stranded Total RNA with Ribo-Zero Gold Human/Mouse/Rat; sequencing: NovaSeq; sequencing coverage: 60 million reads/sample; read length: 100 bp paired end
miRNA	Library type: Illumina transcriptome; library: Illumina TruSeq Small RNA library; sequencing: HiSeq2500 rapid run mode 1x50bp lane-based seq; sequencing coverage: 1/6 lane (120 million reads/lane = 20 million reads/sample); read length: 50 bp single end

The sequencing data was delivered as raw data FASTQ files and analyzed in cooperation by Naama Messika Gold and Dr. Ran Elkon, Department of Human Molecular Genetics and Biochemstry, Sackler Faculty of Medicine, Tel Aviv University, Israel. miRNAs were annotated according to the miRbase v22 microRNA database. miRs were filtered for sequences that were found more than once in a million reads (counts per million (CPM) > 1) in at least 3 samples of a group. Library sizes among samples were normalized using the trimmed mean of M-values (TMM) normalization method (Robinson and Oshlack, 2010). CPM values were $\log_2$CPM transformed and provided as Excel-tables. The global relationship among samples due to their miRNA expression profiles was done by hierarchical clustering based on an Euclidean distance matrix. Because samples for E16 and P0 contained one sample from another batch, data was corrected for batch effects.

Taking the readily normalized CPM values I performed correlation analyses using calculation of the Pearson correlation coefficient r. r quantifies the direction and magnitude of correlation between the miRNA datasets of the P0 cochlea and P0 SOC. A value of r = 0 means no correlation at all, while r = 1 means perfectly correlating data. In this case, if all miRNAs would show the same CPM value for the cochlea and the SOC, r would be = 1. Pearson correlation analyses were performed using GraphPad Prism.

Differentially expressed miRs (P0 vs. E16; P16 vs. P0 and P16 vs. E16) were bioinformatically detected (in cooperation) with the limma-voom R-package with a false discovery rate (FDR) = 0.05 and a fold change (FC) between average expression levels of: |FC| > 1.5. miRNA target-gene predictions were obtained from 3 online databases: TargetScan Mouse v7.2 – August 2018 release, using conserved miRNA families; miRDB v6 – January 2019 release, prediction is based on support vector machines (SVMs) and high-throughput training datasets; miRanda – August 2010 release, makes predictions employing a conservation filter. Raw data from mRNA sequencing was preprocessed by quality assessment and trimming of reads (removing adaptor sequences). Reads were aligned to the reference transcriptome of the house mouse (*mus musculus*). Lowly expressed genes were filtered for a CPM value of at least 0.5 in at least 3 samples of a group. Normalization of library sizes was done using the TMM method and data was $\log_2$CPM transformed. Differentially expressed genes (P0 vs. E16; P16 vs. P0 and P16 vs. E16) were bioinformatically detected with the limma-voom R-package with a false discovery rate (FDR) = 0.0001 and a fold change (FC) between average expression levels of: |FC| > 1.5 miRNAs whose predicted target genes among the mRNA data show significant changes in expression in an anticorrelated manner to the miRNA expression itself were considered as active miRNAs. The workflow of paired miRNA and mRNA NGS data analysis is schematically summarized in **Figure 6**.
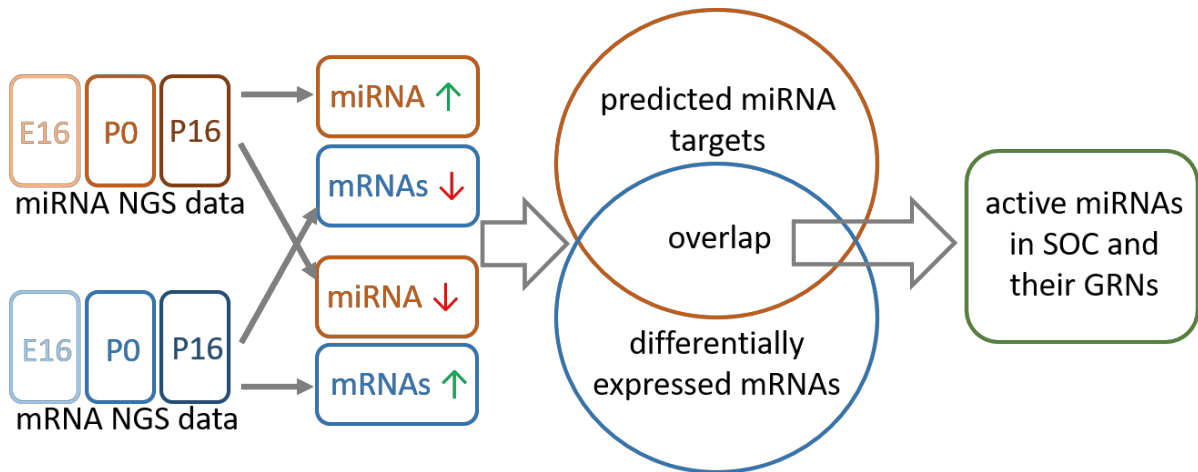
Figure 6: Workflow of paired miRNA and mRNA NGS analysis in the mouse SOC at three timepoints.
miRNA and mRNA NGS data from E16 and P0 SOC samples (N=4) and P16 SOC samples (N=3) of C57Bl6/J mice entered the analysis. Upregulated miRNAs are considered to downregulate their mRNA targets, while downregulated miRNAs should result in an increase of their targeted mRNAs, red and green arrows indicate the direction of regulation. Single, differentially expressed miRNAs were chosen and their predicted targets were compared to anticorrelatedly expressed mRNAs from the NGS dataset. If there was a significant overlap between predicted and differentially expressed mRNAs, the miRNA was defined as actively contributing to a gene regulatory network involved in the development of the SOC. E: embryonic day; GRN: gene regulatory network; P: postnatal day; SOC: superior olivary complex.

3. Results

3.1. Volume reduction of auditory brainstem nuclei in *miR-183/96* ko mice

Dmdo mice carrying a point mutaion in miR-96 displayed smaller volumes of auditory brainstem nuclei (Schlüter et al., 2018). In order to answer the question if this was a consequence from a gain or a loss of function of miR-96, the loss of function scenario was investigated using the *miR-183/96* ko mouse. To investigate the impact of *miR-183/96* ko on auditory hindbrain integrity, the volumes of auditory and non-auditory nuclei of adult *miR-183/96* wt and ko mice at P60 were determined by quantitative analysis of Nissl-stained sections. The DCN, VCN, LSO and MNTB represent auditory nuclei while the 5N, 7N and RtTg served as non-auditory controls. **Figure 7** and **Figure 8** show representative results from Nissl-stained sections, giving clear indications for decreased sizes of the VCN, LSO and MNTB. Whole series of Nissl-stained nuclei were used for the quantitative analysis shown in **Figure 9** and **Figure 10**.
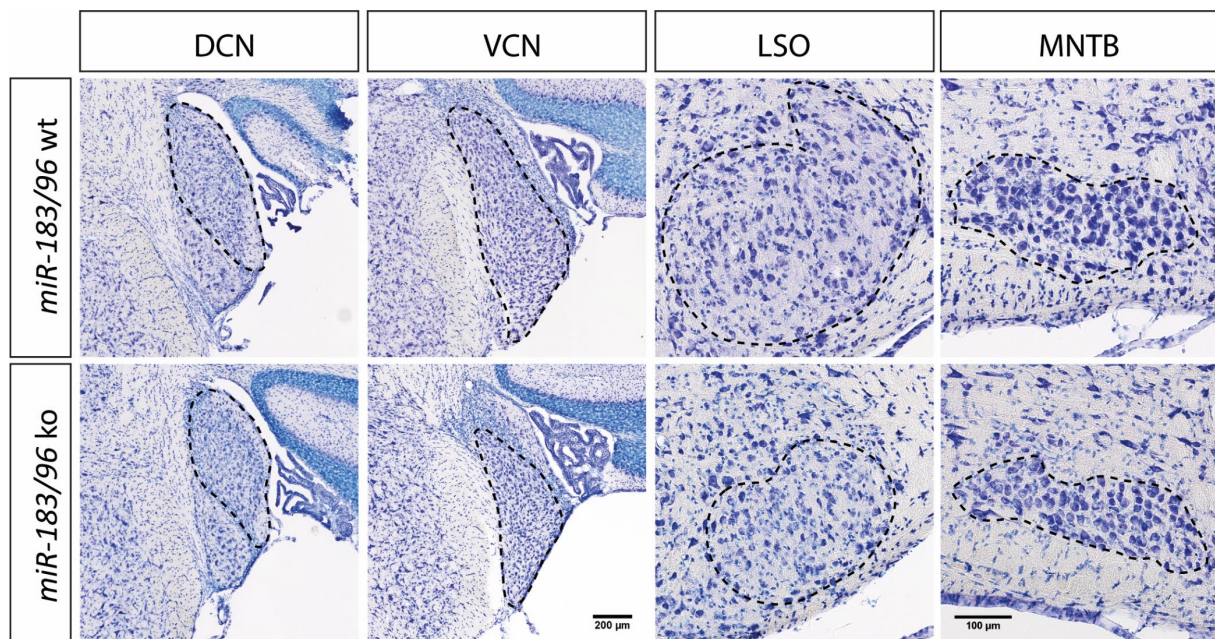
Figure 7: Morphometry of auditory brainstem nuclei in miR-183/86 ko compared to wt littermates.
Images show the auditory brainstem nuclei DCN, VCN, LSO and MNTB on Nissl-stained coronal sections of *miR-183/96* ko and wt mice at comparable section planes. Respective nuclei are outlined with a dashed black line. For the VCN, LSO and MNTB the reduction in size in *miR-183/96* ko mice is evident. DCN: dorsal cochlear nucleus; LSO: lateral superior olive; MNTB: medial nucleus of the trapezoid body; VCN: ventral cochlear nucleus. Scale bars also apply to the upper and left images.
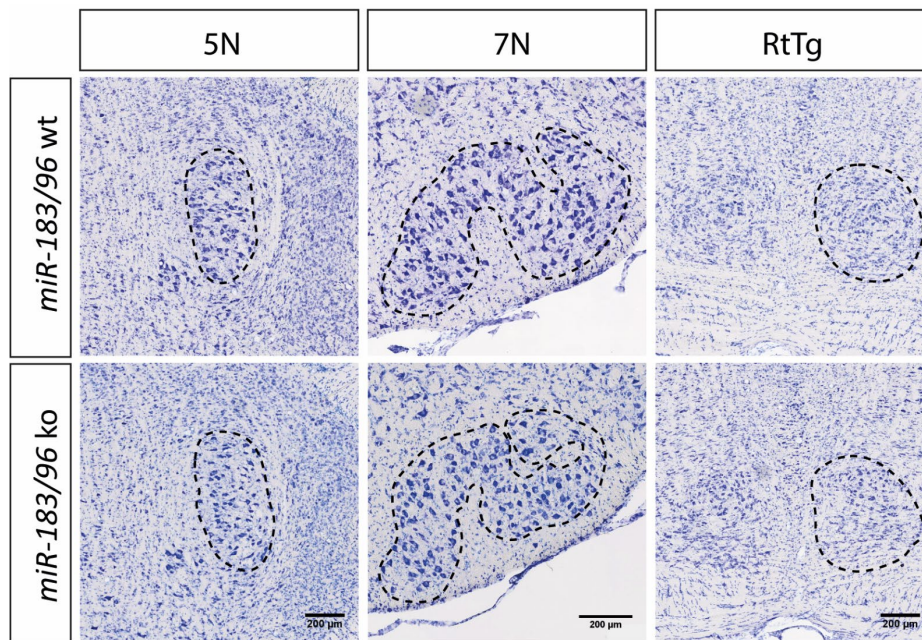
Figure 8: Morphometry of non-auditory brainstem nuclei in miR-183/96 ko compared to wt littermates.
Images show the non-auditory brainstem nuclei 5N, 7N, and RtTg on Nissl-stained coronal sections of *miR-183/96* ko and wt mice at comparable section planes. Respective nuclei are outlined with a dashed black line. Scale bars also apply to the corresponding upper image. 5N: nucleus of the 5th nerve = motor trigeminal nucleus; 7N: nucleus of the 7th nerve = facial nucleus; RtTg: Reticulotegmental nucleus.

To control for a global effect of the *miR-183/96* ko on the brain, the weight of the brains of *miR-183/96* wt (0.47 ± 0.0047 g) and *miR-183/96* ko (0.42 ± 0.0081 g) mice was determined directly after perfusion of the animals. A slight but significant 11% difference was observed (p = 0.0022). However, the effect of *miR-183/96* ko on auditory structures was strikingly compared to only minor effects on nonauditory nuclei as will be shown in subsequent results (**Figure 9**).

Quantitative analysis of Nissl-stained sections demonstrated that three out of four auditory nuclei, i.e. the VCN which is part of the CNC, as well as the LSO and MNTB of the SOC, displayed significant volume reductions, whereas the DCN (also part of CNC) did not (**Figure 9**A).
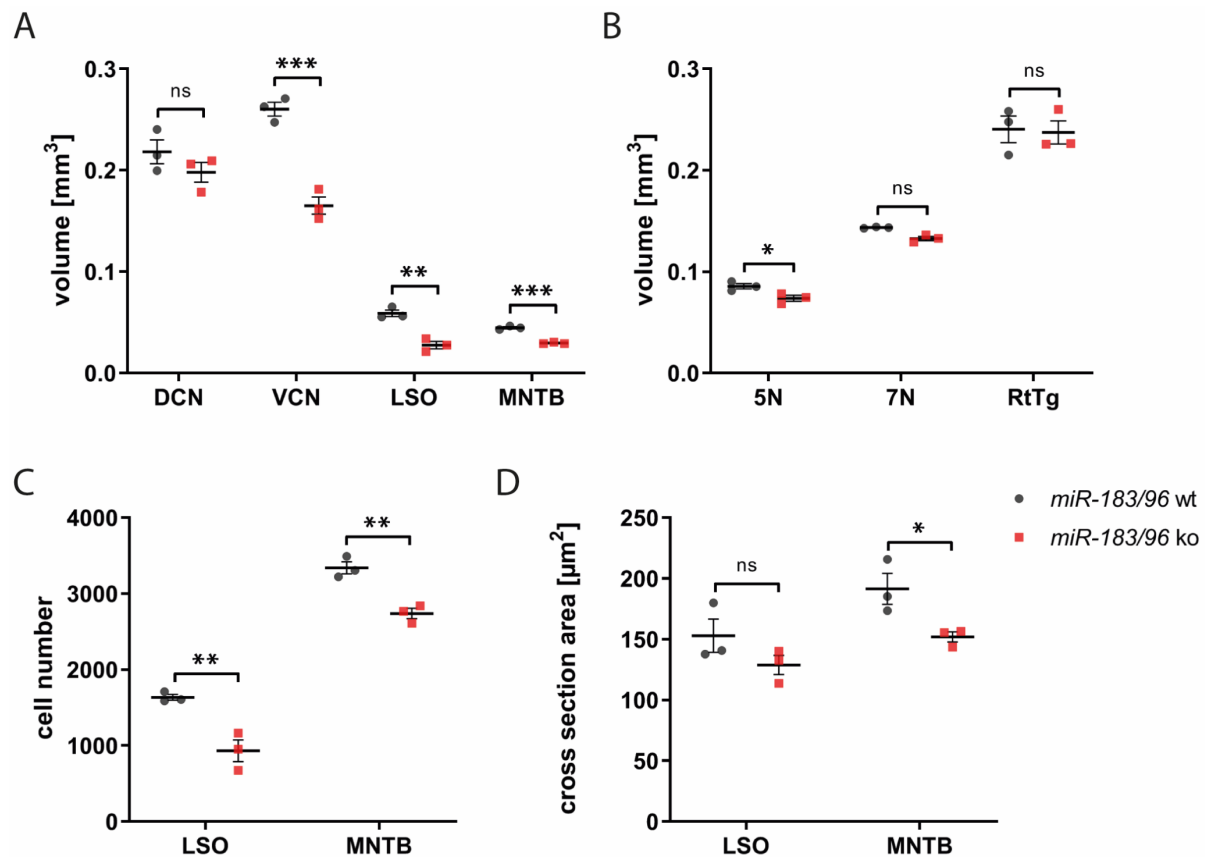
Figure 9: Significantly reduced volumes of auditory brainstem nuclei in miR-183/96 ko mice.
A: Volumes of the VCN, LSO and MNTB were significantly reduced in *miR-183/96* ko mice compared to their wt littermates. Of five nuclei analyzed, only the DCN didn´t show a volume reduction. **B:** Volumes of the non-auditory brainstem nuclei RtTg and 7N were not affected in *miR-183/96* ko mice compared to their wt littermates. Only the 5N showed a slight but significant volume reduction. Volume measurements represent the mean of the left and right side of each nucleus. P-values were calculated by MANOVA. **C:** In the LSO and the MNTB of *miR-183/96* ko mice the number of cells was significantly decreased. Cells have been counted for the left and right side of each nucleus and averaged. **D:** The cross-section area of LSO and MNTB neurons of *miR-183/96* ko mice was slightly decreased, but significantly only for the MNTB. 120 cells per animal have been analyzed and averaged. P-values have been determined by Student´s *t*-test. Scatter dot plots show the individual data points, the mean and SEM for each dataset. 5N, trigeminal motor nucleus; 7N, facial nucleus; DCN, dorsal cochlear nucleus; LSO, lateral superior olive; MNTB, medial nucleus of the trapezoid body; RtTg, reticulotegmental nucleus; VCN, ventral cochlear nucleus. Abbrevations also apply to Fig. 10. ns = not significant; p < 0.05 = *; p < 0.01 = **; p < 0.001 = ***. N = 3, age: P60.

The VCN volume was reduced by 36.53% (wt: 0.26 ± 0.0068 mm3; ko: 0.165 ± 0.0086 mm3; p = 0.00096). The LSO was even 53.15% smaller in miR-183/96 ko animals (wt: 0.059 ± 0.0032 mm3; ko: 0.028 ± 0.0037 mm3; p = 0.0030). The MNTB displayed a volume reduction by 33.80% (wt: 0.045 ± 0.0010 mm3; ko: 0.030 ± 0.00044 mm3; p = 0.00016). The DCN volume was slightly reduced by 9.24%, but this change was not significant (wt: 0.22 ± 0.012 mm3; ko: 0.198 ± 0.010 mm3; p = 0.26). To check for the impact on non-auditory structures, we probed the trigeminal motor nucleus (5N), the facial nucleus (7N) and the reticulotegmental nucleus (RtTg) (**Figure 9**B). The 5N was significantly (13.89%) smaller (wt: 0.086 ± 0.0026 mm3; ko: 0.074 ± 0.0029 mm3; p = 0.039). The 7N showed a slight but non-significant reduction by 7.58% (wt: 0.14 ± 0.00038 mm3; ko: 0.13 ± 0.0020 mm3; p = 0.065), while the RtTg volume was not reduced at all (wt: 0.24 ± 0.013 mm3; ko: 0.24 ± 0.011 mm3; p = 0.87).

To address the question, whether the volume reduction in the LSO and MNTB is due to a decrease in cell number or soma size, both variables were quantified (**Figure 9**C, D). For the LSO, results revealed a significant decrease of 43.04% in cell number (wt: 1,635.42 ± 38.12 cells; ko: 931.67 ± 141.75 cells; p = 0.0087) and a nonsignificant decrease in soma size of 15.70% (wt: 152.89 ± 13.63 μm^2; ko: 128.89 ± 7.89 μm^2; p = 0.20). The MNTB, showed both a significant decrease of 18.01% in cell number (wt: 3,341.58 ± 79.52 cells; ko: 2,739.92 ± 67.98 cells; p = 0.0045) and of 20.71% in cell soma size (wt: 191.58 ± 12.60 μm^2; ko: 151.92 ± 4.16 μm^2; p = 0.040). These results reveal that the decreased volume of the LSO and MNTB is mainly due to fewer cells in the LSO and due to fewer and smaller cells in the MNTB. All values are also listed in **Table 32**.

Table 32: Auditory brainstem morphometric data of miR-183/96 wt and ko mice.

Nucleus	*miR-183/96* wt		*miR-183/96* ko		
-auditory-	mean [mm^3]	SEM	mean [mm^3]	SEM	p-value
DCN	0.22	0.012	0.198	0.010	0.26
VCN	0.26	0.0068	0.165	0.0086	0.00096
LSO	0.059	0.0032	0.028	0.0037	0.0030
MNTB	0.045	0.0010	0.030	0.00044	0.00016
-non-auditory-					
RtTg	0.24	0.013	0.24	0.011	0.87
5N	0.086	0.0026	0.074	0.0029	0.039
7N	0.14	0.00038	0.13	0.0020	0.065
Nucleus	*miR-183/96* wt		*miR-183/96* ko		
	cell number	SEM	cell number	SEM	p-value
LSO	1,635.42	38.12	931.67	141.75	0.0087
MNTB	3,341.58	79.52	2,739.92	67.98	0.0045
	soma size [μm^2]	SEM	soma size [μm^2]	SEM	p-value
LSO	152.89	13.63	128.89	7.89	0.20
MNTB	191.58	12.60	151.92	4.16	0.040

Hindbrain data of the miR-96 *Dmdo* mouse have been compared to the deaf *Cldn14* mouse as a control for effects arising from peripheral deafness (Schlüter et al., 2018). Adding now the *miR-183/96* ko mouse model as the loss of function case for miR-96, the results for changes of volume in auditory nuclei were normalized to nuclei volumes of wt littermates and relative volumes of auditory nuclei were compared amongst the peripherally deaf *Cldn14* mouse, the miR-96 *Dmdo* mouse and the *miR-183/96* ko mouse (**Figure 10**).
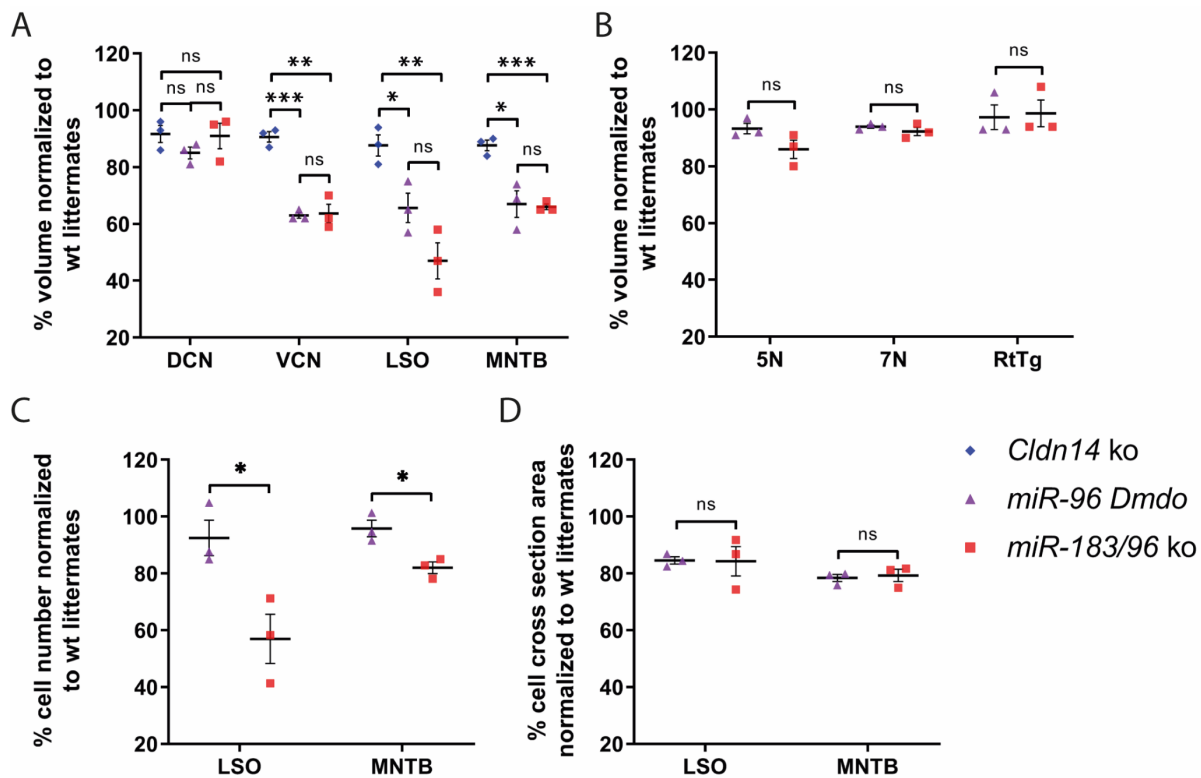
Figure 10: Relative volume reduction of auditory brainstem nuclei in miR-183/96 ko, miR-96 Dmdo and Cldn14 ko mice.
A: The volumes of the VCN, LSO and MNTB are significantly smaller in miR-183/96 ko and miR-96 *Dmdo* mice compared to peripherally deaf *Cldn14* ko mice. Values of miR-183/96 ko mice and miR-96 *Dmdo* mice do not significantly differ. **B:** The relative volumes of the nonauditory brainstem nuclei 5N, 7N and RtTg are not significantly different in *miR-183/96* ko mice compared to miR-96 *Dmdo* mice. Datasets represent the percentage of volume of brainstem nuclei compared to each mouse line's wt littermates. **C:** The relative cell number of the LSO and MNTB in *miR-183/96* ko mice was significantly lower than in miR-96 *Dmdo* mice. **D:** The cross-section area of cells in the LSO and MNTB was not significantly different between *miR-183/96* ko and miR-96 *Dmdo* mice. P-values were calculated using Student's *t*-test. ns = not significant; $p < 0.05$ = *; $p < 0.01$ = **; $p < 0.001$ = ***. N = 3.

Comparing the relative volume reduction of auditory nuclei between miR-96 *Dmdo* and *miR-183/96* ko mice (relative to their wt littermates), revealed no significant differences (**Figure 10** A) (DCN: miR-96 *Dmdo*: 14.89 ± 1.59%; *miR-183/96* ko: 9.24 ± 3.67%, p = 0.31; VCN: miR-96 *Dmdo*: 36.94 ± 0.76%; *miR-183/96* ko: 36.53 ± 2.68%, p = 0.91; LSO: miR-96 *Dmdo*: 38.96 ± 4.22%; *miR-183/96* ko: 53.15 ± 5.11%, p = 0.082; MNTB: miR-96 *Dmdo*: 33.86 ± 3.89%; *miR-183/96* ko: 33.80 ± 0.80%, p = 0.88). Effects for the VCN and MNTB have been the same. The finding of nonsignificant differences also applies to the volume differences of non-auditory nuclei (**Figure 10**B) (5N: miR-96 *Dmdo*: 6.55 ± 1.59%; *miR-183/96* ko: 13.89 ± 2.78%, p = 0.13; 7N: miR-96 *Dmdo*: 7.14 ± 0.54%; *miR-183/96* ko: 7.58 ± 1.16%, p = 0.39; RtTg: miR-96 *Dmdo*: 2.71 ± 3.74%; *miR-183/96* ko: 1.26 ± 3.84%, p = 0.84). The relative volume reduction of the DCN, VCN, LSO and MNTB has also been investigated for the *Cldn14* ko compared to its wt littermates, revealing no significant differences (Schlüter et al., 2018). **Figure 10**A shows the comparison of the relative volume reduction of the *Cldn14* ko, the miR-96 *Dmdo* and *miR-183/96* ko which was highly significant in all cases except for the DCN.

The cell number in the LSO and MNTB has been more affected by the *miR-183/96* ko showing significant differences in decreased percentage of cells compared to the miR-96 *Dmdo* mouse line in the LSO (miR-96 *Dmdo*: 7.51 ± 5.10%; *miR-183/96* ko: 43.03 ± 7.08%, p = 0.029) and the MNTB (miR-96 *Dmdo*: 4.71 ± 2.36%; *miR-183/96* ko: 18.01 ± 1.66%, p = 0.017) (**Figure 10**C). Differences between the soma sizes of miR-96 *Dmdo* and *miR-183/96* ko mice have been minor and not significant (**Figure 10**D) (LSO: miR-96 *Dmdo*: 15.42 ± 1.02%; *miR-183/96* ko: 15.70 ± 4.22%, p = 0.96; MNTB: miR-96 *Dmdo*: 21.59 ± 1.05%; *miR-183/96* ko: 20.70 ± 1.77%, p = 0.74). All values for relative comparison are also listed in **Table 33**.

Table 33: Relative auditory brainstem morphometric data comparing miR-96 Dmdo and miR-183/96 ko mice.

Nucleus	miR-96 *Dmdo*		*miR-183/96* ko		
-auditory-	reduction [%]	SEM	reduction [%]	SEM	p-value
DCN	14.89	1.59	9.24	3.67	0.31
VCN	36.94	0.76	36.53	2.68	0.91
LSO	38.96	4.22	53.15	5.11	0.082
MNTB	33.86	3.89	33.80	0.80	0.88
-non-auditory-					
RtTg	2.71	3.74	1.26	3.84	0.84
5N	6.55	1.59	13.89	2.78	0.13
7N	7.14	0.54	7.58	1.16	0.39
Nucleus	miR-96 *Dmdo*		*miR-183/96* ko		
	reduction of cell number [%]	SEM	reduction of cell number [%]	SEM	p-value
LSO	7.51	5.10	43.03	7.08	0.029
MNTB	4.71	2.36	18.01	1.66	0.017
	reduction of soma size [%]	SEM	reduction of soma size [%]	SEM	p-value
LSO	15.42	1.02	15.70	4.22	0.96
MNTB	21.59	1.05	20.70	1.77	0.74

3.2. Unchanged expression of potassium channel subunits in *miR-183/96* ko mice

The *miR-96 Dmdo* mutation leads to decreased expression of the potassium channel subunits Kv1.6 and BKβ2 in the LSO and MNTB (Schlüter et al., 2018). The fact that the genes coding for these proteins, *KCNA6* and *KCNMB2*, have been predicted targets for the mutated miR-96 and the reduced expression of their gene products in the *miR-96 Dmdo* mouse suggests the changed potassium channel subunit expression to be a gain of function of the mutated miR-96. The *miR-183/96* ko mouse model was used to check the expression of K_V1.6 and BKβ2 again to control for any loss of function effects. First, the mRNA expression of the *KCNA6* and *KCNMB2* genes was checked by quantitative PCR. mRNA levels of *KCNA6* (mean rel. expression wt: 0.0226 ± 0.0020; mean rel. expression ko: 0.0198 ± 0.0017; p = 0.14) and *KCNMB2* (mean rel. expression wt: 0.0016 ± 0.00019; mean rel. expression ko: 0.0018 ± 0.00039; p = 0.50) did not significantly differ between wt and *miR-183/96* ko SOC tissues (**Figure 11**A). Because miRNA function takes place on the posttranscriptional level not only degrading mRNAs but also inhibiting binding of ribosomes on the mRNA, the expression of the final endproducts of the *KCNA6* and *KCNMB2* genes, the immunoreactive signals of the proteins K_V1.6 and BKβ2 were analyzed in cooperation with Ali Jason Saleh MS, Devision for Neurogenetics. After immunohistochemistry against K_V1.6 and BKβ2, we found no significant differences in grey values, neither for Kv1.6 (LSO: wt: 1.91 ± 0.13; ko: 1.96 ± 0.12; p = 0.42; MNTB: wt: 1.86 ± 0.19; ko: 1.93 ± 0.17; p = 0.48) nor for BKβ2 between *miR-183/96* ko mice and wt littermates (LSO: wt: 2.13 ± 0.14; ko: 2.09 ± 0.13; p = 0.68; MNTB: wt: 2.08 ± 0.15; ko: 2.08 ± 0.14; p = 0.92), (**Figure 11**B). The absence of significant differences in expression either of the genes *KCNA6* and *KCNMB2* or the proteins corroborates the previous assumption of a gain of function phenotype in the *miR-96 Dmdo* mouse.
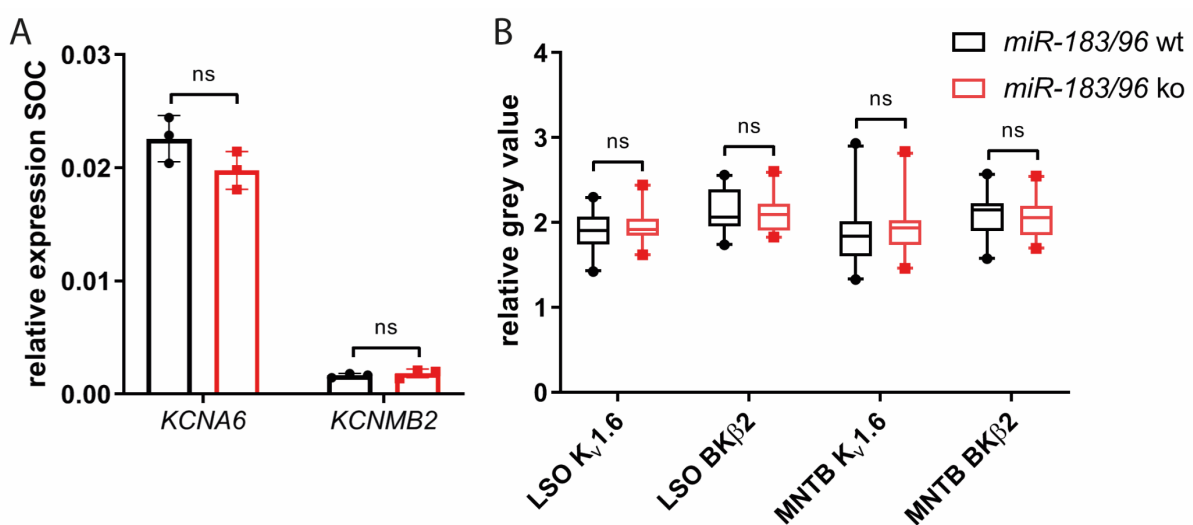
Figure 11: Unchanged expression of the genes KCNA6 and KCNMB2 and their protein products KV1.6 and BKβ2 in miR-183/96 ko mice.

A: qPCR of *KCNA6* and *KCNMB2* at SOC RNA of *miR-183/96* wt and ko mice. No changes were observed in the mRNA levels of the potassium channel subunits *KCNA6* and *KCNMB2* in the SOC of P30 *miR-183/96* ko mice compared to their wt littermates. Barplots represent the relative expression of respective genes compared to the expression of *RPL3*. Single data points represent each n, the error bars show the standard deviation among samples. N = 3 per genotype. **B:** Analysis of relative grey values of $K_V1.6$ and BKβ2 immunoreactivity in the LSO and MNTB. No changes were observed in the immunoreactivity of the potassium channel subunits $K_V1.6$ and BKβ2 in the LSO and MNTB of P30 *miR-183/96* ko mice compared to their wt littermates. 20 sections of each nucleus (left and right together) of n = 3 animals per genotype have been analyzed. Boxes show the median and the upper and lower quartile of each dataset. Whiskers show the 5-95 percentile of each dataset. Data points beyond that are shown separately. Statistical significance of differences between groups was tested using Student´s *t*-test. ns = not significant. B: data obtained by Ali Jason Saleh, MS.

3.3. SV2 expression at the *miR-183/96* ko presynapse

Dmdo mutant mice show deficits in structural maturation of the calyx of Held synapse, i.e. the formation of distinct SV2 puncta (Schlüter et al., 2018). The latter probably reflects the fenestration of the synapse from a cup-like structure into stalks.
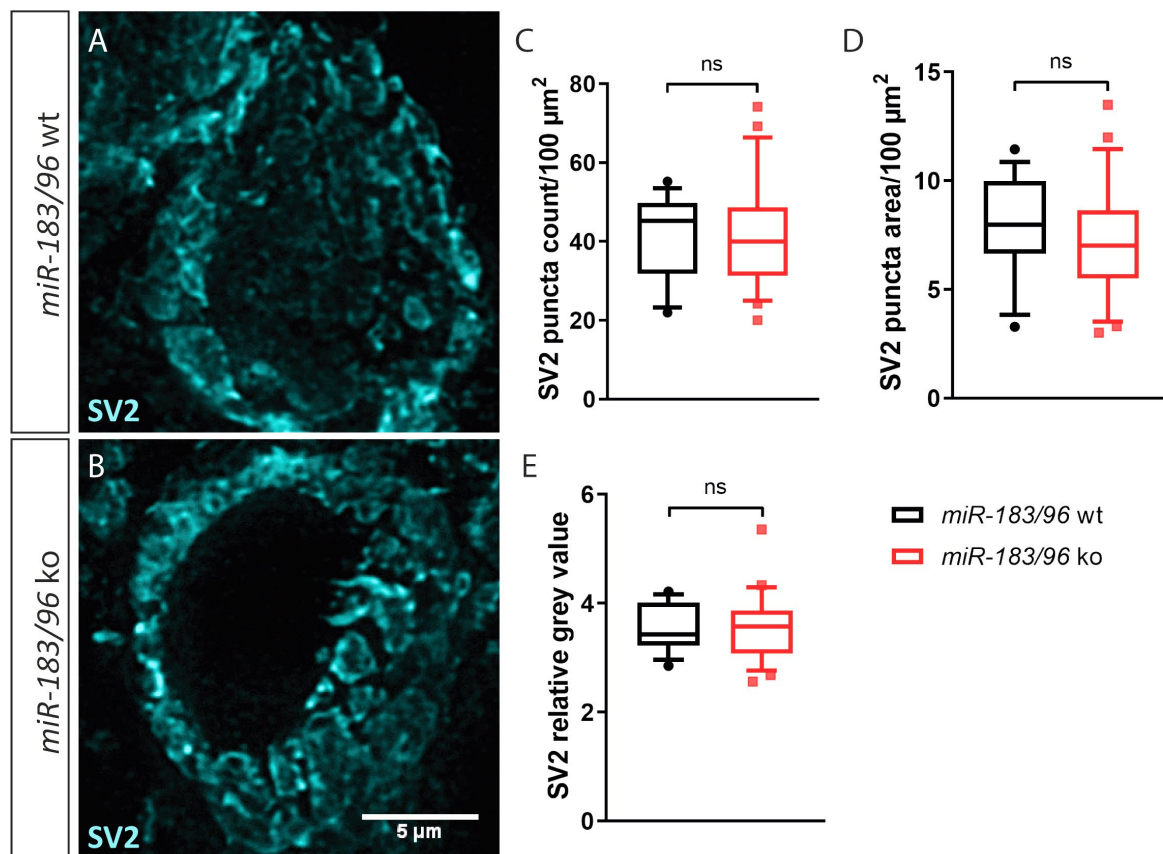
Figure 12: No changes in SV2 expression in miR-183/96 ko mice.
A, B: Immunohistochemistry of SV2 showing the presynaptic terminals on single MNTB neurons. **C:** The number of SV2 puncta in the calyx of Held presynapse of the MNTB was not changed in *miR-183/96* ko mice compared to their wt littermates, nor was the SV2 cluster area (**D**) or immunoreactivity of SV2 (**E**). Boxes show the median and the upper and lower quartile of each dataset. Whiskers show the 5-95 percentile of each dataset. Data points beyond that are shown separately. P-values were calculated using Student´s *t*-test. ns = not significant. N = 45 cells from 3 animals per genotype at the age of P30.

In *miR-183/96* ko, the SV2 immunoreactive signal appeared normal with ring-like clusters as in wt animals (**Figure 12**A and B). Quantitative analysis of the distribution of SV2 immunoreactive puncta in P30 *miR-183/96* ko calyces showed no differences compared to wt

littermates (**Figure 12**C) (wt: 41.55 ± 2.6 clusters/100 µm^2; ko: 41.76 ± 2.96 clusters/100 µm^2; p = 0.96). Also, the area of SV2 puncta was measured (**Figure 12**D) (wt: 7.98 ± 0.58 µm^2; ko: 7.16 ± 0.56 µm^2; p = 0.32), and the relative immunoreactivity of SV2 was quantified (**Figure 12**E) (wt: 3.56 ± 0.11; ko: 3.54 ± 0.13; p = 0.92). In all cases, no significant differences between genotypes have been found. This suggests an unperturbed maturation of the calyx of Held in *miR-183/96* ko mice, which is in striking contrast to the immature phenotype seen in *Dmdo* mice (Schlüter et al., 2018). Observed changes in the *Dmdo* mouse therefore likely reflect again a gain of function of the point mutation.

3.4. Increased synaptic transmission at the calyx of Held in *miR-183/96* ko mice

In cooperation with Dr. Christoph Körber (Institute of Anatomy und Cell Biology, Department of Functional Neuroanatomy, Heidelberg University) the functional impact of *miR-183/96* ko on synaptic transmission at the well-studied calyx of Held synapse in the MNTB was analyzed electrophysiologically. To this end, spontaneous EPSCs (sEPSCs) were recorded from MNTB principal neurons in acute brainstem slices prepared from *miR-183/96* ko mice and wt littermates at P25-27.
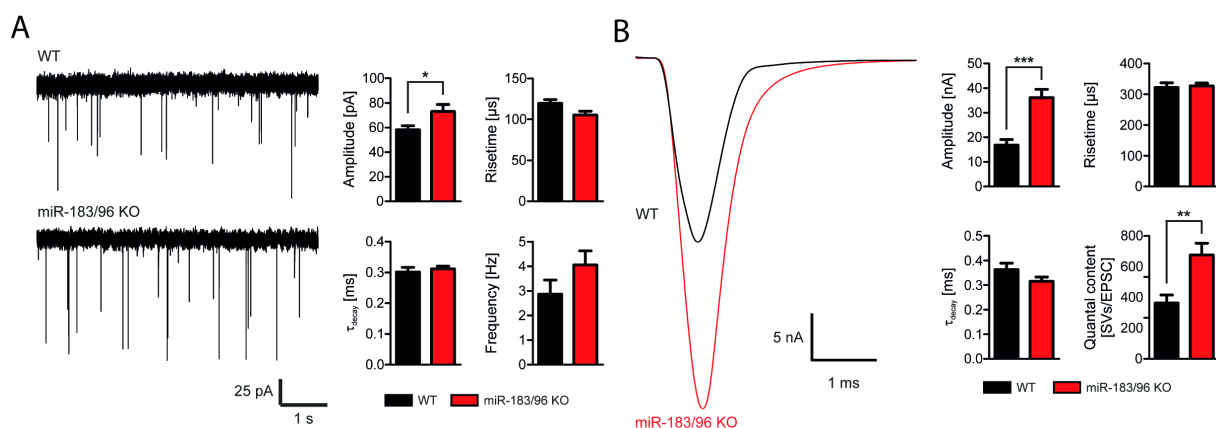
Figure 13: Increased spontaneous and evoked synaptic transmission at the calyx of Held in miR-183/96 ko.
A: Representative sample current traces of sEPSCs and quantification of spontaneous release parameters like sEPSC amplitude, frequency, risetime and decay time from calyces of *miR-183/96* ko and wt mice. The amplitude of sEPSCs is significantly increased in the ko animals. **B:** Representative sample current traces of evoked EPSCs and quantification of evoked release parameters like eEPSC amplitude, risetime, decay time and quantal content from calyces of *miR-183/96* ko and wt mice. The amplitude of the eEPSC and the quantal content in terms of released synaptic vesicles per eEPSC are significantly increased in the ko animals. Statistical significance was determined by unpaired two-tailed Students *t*-test using Prism 5.0 software (Graphpad software, La Jolla, CA). Data is presented as mean ± SEM. p < 0.05 = *; p < 0.01 = **; p < 0.001 = ***. sEPSCs wt: n = 9 cells, ko: n = 6 cells, eEPSCs wt: n = 10 cells, ko: n = 12 cells. Figure in collaboration with Dr. Christoph Körber.

miR-183/96 ko resulted in an increase in sEPSC amplitude of 29.9% (wt: 56.2 ± 3.2 pA; ko: 73.0 ± 5.7 pA; p = 0.0299), while leaving sEPSC frequency and kinetics like rise time and decay time unaffected (**Figure 13**A, appendix **Table 42**). Next, single calyx of Held evoked EPSCs (eEPSCs) induced at low frequency (0.1 Hz) were recorded. In line with the results obtained for sEPSCs,

eEPSCs recorded from *miR-183/96* ko calyces were found to be drastically increased of 114% resulting in enormous eEPSCs amplitudes (wt: 16.81 ± 2.32 pA; ko: 36.1 ± 3.41 pA; p = 0.0002) with no changes in eEPSC kinetics like risetime or decay time (**Figure 13**A, appendix **Table 42**). However, when the quantal content in terms of released SVs of single low frequency eEPSCs was calculated, *miR-183/96* ko calyces were found to release 86.4% more SVs per eEPSC as compared to their wt controls (wt: 272 ± 39 SVs/eEPSC; ko: 507 ± 57 SVs/eEPSC; p = 0.0041) (**Figure 13**B, appendix **Table 42**). The increase in quantal content argues against a purely postsynaptic effect as the quantal content is dependent on presynaptically abundant readily releasable SVs.
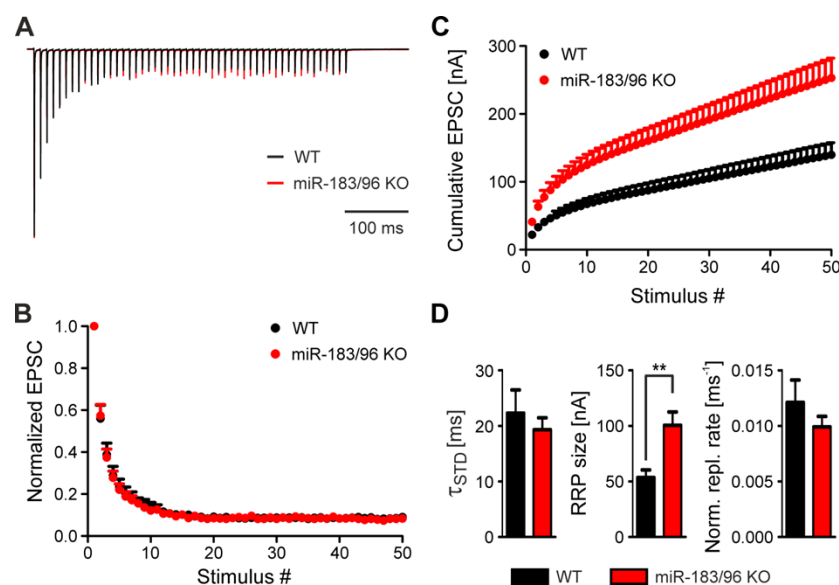
Figure 14: Knock-out of miR-183/96 has no effect on short-term plasticity but increases the RRP.
A: Superimposed scaled representative eEPSC current traces recorded during 100 Hz stimulus trains (50 stimuli). **B:** Averaged normalized eEPSC amplitudes during 100 Hz trains. **C:** Averaged cumulative eEPSCs amplitudes during 100 Hz trains. **D:** Quantification of the time constant of eEPSC amplitude decay during 100 Hz trains (left), the RRP size (middle) and the replenishment rate normalized to the eEPSC amplitude (right). Statistical significance was determined by unpaired two-tailed Students *t*-test using Prism 5.0 software (Graphpad software, La Jolla, CA). Data is presented as mean ± SEM. p < 0.01 = **. wt: n = 10 cells, ko: n = 11 cells. Figure in collaboration with Dr. Christoph Körber.

A hallmark of the calyx of Held is the prominent short-term depression (STD) attributed to the depletion of the readily releasable SVs during periods of repeated synaptic activity (Borst et al., 1995; Taschenberger and Gersdorff, 2000; Körber et al., 2015). Therefore, STD during trains of action potentials delivered at a frequency of 100 Hz was investigated. Surprisingly, no differences in the STD parameters measured between the genotypes were detected. Those were the time constant of eEPSC amplitude decay, the extent of depression and the paired-pulse ratio (PPR). The PPR is the ratio between the amplitudes of the first and second eEPSC which can be used as a measure of the release probability of SVs. The only difference observed was an 82.9% increase in the steady state eEPSC amplitude during the late phase of the 100 Hz stimulation train in the *miR-183/96* ko (wt: 1.70 ± 0.25 pA; ko: 3.11 ± 0.43 pA; p = 0.0037)

(**Figure 14**A, B, D, appendix **Table 42**). Next, the size and dynamics of the readily releasable pool (RRP) of SVs was investigated, employing the cumulative eEPSC method (Schneggenburger et al., 1999) (**Figure 14**C). Line fits to the linear part of the cumulative EPSC plot and back extrapolation to the intercept with the Y-axis revealed significant increases for the *miR-183/96* ko in both RRP size (wt: 53.49 ± 6.89 nA; ko: 100.6 ± 11.86 nA; p = 0.0034) (**Figure 14**D) and SV replenishment rate (wt: 0.177 ± 0.026 nA/ms; ko: 0.329 ± 0.035 nA/ms; p = 0.0029). The RRP size was then normalized to the sEPSC amplitude to calculate the number of SVs in the RRP and again a roughly 50% increase in the number of RRP SVs in *miR-183/96* ko calyces was found (wt: 899 ± 79 SVs; ko: 1386 ± 156 SVs; p = 0.0142). However, when the replenishment rate was normalized to the first eEPSC in the train, to take the intrinsically high variance of eEPSC amplitudes into account, no difference in the normalized replenishment rate was observed anymore (**Figure 14**D, appendix **Table 42**). Thus, the effect of *miR-183/96* ko on the replenishment rate seems to be an adjustment to the increased eEPSC and RRP size. Moreover, the increase in eEPSC amplitude observed in *miR-183/96* ko calyces can be explained, at least partially, by an increase in RRP size, while the vesicular probability of release (Pr) remains unaffected (appendix **Table 42**).

The refilling of the RRP during periods of rest was then determined, following RRP depletion. RRP refilling in *miR-183/96* ko synapses did not differ when compared to wt controls (**Figure 14**D, **Table 42**). Summarized, *miR-183/96* deficiency at the calyx of Held synapse resulted in an enormous increase in AP-evoked EPSC amplitude that is probably the result of a combination of two effects: an increase in sEPSC/quantal amplitude and an increase in the size of the RRP, while the Pr remains constant. In other words: *miR-183/96* ko calyces release more SVs per EPSC and each of them causes a larger current influx in the postsynaptic MNTB principal neuron, taking also a postsynaptic effect into account.

However, since the EPSCs recorded from *miR-183/96* ko synapses were very large, it could not be excluded that AMPAR saturation influences the interpretation of our data. Therefore, the experiments on AP-evoked EPSCs were repeated in the presence of 1 mM kynurenic acid (Kyn), which is a partial AMPAR antagonist with fast off-kinetics that prevents AMPAR saturation (Traynelis et al. 2010). When EPSCs at 0.1 Hz frequency were evoked, again, a prominent 73.4% increase in eEPSC amplitude was seen in *miR-183/96* ko synapses (wt: 1.92 ± 0.21 nA; ko: 3.33 ± 0.38 nA; *p* = 0.0037), although this time accompanied by a slowing of the eEPSC decay time constant (wt: 0.308 ± 0.008 ms; ko: 0.341 ± 0.012 ms; *p* = 0.0377) (**Figure 15**A, B). This increase in eEPSC amplitude was again reflected in an increase in quantal content (SVs/EPSC), as seen in the initial experiments performed in the absence of Kyn (wt: 289 ± 32 SVs/EPSC; ko: 494 ± 56 SVs/EPSC; *p* = 0.0046) (appendix **Table 43**). Also in line with the initial findings, STD was unaffected by *miR-183/96* ko (**Figure 15**D, appendix **Table 43**). Of note, the increase in steady state EPSC amplitude during 100 Hz stimulation seen in the absence of Kyn, did not reach significance anymore when Kyn was present (p = 0.07). This was probably due to the reduced absolute difference of values (appendix **Table 43**). Re-examination of RRP size and SV replenishment in presence of Kyn confirmed the results obtained previously, as an increase in RRP size was again detected (wt: 8.47 ± 0.89 nA; ko: 13.39 ± 1.17 nA; p = 0.0029) but not in replenishment rate in calyces from *miR-183/96* ko mice (**Figure 15**F, H, appendix

Table 43). Finally, the lack of an effect of *miR-183/96* ko on RRP refilling during periods of rest could be confirmed in the presence of Kyn. Taken together, these control experiments in abundance of Kyn confirm the interpretation that *miR-183/96* ko results in increases in EPSC quantal content and RRP size.
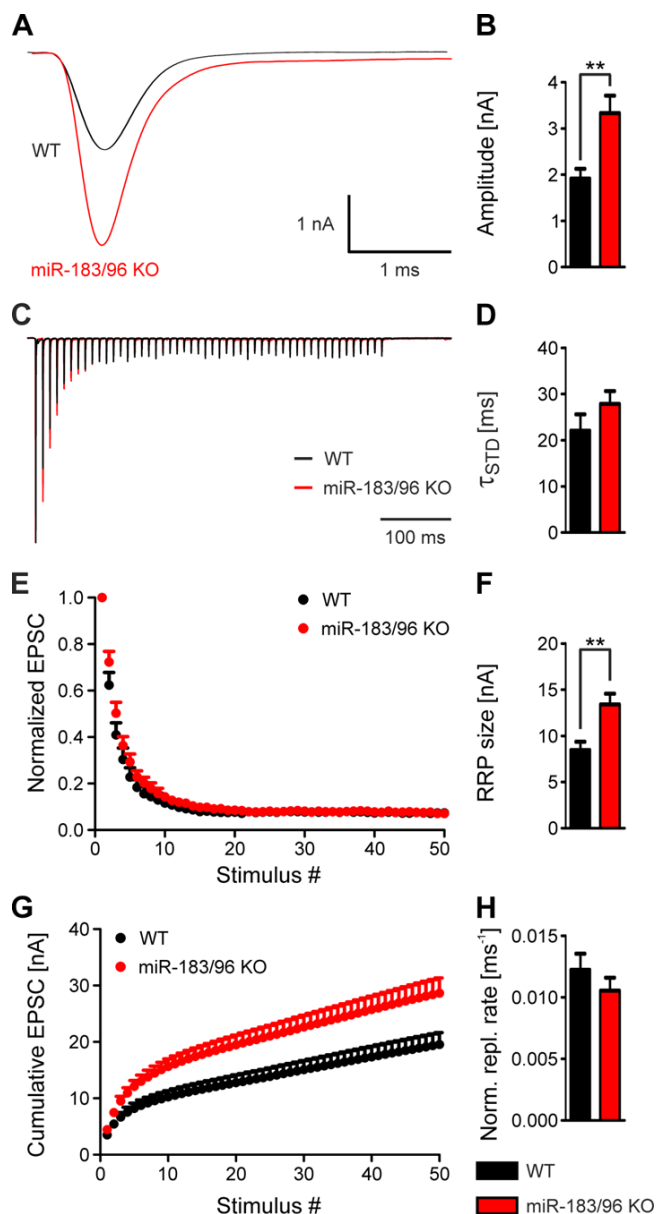
Figure 15: Increased eEPSC amplitude and RRP size in miR183/96 ko calyces are not due to AMPAR saturation since they persist in the presence of kynurenic acid.
A: Representative sample current traces of eEPSCs. **B:** Quantification of eEPSC amplitudes. **C:** Superimposed scaled representative current traces recorded during 100 Hz stimulus trains (50 stimuli). **D:** Quantification of the time constant of eEPSC amplitude decay during 100 Hz trains. **E:** Averaged normalized eEPSC amplitudes during 100 Hz trains. **F:** Quantification of the RRP size **G:** Averaged cumulative eEPSCs amplitudes during 100 Hz trains. **H:** Quantification of the replenishment rate normalized to the eEPSC amplitude. Statistical significance was determined by unpaired two-tailed Students *t*-test using Prism 5.0 software (Graphpad software, La Jolla, CA). Data is presented as mean ± SEM. $p < 0.01 =$ **. wt: n = 15 cells, ko: n = 17 cells. Figure in collaboration with Dr. Christoph Körber.

3.5. Increased active zone size of the presynaptic proteins Bassoon and Piccolo in *miR-183/96* ko mice

Having established an increase in the RRP in calyces of miR-183/96 ko mice, we investigated whether this was accompanied by an increase in the number and size of active zones (AZs). Therefore, we performed immunolabeling and particle analysis of the AZ marker proteins Bassoon and Piccolo (**Figure 16**A-D).
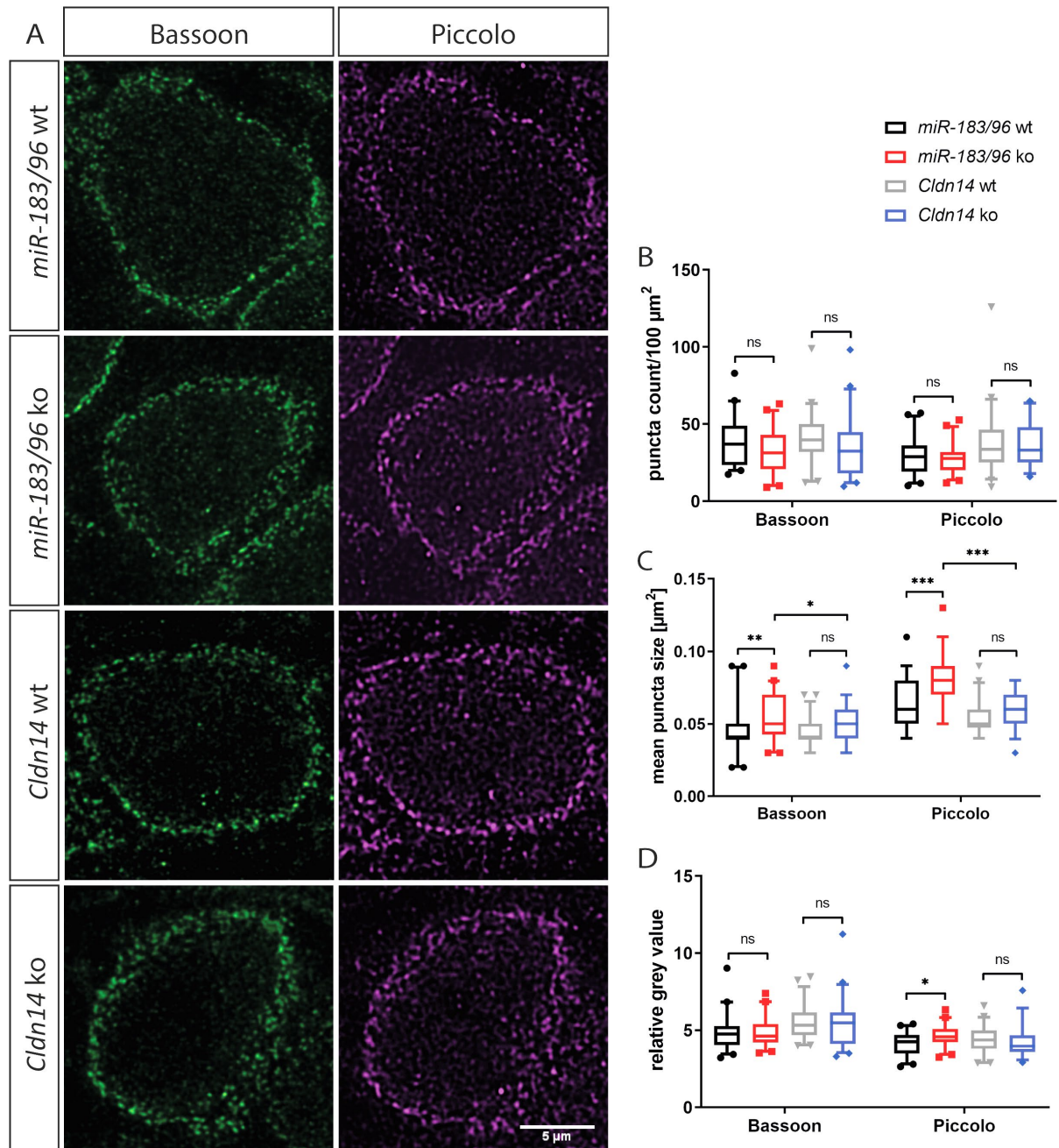
Figure 16: Increased puncta size of the presynaptic proteins Bassoon and Piccolo in miR-183/96 ko mice.
A: Immunohistochemistry of Bassoon and Piccolo for *miR-183/96* wt and ko and *Cldn14* wt and ko showing the presynaptic active zones of the calyx of Held on single MNTB neurons. **B:** The number of Bassoon and Piccolo puncta was not significantly affected in the calyx of Held presynapse of the MNTB of *miR-183/96* ko mice and in *Cldn14* mice compared to their wt littermates. **C:** The mean size of Bassoon and Piccolo puncta was significantly increased in *miR-183/96* ko mice compared to their wt littermates. For Piccolo, there was also a slight increase in puncta size for the peripherally deaf *Cldn14* ko mouse. **D:**

The immunoreactivity of Piccolo was significantly increased in *miR-183/96* ko mice compared to their wt littermates. Boxes show the median and the upper and lower quartile of data. Whiskers show the 5-95 percentile of data. Data points beyond that are shown separately. P-values were calculated using ANOVA followed by Sidak´s post-hoc test. ns = not significant; p < 0.05 = *; p < 0.01 = **; p < 0.001 = ***. N = 45 cells from 3 animals per genotype at the age of P30.

No changes in the number of Bassoon and Piccolo puncta were found between *miR-183/96* wt and ko calyces (**Figure 16**B) (Bassoon: wt: 38.19 ± 2.29 particles/100 µm^2; ko: 32.44 ± 2.10 particles/100 µm^2; p = 0.067; Piccolo: wt: 28.81 ± 1.83 particles/100 µm^2; ko: 27.45 ± 1.67 particles/100 µm^2; p = 0.56). However, the mean size of puncta was significantly increased in *miR-183/96* ko mice by 7.1% for Bassoon and 29% for Piccolo when compared to wt (Bassoon: wt: 0.046 ± 0.0024 µm^2; ko: 0.056 ± 0.0022 µm^2; p = 0.0031; Piccolo: wt: 0.062 ± 0.0025 µm^2; ko: 0.080 ± 0.0028 µm^2; p = 0.000011) (**Figure 16**C). Along the same lines, the quantification of the relative intensity of the immunoreactivity revealed an increase of 12.1% for Piccolo in *miR-183/96* ko mice, but not for Bassoon (Piccolo: wt: 4.13 ± 0.11; ko: 4.63 ± 0.12; p = 0.02; Bassoon: wt: 4.85 ± 0.17; ko: 4.89 ± 0.15; p = 0.85) (**Figure 16**D).

To control for effects caused by deafness, the peripherally deaf *Cldn14* ko mouse was included as further control (**Figure 16**A-D). Comparing the *Cldn14* ko with its wt, numbers of Bassoon and Piccolo puncta were not significantly changed (Bassoon: wt: 40.28 ± 2.30 particles/100 µm^2; ko: 34.37 ± 2.75 particles/100 µm^2; p = 0.11; Piccolo: wt: 37.18 ± 2.95 particles/100 µm^2; ko: 36.06 ± 2.03 particles/100 µm^2; p = 0.77). Regarding mean puncta size, there has been a slight but significant 12.9% increase in the *Cldn14* ko for Piccolo but not for Bassoon (Bassoon: wt: 0.044 ± 0.0014 µm^2; ko: 0.048 ± 0.0019 µm^2; p = 0.057; Piccolo: wt: 0.054 ± 0.0016 µm^2; ko: 0.061 ± 0.0020 µm^2; p = 0.013). Relative immunoreactivity measurements didn´t reveal any significant changes in the *Cldn14* ko mouse (Bassoon: wt: 5.50 ± 0.15; ko: 5.40 ± 0.21; p = 0.73; Piccolo: wt: 4.39 ± 0.13; ko: 4.27 ± 0.16; p = 0.57). Comparison of *miR-183/96* ko synapses to *Cldn14* ko ones revealed also significant changes in mean puncta sizes of Bassoon (*miR-183/96* ko: 0.056 ± 0.0022 µm^2; *Cldn14* ko: 0.048 ± 0.0019 µm^2; p = 0.0238) and Piccolo (*miR-183/96* ko: 0.080 ± 0.0028 µm^2; *Cldn14* ko: 0.061 ± 0.0020 µm^2; p < 0.0001). These findings suggest that *miR-183/96* ko results in an increase in AZ size rather than in the formation of additional AZs and could explain at least a part of the increase in eEPSC amplitudes and RRP size described above. Although this may in part be induced by the deafness of the animal, as inferred from *Cldn14* ko results, *miR-183/96* ko increases the effect drastically.

3.6. *miR-183/96* ko leads to an increased number and size of synaptic GluA1 clusters

The increase in AZ size described here does not explain the increase in sEPSC amplitude, because the AZ are localized presynaptically, whereas the sEPSC amplitudes are a postsynaptic component. However, the AMPA receptor (AMPAR) subunit GluA1 is a known target of miR-96 (Jensen and Covault, 2011; Dambal et al., 2015). Therefore, the expression of GluA1-4 encoding genes *GRIA1-4* respectively was analyzed by qPCR. mRNA expression levels of *GRIA1* (mean rel. expression wt: 0.0278 ± 0.0025; mean rel. expression ko: 0.024 ± 0.0049; p = 0.39),

GRIA2 (mean rel. expression wt: 0.0246 ± 0.0041; mean rel. expression ko: 0.0263 ± 0.0047; p = 0.73), *GRIA3* (mean rel. expression wt: 0.0102 ± 0.0014; mean rel. expression ko: 0.0098 ± 0.0008; *p* = 0.72) and *GRIA4* (mean rel. expression wt: 0.0227 ± 0.0011; mean rel. expression ko: 0.023 ± 0.00044; p = 0.65) did not significantly differ (appendix **Figure 30**).

Because microRNA function can affect the posttranscriptional level by inhibiting protein biosynthesis, it was thus investigated whether the *mir-183/96* ko had an effect on the GluA1 protein level and - more important - its localization to the postsynaptic density (PSD). Therefore, the abundance of GluA1 in the MNTB principal cell and its synaptic localization was analyzed by means of immunohistochemistry (**Figure 17**, **Figure 18**).
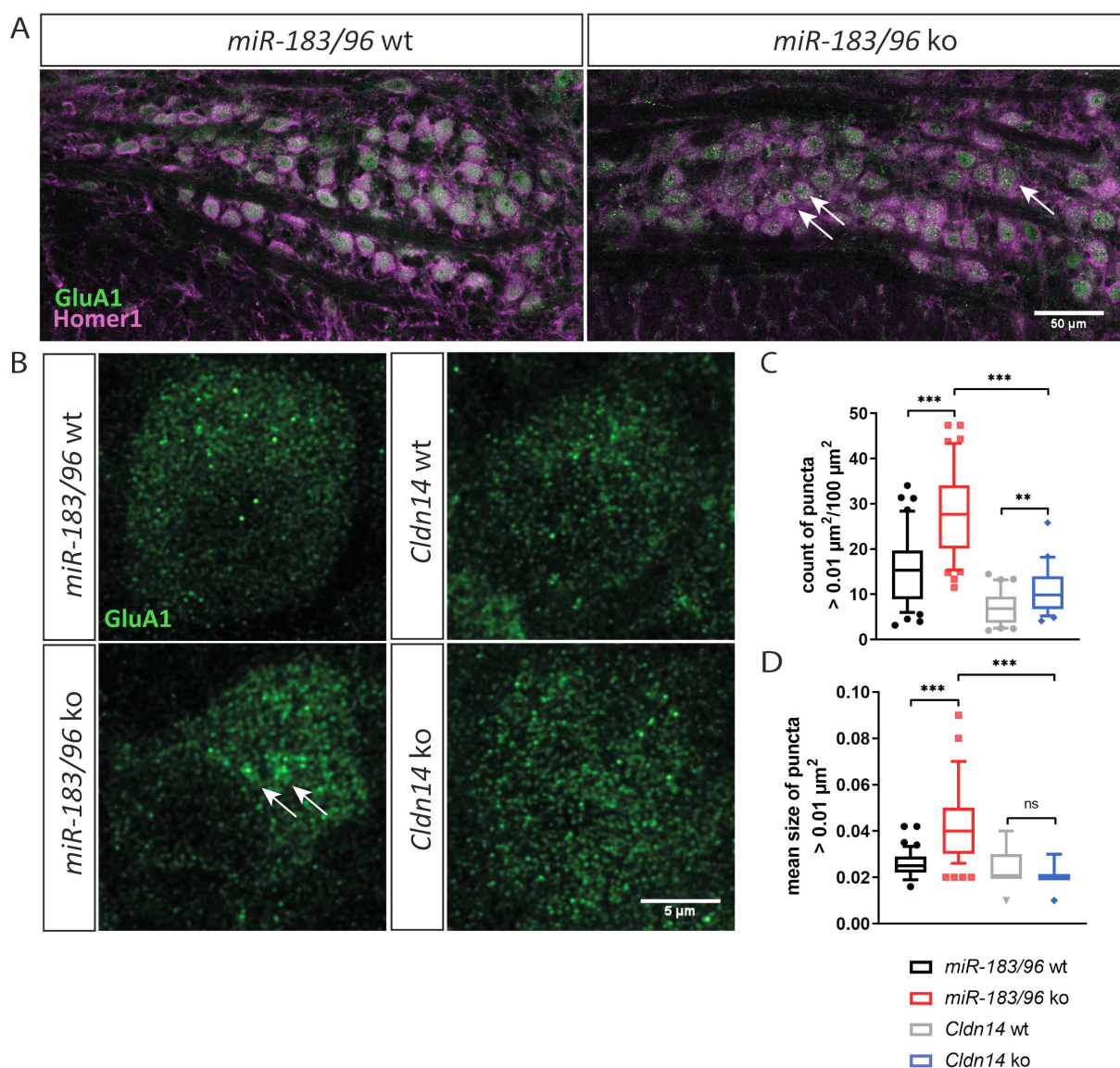
Figure 17: Increased number and size of GluA1 puncta in miR-183/96 ko mice.
A: Overview pictures of whole MNTBs after immunohistochemistry against GluA1 and Homer1. Arrows highlight the larger GluA1 puncta in the *miR-183/96* ko. **B:** Representative whole MNTB principal cell pictures after immunohistochemistry against GluA1 in *miR-183/96* wt and ko and *Cldn14* wt and ko. Arrows indicate the bigger GluA1 puncta in the *miR-183/96* ko. **C:** The number of GluA1 puncta in MNTB principal neurons that are bigger than 0.01 μm^2 was strongly and highly significantly

elevated in *miR-183/96* ko mice compared to their wt littermates. The number of these GluA1 puncta was also significantly elevated in *Cldn14* ko mice but the effect in *miR-183/96* ko mice was bigger. **D:** The mean GluA1 puncta size of GluA1 accumulations bigger than 0.01 μm^2 was strongly increased in *miR-183/96* ko mice compared to their wt littermates. There was no difference in GluA1 puncta size between *Cldn14* ko and *Cldn14* wt mice. Boxes show the median and the upper and lower quartile of each dataset. Whiskers show the 5-95 percentile of each dataset. Data points beyond that are shown separately. P-values were calculated using ANOVA followed by Sidak´s post-hoc test. ns = not significant; $p < 0.05$ = *; $p < 0.01$ = **; $p < 0.001$ = ***. N = 45 cells from 3 animals per genotype at the age of P30.

GluA1 particles were found to form larger clusters in the cell interior in *miR-183/96* ko mice as compared to wt littermates (**Figure 17**A, B). Quantification of number and mean size of GluA1 puncta larger than 0.01 μm^2 resulted in a strongly and highly significantly elevated number of these larger GluA1 clusters by 83.4% in *miR-183/96* ko (wt: 15.15 ± 1.19 puncta/100 μm^2; ko: 27.78 ± 1.39 puncta/100 μm^2; $p = 8.26E^{-10}$) (**Figure 17**C). Moreover, a strong increase in the average size of these puncta by 57.57% was oberved (wt: 0.026 ± 0.00084 μm^2; ko: 0.041 ± 0.0024 μm^2; $p = 2.91E^{-8}$) (**Figure 17**D).

In *Cldn14* ko mice, a significant increase in number of GluA1 puncta larger than 0.01 μm^2 of 57% was evident (wt: 6.92 ± 0.86 puncta/100 μm^2; ko: 10.89 ± 0.98 puncta/100 μm^2; $p = 0.001$) (**Figure 17**C). The mean size of GluA1 puncta was unchanged compared to the respective wt littermates (wt: 0.024 ± 0.00073 μm^2; ko: 0.021 ± 0.00074 μm^2; $p = 0.59$) (**Figure 17**D). GluA1 puncta count was ~2.5 times higher in *miR-183/96* ko synapses (27.78 ± 1.39 puncta/100 μm^2) compared to the *Cldn14* ko ones (10.89 ± 0.98 puncta/100 μm^2), which was highly significant ($p < 0.0001$). This also holds true for comparison of the mean puncta size, which was twice as large in the *miR-183/96* ko calyx (0.041 ± 0.0024 μm^2) than in the *Cldn14* ko synapse (0.021 ± 0.00074 μm^2, $p < 0.0001$) (**Figure 17**C, D).

To investigate whether the increase in number and size of GluA1 puncta led to a stronger incorporation of GluA1 subunits into the postsynaptic receptor complexes, the number of GluA1 puncta in close proximity to the AZ was examined, delineated by the presynaptic protein Piccolo. Co-labeling of GluA1 and Piccolo was performed and defined those GluA1 puncta as postsynaptically localized that overlapped at least 1% with Piccolo immunoreactivity in maximum intensity projections of small confocal image stacks (**Figure 18**).
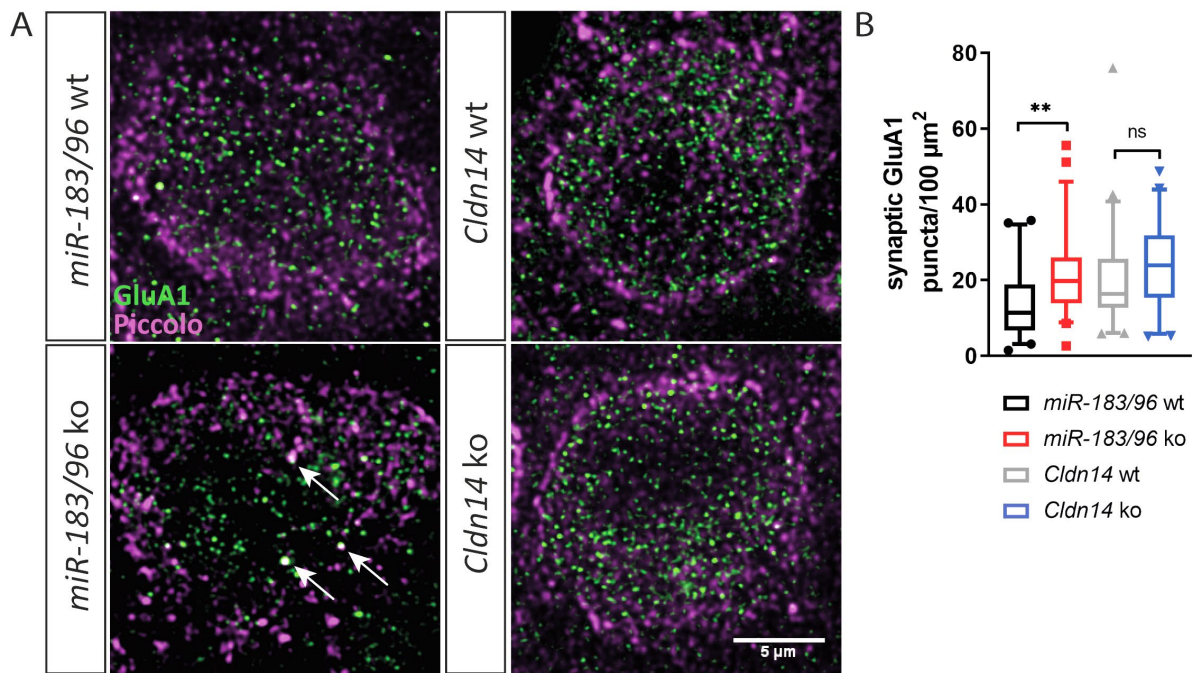
Figure 18: Increased synaptic GluA1 in miR-183/96 ko.
A: Whole MNTB principal cells after immunohistochemistry against GluA1 (green, postsynaptic) and Piccolo (magenta, presynaptic active zones) in *miR-183/96* wt and ko and *Cldn14* wt and ko mice. Arrows indicate overlapping GluA1 and Piccolo signals showing larger GluA1 puncta that are located near the active zones of the presynapse in the *miR-183/96* ko. **B:** Quantification of synaptic GluA1 showing at least 1% overlap with a Piccolo particle. Boxes show the median and the upper and lower quartile of each dataset. Whiskers show the 5-95 percentile of each dataset. Data points beyond that are shown separately. P-values were calculated using ANOVA followed by Sidak´s post-hoc test. ns = not significant, $p < 0.001$ = ***. N = 45 cells from 3 animals per genotype at the age of P30.

These GluA1 puncta are refered to as "synaptic GluA1". GluA1 was significantly elevated at the PSD of *miR-183/96* ko MNTB neurons as the number of synaptic GluA1 puncta increased by ~50% (wt: 13.82 ± 1.31 puncta/100 μm^2; ko: 21.61 ± 1.52 puncta/100 μm^2; $p = 0.0017$) (**Figure 18**B). Importantly, this increase in synaptic GluA1 was not caused by homoeostatic upregulation of GluA1 due to peripheral deafness, since no significant differences in synaptic GluA1 in *Cldn14* ko synapses was observed (wt: 20.08 ± 1.76 puncta/100 μm^2; ko: 24.21 ± 1.67 puncta/100 μm^2; $p = 0.19$). Notably, number of synaptic puncta in this mouse line with a NMRI background seems to be generally on a higher level as compared to C57BL/6N mice.

Taken together, these data reveal an increase in postsynaptic GluA1 protein that is incorporated into the AMPAR complexes in the PSD of *miR-183/96* ko MNTB neurons. This increase at least partially explains the higher amplitudes of sEPSCs and eEPSCs in *miR-183/96* ko animals and reveals a role for miR-183/96 in the regulation of synaptic strength pre- and postsynaptically.

3.7.   MiRNAs from the cochlea are also expressed in the auditory brainstem

3.7.1. Spatial expression of miRNA precursors in the auditory hindbrain

Due to its function in both, the peripheral and central auditory system, miR-96 was added to the list of deafness genes with an essential role beyond the cochlea (Michalski and Petit, 2019). miR-96 represented the first miRNA on that list, raising the question if there are more miRNAs with an important role in the central as well as the peripheral auditory system. Therefore, a first cue for a possible function of miRNAs in both systems is their expression in respective tissues. Knowing the most highly expressed miRNAs from cochlear and vestibular epithelia at P0 (Rudnicki et al., 2014a), the 12 highest expressed miRNAs of that study were chosen for visualization of their precursor expression in the auditory brainstem because of their strong abundance in the auditory periphery. These were miR-22, -26a, -27b, -127, -143, -181a, -181b, -181c, -183, -191, -204, and -let-7c. Visualization of miRNA precursor expression was done by *in-situ* hybridization, delivering non-quantitative information about miRNA expression. Regarding auditory brainstem tissue, P4 was chosen representing the pre-hearing stage (and not P0 as in the Rudnicki et al. study) and P30 was analyzed representing the adult condition. P4 was chosen instead of P0 because this increased the manageability of the experiment (perfusion of mice, performing cryosections and *in-situ* hybridization) and presentability of distinct auditory brainstem structures. All miRNA precursors analyzed in this study were broadly and homogeneously expressed in nuclei throughout the auditory brainstem at P4 (**Figure 19**A - **Figure 21**A). The subsequent paragraph will deal with the description of the results obtained from the P30 tissue because expression patterns of miRNA precursors were better differentiated at that stage.

Images of expression of mir-let-7c, mir-22,-26a and- 27b are shown in **Figure 19**A: In P30, mir-let-7c was less expressed in the GCD of the DCN and VCN than in the magnocellular domains of the CNC. A gradual increase of mir-let-7c expressing neurons in the VCN following the tonotopic axis from low to high frequency tuned neurons was observed, though not quantified. Expression in principal cells of the MNTB was found to be very prominent whereas in the LSO only a few neurons displayed prominent mir-let-7c expression. mir-22 expression at P30 was lower in the GCD of the DCN and the VCN than in the magnocellular regions of the CNC. In the DCN there were only a few neurons expressing mir-22. The MNTB showed a very prominent mir-22 signal. In the P30 LSO there was a visible expression gradient of mir-22 positive neurons following the tonotopic axis from low to high frequency (**Figure 22**). There was a notably high expression of mir-22 in the LNTB. mir-26a abundance was decreased in the GCD of the DCN and VCN, only few positive neurons were left in the DCN. An increasing number of positive neurons in the aVCN along the tonotopic axis appeared from low to high frequencies (not quantified). mir-26a expression was prominent in the adult MNTB and sparse in the adult LSO, but in the LSO with an obvious expression gradient from dorso-medial to ventral parts (**Figure 22**). mir-27b was lowly expressed in the DCN and VCN with almost no expression in the GCDs. Prominent abundance of mir-27b only remained in the MNTB and in

a few neurons of the LSO. mir-181a, -b and-c belong to the miR-181 family and were therefore grouped together in **Figure 20**A. There was almost no expression of mir-181 family members in the GCD of the DCN, with the exception of few cells in the GCN of the VCN with the highest expression at the border between the GCN and the magnocellular domain. mir-181 family abundance in the cores of the CNC nuclei was homogeneous. In the SOC, the MNTB and VNTB displayed the strongest mir-181 expression whereas in the LSO there was some punctual expression. mir-183 had the same expression pattern in the CNC as the mir-181 family. In the SOC mir-183 was strongly abundant in the MNTB, SPN and VNTB. Images of expression of mir-127, -143, -191 and -204 are shown in **Figure 21**A: mir-127 was almost absent in the GCD of the DCN and VCN. In the core DCN, there was a strong mir-127 signal that also appears in the aVCN, but here again with an increasing number of mir-127 expressing neurons along the tonotopic axis. In the SOC, mir-127 was prominently expressed in the MNTB and there also was expression in a few LSO neurons located at the medially dorsally edge of the nucleus (**Figure 22**). For mir-143 there was homogeneous expression in the CNC but not in the GCD. The most prominent mir-143 expression of the SOC was observed in the MNTB and in some neurons of the VNTB. mir-191 showed strong abundance in the CNC with some expression in the GCD. mir-191 was also strongly expressed throughout the SOC including the MNTB, the entire LSO, SPN, LNTB and VNTB. mir-204 was absent in the GCD of the DCN and only sparse in the pVCN. It was homogeneously distributed within the core of the DCN and the entire aVCN, including the GCD. In the SOC mir-204 expression was barely detectable, with some principal cells of the MNTB expressing this miR.

Summarized, all precursors of the 12 chosen miRNAs that have been found to be highly abundant in the auditory periphery (Rudnicki et al., 2014a) were observed in the central auditory pathway at P4 and P30 as well, suggesting a role for them in development and maintenance in both the peripheral and central auditory system.
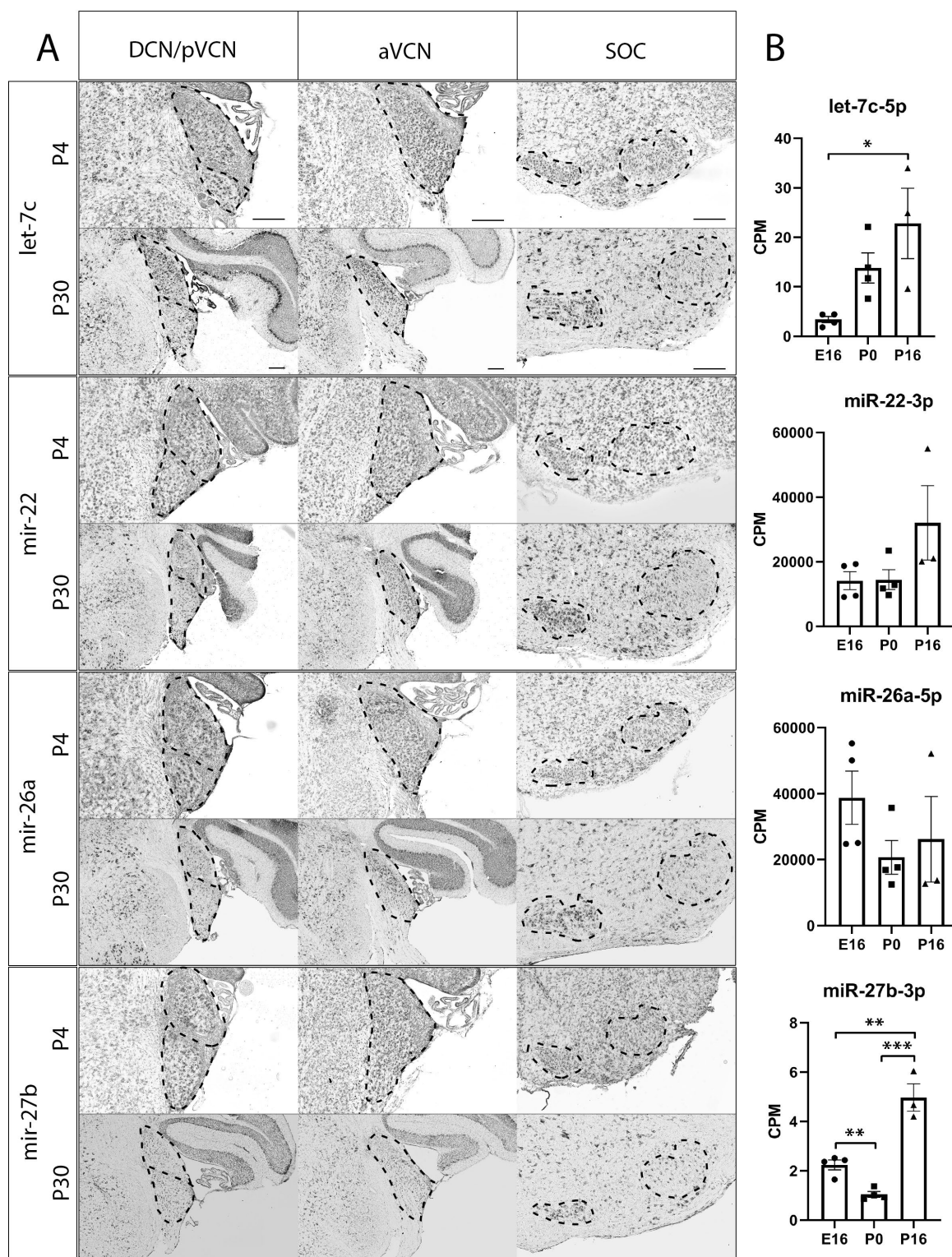
Figure 19: Expression of pre-miR- let-7c, -22, -26a, -27b and quantification of respective mature miRNA expression.
A: RNA *in-situ* hybridization of coronal sections through the mouse auditory brainstem of P4 and P30 animals. Sections were hybridized with DIG-labeled RNA antisense probes. The dashed lines indicate the positions of respective auditory nuclei. aVCN: anterior ventral cochlear nucleus; DCN: dorsal cochlear nucleus; LSO: lateral superior olive; MNTB: medial nucleus of the trapezoid body; MSO: medial superior olive; P: postnatal day; pVCN: posterior ventral cochlear nucleus; SOC: superior olivary complex; VNTB: ventral nucleus of the trapezoid body. Representative results from at least 3 independent experiments are shown. Scale bars: 200 µm. **B**: Quantification of mature miRNA expression in the SOC of E16, P0 and P16 mice from NGS data. The x-axis shows the age of specimen, E16, P0 and P16. The y-axis shows the counts per million (CPM) at different scales.

Bargraphs show the mean CPM values, single data points and SEM. CPM: counts per million; E: embryonic day; P: postnatal day. *P*-values were calculated using Student´s *t*-test; p < 0.05 = *; p < 0.01 = **; p < 0.001 = ***. N = 4 for E16 and P0, n = 3 for P16. This also applies to figures 20 and 21.
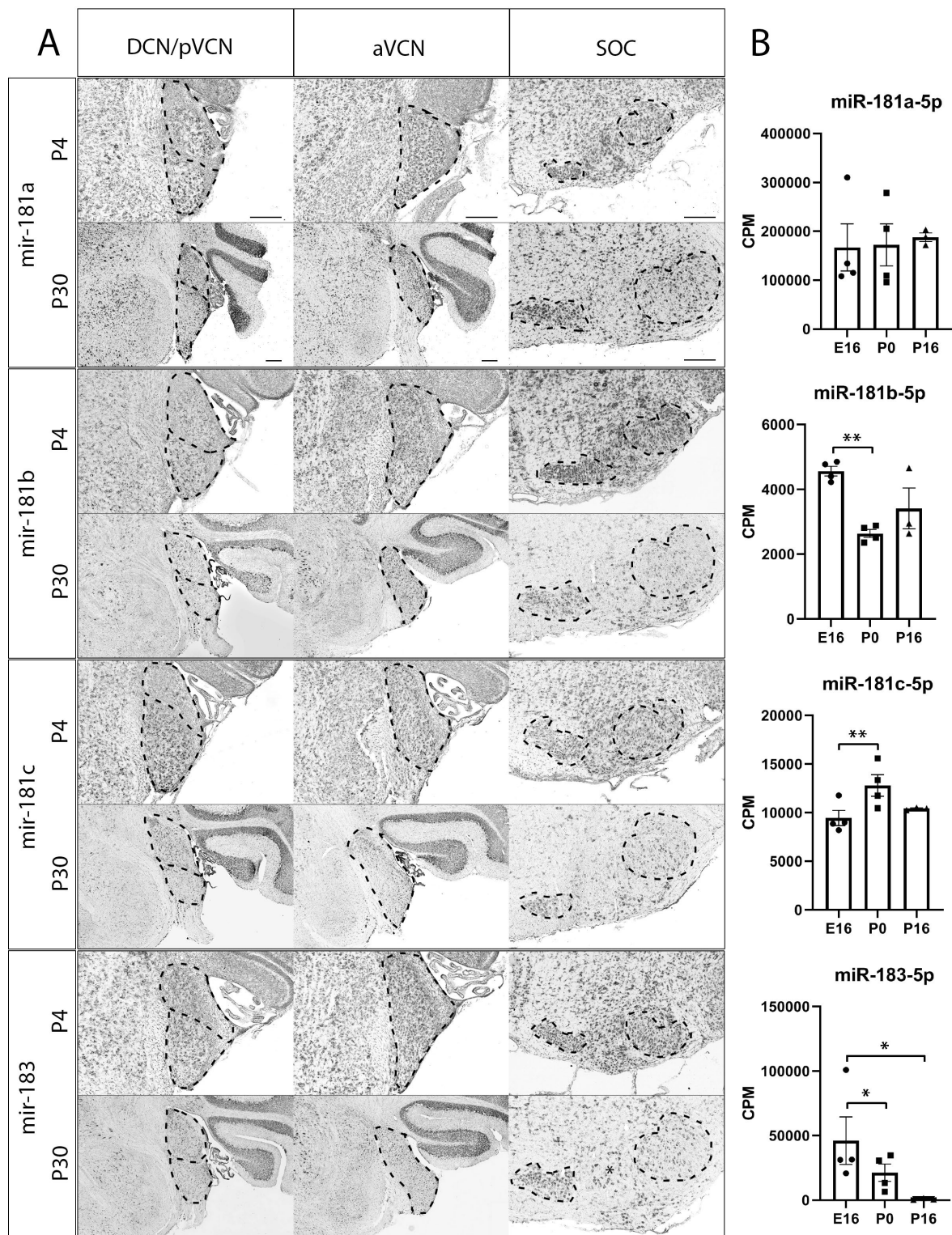
Figure 20: Expression of pre-miR-181a, -181b, -181c, -183 and quantification of respective mature miRNA expression.
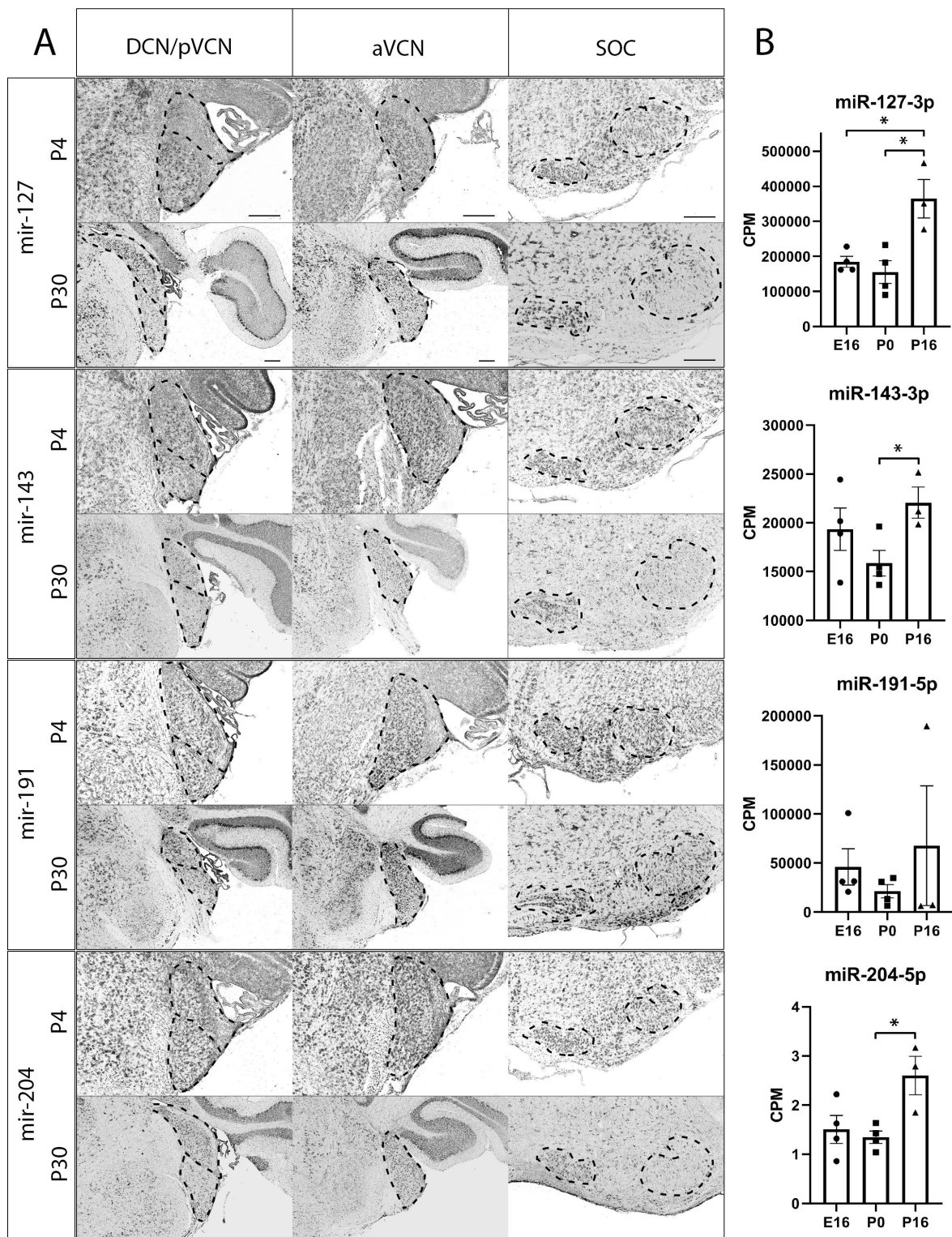
Figure 21: Expression of pre-miR-127, -143, -191, -204 and quantification of respective mature miRNA expression.
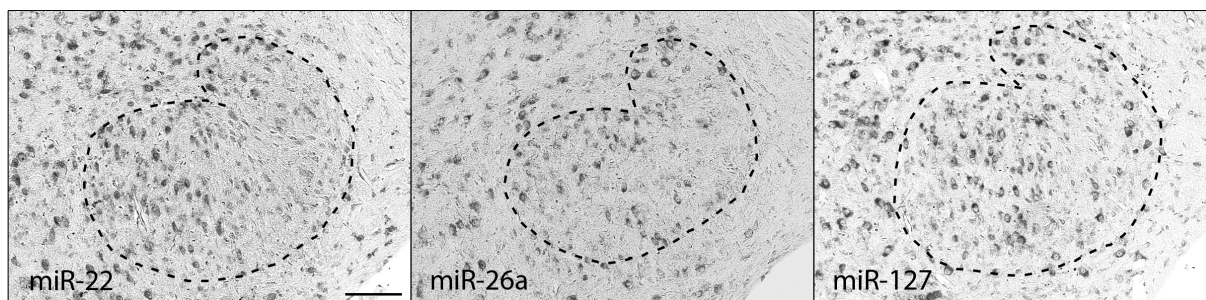
Figure 22: Gradients of pre-miRNA expression in the LSO.
In-situ hybridization images of pre-miR-22, -26a and -127 showing the LSO (dashed line) indicating an expression gradient. For miR-22 and -127 this gradient is evident along the tonotopic axis with most stained cells at the more high frequency regions. The high to low frequency tonotopy of the LSO goes always from the left to the right side of the LSO. Scale bar = 100 µm.

3.7.2. Quantification of mature miRNA expression during development

After qualitative, spatial analysis of miRNA precursor expression by *in-situ* hybridization, I aimed to quantify the expression of mature miRNAs at the timepoints E16, P0 and P16. E16 was chosen as a stage where neuronal migration is completed. P0 represents a timepoint when auditory brainstem neurons gain their functional maturity being integrated into their neuronal circuits but still prior to hearing onset (Marrs and Spirou, 2012). P16 is after hearing onset that takes place around P12. (Ehret, 1976; Sonntag et al., 2009). For P16, it is known that from that stage on, for the SOC, there are no significant changes in gene expression any more until adulthood (Ehmann et al., 2013). Therefore data from that stage is comparable to data from later stages, e.g. P30 data from the *in-situ* hybridizations. For sequencing of miRNAs, a NGS approach was used, delivering relative expression levels of all detectable mature miRNAs in a sample in counts per million (CPM) miRNA molecules. miRNA sequencing revealed identification of 674 miRNAs being abundant in at least one of the developmental stages. Global relationship of sequencing data reflected the biological relationship among samples (E16, P0, P16). Here, this NGS dataset was used to analyze the 12 previously chosen miRNAs that were highly expressed in the cochlea at P0 (Rudnicki et al., 2014a) and which expression patterns have been visualized by *in-situ* hybridization in the SOC (**Figure 19** - **Figure 21**A). The results from the quantification of mature miRNA expression obtained from the NGS data for this subset of miRNAs are shown in **Figure 19** - **Figure 21**B, always next to respective *in-situ* hybridization images of their precursor expression. **Table 34** shows summarized statistical data of miRNA expression for these 12 miRNAs obtained from the NGS dataset.

Table 34: Expression of 12 highly expressed miRNAs from the cochlea in the SOC at E16, P0 and P16.
Each row shows one highly expressed miRNA from P0 cochlear data with its expression level at E16, P0 and P16 as well as statistical *p*-values for comparison of expression levels between timepoints P0 and E16, P16 and P0; P16 and E16. CPM: counts per million; E: embryonic day; P: postnatal day; SEM: standard error of the mean.

miRNA	E16 CPM ± SEM	P0 CPM ± SEM	P16 CPM ± SEM	p-value P0 vs. E16	p-value P16 vs. P0	p-value P16 vs. E16
miR-let-7c-5p	3.38 ± 0.56	13.84 ± 2.64	22.84 ± 5.03	0.054	0.253	0.023
miR-22-3p	14,175.81 ± 2,426.17	14,480.39 ± 2,658.46	32,091.42 ± 9,389.49	0.928	0.147	0.139
miR-26a-5p	38,801.55 ± 7,000.62	20,713.91 ± 4,443.30	26,209.80 ± 10,602.71	0.119	0.677	0.424
miR-27b-3p	2.25 ± 0.18	1.05 ± 0.10	4.97 ± 0.45	0.005	0.0005	0.003
miR-127-3p	184,399.67 ± 13,445.98	155,199.23 ± 27,968.99	364,440.11 ± 44,853.31	0.521	0.017	0.015
miR-143-3p	19,347.96 ± 1,882.00	15,869.88 ± 1,129.00	22,074.53 ± 1,305.43	0.315	0.029	0.390
miR-181a-5p	166,923.49 ± 41,636.83	172,181.35 ± 37,232.48	187,702.54 ± 7,347.48	0.870	0.775	0.732
miR-181b-5p	4,563.32 ± 129.32	2,639.89 ± 107.80	3,411.96 ± 512.88	0.006	0.146	0.092
miR-181c-5p	9,457.36 ± 683.70	12,792.95 ± 960.30	10,405.90 ± 65.66	0.007	0.129	0.358
miR-183-5p	23,631.29 ± 4,921.11	3,959.05 ± 1,306.86	836.84 ± 315.07	0.027	0.146	0.020
miR-191-5p	46,107.39 ± 15,981.96	21,312.11 ± 5,855.38	67,723.35 ± 49,812.87	0.366	0.410	0.713
miR-204-5p	1.50 ± 0.25	1.35 ± 0.11	2.61 ± 0.32	0.454	0.018	0.067

Notably, the miRNA expression levels over time seem to differ between the precursor as observed by *in-situ* hybridization experiments and the mature miRNA data obtained by NGS (**Figures 19 – 21**). Looking at the timepoints P0/P4 to P16/P30 (NGS/ *in-situ* hybridization respectively), for some of the miRNAs (let-7c, miR-27b, -127, -143, 204), the precursor molecules seem to be expressed in fewer cells of the CNC/SOC at later stages. Contrary, the mature miRNA expression gets significantly upregulated as indicated by the NGS data (**Figures 19 - 21, Table 34**). Only the level of mature miRNA-183 expression shown by the NGS data seems to follow the downregulation of precursor expression as indicated by the *in-situ* hybridization data.

Because of these discrepancies, another approach of quantitative expression analysis of mature miRNAs was chosen for miRNAs 127-3p and 181c-5p. This served for comparison to

the NGS data and its validation: miR-127-3p and miR-181c-5p were probed at three different timepoints (E16, P0, P30) in the SOC using a TaqMan qPCR approach (**Figure 23**).
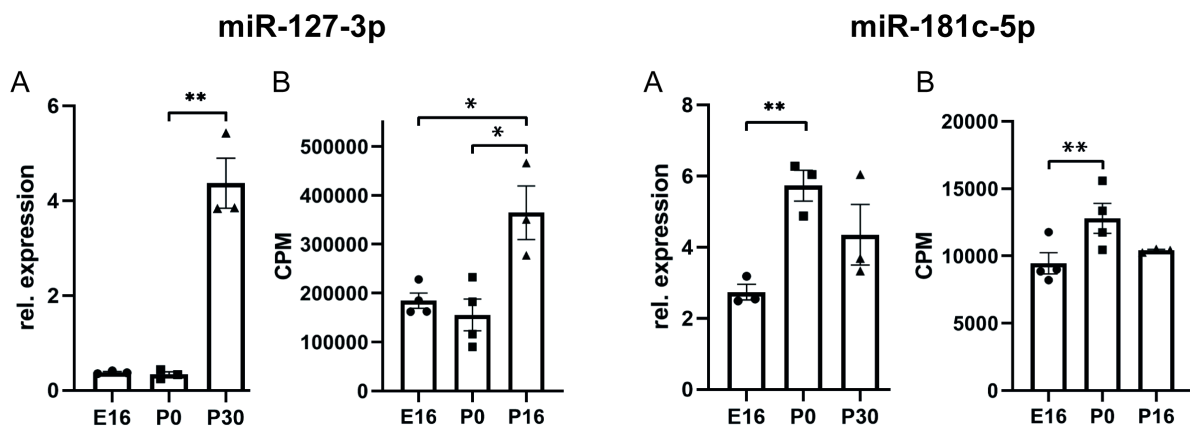
Figure 23: Expression levels of miR-127-3p and -181c-5p in the developing SOC from qPCR and NGS data.
A: relative miRNA expression from qPCR data at E16, P0 and P30. **B**: expression levels from NGS data at E16, P0 and P16. miR-127-3p was upregulated in the SOC of older animals compared to younger stages in both datasets. miR-181c-5p was upregulated in the SOC at P0 vs. E16 in both datasets. Single data points represent each n, the error bars show the SEM. N = 3 per genotype. Statistical significance of differences between groups was tested using Student´s *t*-test. CPM: counts per million, E: embryonic day, P: postnatal day. $p < 0.05$ = *; $p < 0.01$ = **.

Analysis of qPCR data revealed significant relative upregulation for miR-127-3p in the SOC at older vs. younger stages but not at P0 vs. E16. For miR-181c-5p, significant upregulation was found only for P0 vs. E16 (results summarized in **Table 35**). Overall, the qPCR results grossly matched the NGS results (see also **Table 34**) regarding the regulation pattern over time for the SOC with significant upregulation of miR-127-3p at P16/P30 and of miR-181c-5p at P0 (**Figure 23**).

Table 35: qPCR data for quantification of miRNA expression of miR-127-3p and -181c-5p.
Values represent relative expression of miRNAs compared to the expression of U6snRNA ± SEM.

miRNA	E16	P0	P30	p-value P0 vs. E16	p-value P30 vs. P0
miR-127-3p	0.38 ± 0.015	0.34 ± 0.045	4.37 ± 0.43	0.54	0.0016
miR-181c-5p	2.74 ± 0.18	5.73 ± 0.35	4.35 ± 0.7	0.0036	0.22

Summarized, quantification of expression of the 12 chosen mature miRNAs from the most highly expressed ones by the NGS approach (Rudnicki et al., 2014a) revealed high abundance for most of them in the SOC, except miRNAs let-7c, -27b and 204, which seemed to be only lowly expressed as indicated by the NGS data. Discrepancies occurred when comparing the precursor expression of some of the miRNAs to the expression of their mature forms over time, but the regulation pattern of at least two mature miRNAs was validated using another method which corroborated the NGS data.

3.8. Paired miRNA and mRNA expression in the SOC at E16; P0 and P16

Analyzing NGS data of tissues from different time points provides the possibility to obtain a global view on differential expression of miRNAs and mRNAs during development. Knowing the biological function of miRNAs, which is inhibition of protein biosynthesis by destabilizing mRNAs, an active regulatory miRNA that is upregulated over time would have an inhibitory effect on a significant portion of its predicted target mRNAs, resulting in their decreasing expression level. Analyzing both, miRNA expression and their predicted targets´ mRNA expression levels, allows for integration of their expression patterns to determine anticorrelations of their expression levels over time. This approach of "paired" or "integrated" miRNA and mRNA expression analysis was used here to search for miRNA candidates that are putatively contributing to the development and maintenance of auditory brainstem structures. These miRNAs will be specified as "active, regulatory miRNAs with a putative role in the central auditory system ".

Paired miRNA and mRNA expression analysis of NGS data from E16, P0 and P16 SOC was done in cooperation with Naama Messika Gold and Dr. Ran Elkon (Department of Human Molecular Genetics and Biochemstry, Sackler Faculty of Medicine, Tel Aviv University, Israel) using NGS data that was generated by myself. Among the NGS dataset, 214 miRNAs were detected as differentially expressed in an either intermediate-upregulated (96 miRNAs) or intermediate-downregulated (118 miRNAs) expression pattern over time. Tables showing individual differentially expressed miRNAs can be found in the appendix (appendix, **Table 44** and **Table 45**). mRNA expression data revealed 15,489 expressed genes among specimen of all ages. The global relationship (Euclidean distance measurement) revealed matching relation of biological samples and relation of RNA sequencing data without any batch effects. 3,546 genes were detected as differentially expressed. Upregulated genes clustered in three expression patterns between E16, P0 and P16: Early up (147 mRNAs); intermediate-up (1,535 mRNAs) and transient up (142 mRNAs). Down-regulated genes clustered in four regulatory patterns over time: early-down (193 mRNAs); intermediate-down (722 mRNAs); late-down (670 mRNAs) and transient-down (137 mRNAs). Integration of differentially expressed mRNAs and miRNA revealed candidate miRNAs that are downregulating their target mRNAs and to be therefore involved in gene regulatory networks underlying the development of the SOC. **Table 36** sums up the characteristics of integrated miRNA and mRNA sequencing analysis about evaluated candidate miRNAs being possibly involved in auditory brainstem functional maturation. 37 candidate miRNAs were either classified as "strong" or "weak" due to the consistency of "predicted target" – "differentially expressed genes" overlap among the databases TargetScan, miRDB and miRanda. The order of miRNAs in the following tables and figures was given by candidate classification, regulation of miRNAs, significance of predicted target/differentially expressed gene overlap among databases. For a better overview of the procedure please also see **Figure 6** from the Materials and Methods section again.

Table 36: Paired analysis of differentially expressed miRNAs regulating predicted targets among mRNA NGS data.
The table shows 37 miRNA candidates from paired miRNA/mRNA expression analysis being anticorrelatedly expressed during development of the SOC. The direction of miR-regulation over time is indicated by the arrows, green for upregulated, red for downregulated. Differentially expressed mRNAs (here also referred to as genes) are grouped into gene expression clusters due to their timing of increase/decrease in expression. To each found cluster the number of differentially expressed mRNAs is assigned. The last cloumn shows the overlap of predicted target genes and differentially expressed genes for every found mRA expression cluster. Order of miRNA candidates is due to their relevance among the target prediction databases. DE: differentially expressed, -: not available. Table created with analyzed data from Naama Messika Gold.

miRNA	predicted target genes	gene expression cluster	DE genes in cluster	common predicted targets/DE genes
strong candidates				
miR-124-3p ↑	1,246	early-down	193	94
		intermediate-down	722	216
		transient-down	137	80
miR-30d-5p ↑	789	early-down	193	62
miR-338-3p ↑	309	transient-down	137	21
miR-139-5p ↑	406	transient-down	-	12
miR-96-5p ↓	752	intermediate-up	1,535	278
miR-130b-3p ↓	465	intermediate-up	1,535	297
miR-17-5p ↓	605	intermediate-up	1,535	406
miR-20a-5p ↓	658			
miR-20b-5p ↓	620			
miR-106b-5p ↓	783			
miR-18a 5p ↓	225	intermediate-up	-	96
miR-25-3p ↓	413	intermediate-up	1,535	258
miR-92b-3p ↓	401			
miR-363-3p ↓	457			
miR-203-3p ↓	674	intermediate-up	1,535	189
miR-182-5p ↓	903	intermediate-up	-	319
miR-140-5p ↓	286	intermediate-up	-	109
miR-148a-3p ↓	545	intermediate-up	-	206
miR-148b-3p ↓	389			
miR-152-3p ↓	401			
miR-351-5p ↓	430	intermediate-up	-	216
miR-7b-5p ↓	349	intermediate-up	-	165
miR-223-3p ↓	306	intermediate-up	-	112
miR-216b-5p ↓	278	intermediate-up	-	90
miR-205-5p ↓	426	intermediate-up	-	178
weak candidates				
miR-29b-3p ↑	517	early-down	193	40
		intermediate-down	722	90
		late-down	670	194
miR-27b-3p ↑	706	transient/late-down	-	113
let-7b-5p ↑	434	early/late-down	-	106
let-7c-5p ↑	418			
let-7d-5p ↑	600			
miR-200c-3p ↓	566	early/intermediate-up	1,682	299
miR-429-3p ↓	573			
miR-295-3p ↓	397	intermediate/transient-up	-	246
miR-322-5p ↓	646	early/intermediate-up	-	356
miR-302d-3p ↓	413	intermediate/transient-up	-	246
miR-449a-5p ↓	414	early/intermediate-up	-	215
miR-183-5p ↓	380	intermediate-up	-	68

MiR-124-3p, miR-30d-5p, miR-338-3p and miR-139-5p were among the upregulated miRNAs the strongest candidates. They seem to have impact on the development of the auditory hindbrain by downregulating a significant portion of their predicted targets. For miR-124-3p a total of 1,246 predicted targets have been found among the SOC mRNA data including 390 of them that were significantly downregulated. miR-30d-5p shows 789 predicted targets and 62 significantly downregulated genes. miR-338-3p seems to actively downregulate 21 out of 309 predicted genes. The regulation of these miRNA candidates from E16 to P16 is shown in **Figure 24**, **Figure 25** and **Table 37**. A larger subset of miRNAs was downregulated over time, while a significant portion of their predicted target genes was upregulated. This was true for the identified strong candidates miR-96-5p, miR-130b-3p, miR-17-5p, miR-20a-5p, miR-20b-5p, miR-106b-5p, miR-18a-5p, miR-25-3p, miR-92b-3p, miR-363-3p, miR-203-3p, miR-182-5p, miR-140-5p, miR-148a-3p, miR-148b-3p, miR-152-3p, miR-351-5p, miR-7b-5p, miR-223-3p, miR-216b-5p and miR-205-5p.

Among the downregulated miRNA, miR-96-5p popped out as the most promising candidate for a critical role in the auditory brainstem. From its 752 predicted target genes, 278 were significantly upregulated. miR-130b-3p seems to regulate 297 out of 465 predicted targets. miR-17-5p, miR-20a-5p, miR-20b-5p and miR-106b-5p were grouped together because they all seem to regulate the same 406 genes among their 605 to 783 predicted targets. Together with miR-18a-5p, they belong to the miR-17 gene family (miRbase) showing high sequence homology in their stem sequence (appendix, **Figure 31**). miR-25-3p, miR-92b-3p and miR-363-3p all target the same 258 genes among their 401 to 457 predicted targets and therefore also were grouped together. miR-25 and miR-92b belong to the miR-25 gene family (miRbase) and show almost identical seed sequences in their stems (appendix, **Figure 31**). Another miRNA family shows up among the strong candidates, the miR-148 family with miR-148a-3p, miR-148b-3p and miR-152-3p. Members of this family seem to regulate the same 206 of their predicted target genes. The regulation of the strong candidates that were themselves downregulated over time is shown in **Figure 24** with underlying statistical data in **Table 37**. Classified as weak candidates were miR-29b-3p, miR-27b-3p, let-7b-5p, let-7c-5p, let-7d-5p, miR-200c-3p, miR-429-3p, miR-295-3p, miR-322-5p, miR-302d-3p, miR-449a-5p and miR-183-5p. miR-29b-3p was upregluated over time and seemed to significantly regulate 324 of its 517 predicted target genes. miR-200c-3p was downregulated over time and 299 of its 566 predicted targets were actually upregulated. For regulation of these miRs see **Figure 25** and **Table 37**. miRNA families were identified among the weak candidates as well, namely members of the miR-8 family, miR-200c-3p and miR-429-3p and of the let-7 family, let-7b-5p, let-7c-5p and let-7d-5p.
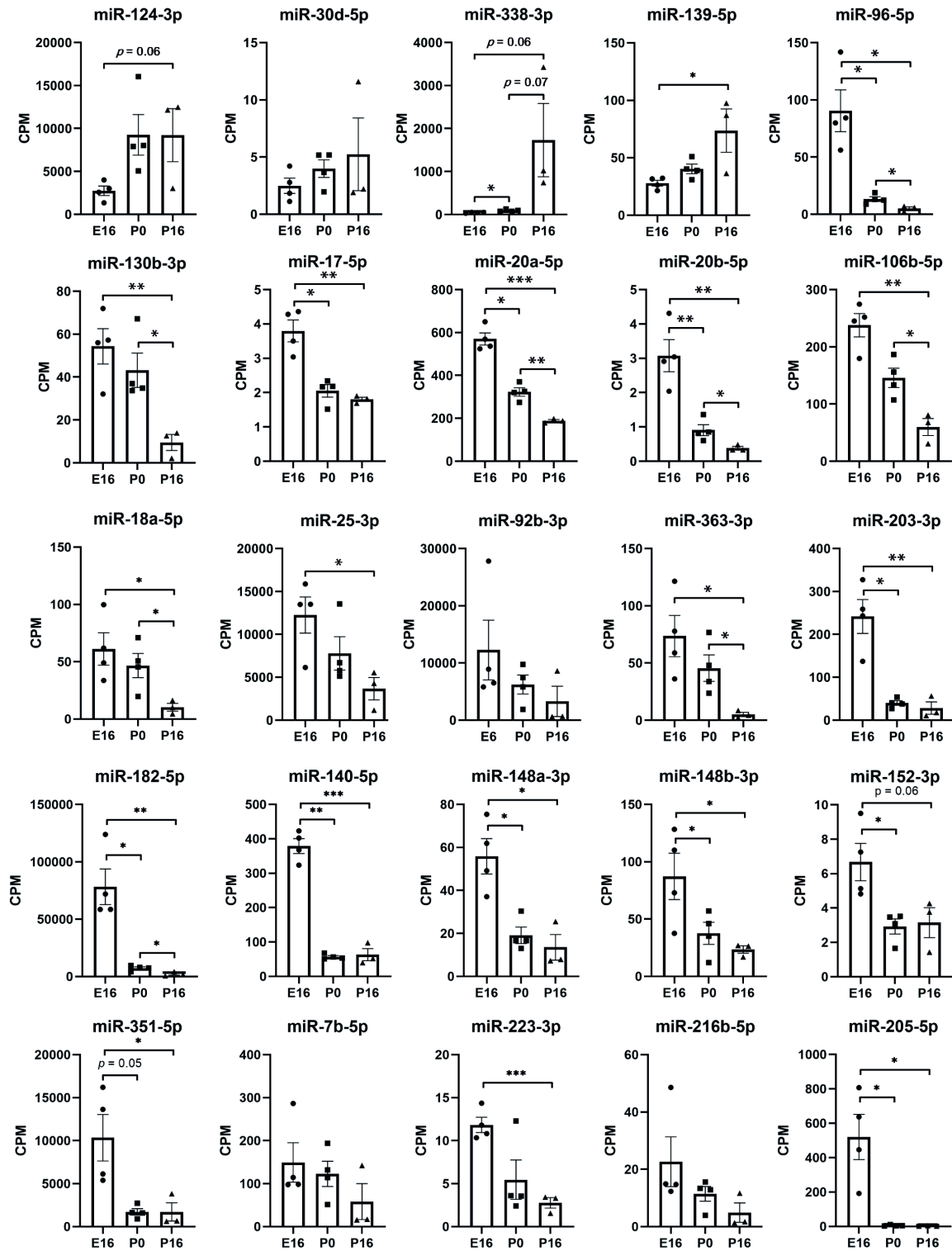
Figure 24: Regulation of strong miRNA candidates being possibly involved in auditory brainstem functional development.
The x-axis shows the age of specimen, E16, P0 and P16. The y-axis shows the counts per million (CPM) miRNA molecules at different scales. Bargraphs show the mean CPM values, single data points and SEM. *P*-values were calculated using Student´s *t*-test; *p* < 0.05 = *; *p* < 0.01 = **; *p* < 0.001 = ***. N = 4 for E16 and P0, n = 3 for P16. Plots were created using the NGS data analyzed by Naama Messika Gold.

73
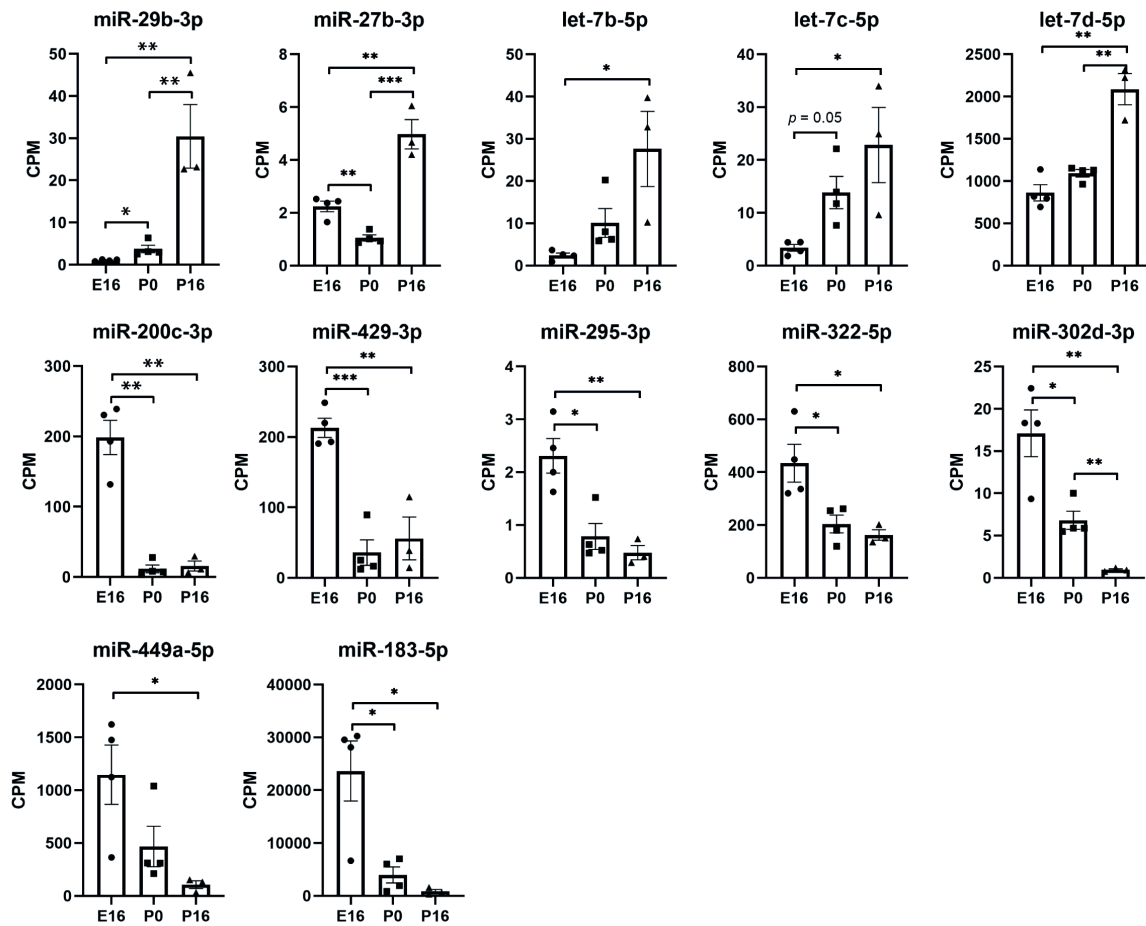
Figure 25: Regulation of weak miRNA candidates being possibly involved in auditory brainstem functional development.
The x-axis shows the age of specimen, E16, P0 and P16. The y-axis shows the counts per million (CPM) miRNA molecules at different scales. Bargraphs show the mean CPM values, single data points and SEM. *P*-values were calculated using Student´s t-test; $p < 0.05$ = *; $p < 0.01$ = **; $p < 0.001$ = ***. N = 4 for E16 and P0, n = 3 for P16. Plots were created using the NGS data analyzed by Naama Messika Gold.

Table 37: Expression of miRNA candidates for auditory function from paired miRNA/mRNA analysis at E16, P0 and P16.
Each row shows one miRNA candidate for possibly auditory-related developmental processes with its expression level at E16, P0 and P16 as well as statistical p-values for comparison of expression levels between timepoints P0 and E16, P16 and P0; P16 and E16. CPM: counts per million; E: embryonic day; P: postnatal day; SEM: standard error of the mean. Table created using the NGS data analyzed by Naama Messika Gold.

miRNA	E16 CPM ± SEM	P0 CPM ± SEM	P16 CPM ± SEM	*p*-value P0 vs. E16	*p*-value P16 vs. P0	*p*-value P16 vs. E16
miR-124-3p	2,736.96 ± 479.09	9,258.25 ± 2,045.50	9,217.97 ± 2,528.69	0.100	0.992	0.060
miR-30d-5p	2.49 ± 0.58	3.99 ± 0.66	5.24 ± 2.60	0.369	0.676	0.367
miR-338-3p	42.43 ± 4.33	92.36 ± 10.85	1,729.97 ± 695.81	0.045	0.070	0.064
miR-139-5p	27.93 ± 2.21	40.37 ± 3.58	73.67 ± 13.35	0.153	0.100	0.036
miR-96-5p	90.44 ± 15.77	13.23 ± 1.80	5.04 ± 1.14	0.024	0.030	0.011
miR-130b-3p	54.34 ± 7.14	43.17 ± 6.95	9.52 ± 3.04	0.532	0.020	0.007
miR-17-5p	3.80 ± 0.27	2.05 ± 0.16	1.80 ± 0.05	0.033	0.316	0.003
miR-20a-5p	570.03 ± 24.59	322.82 ± 16.98	188.55 ± 4.54	0.013	0.002	0.000
miR-20b-5p	3.07 ± 0.41	0.91 ± 0.14	0.38 ± 0.04	0.006	0.043	0.005
miR-106b-5p	237.79 ± 17.65	145.75 ± 14.65	59.73 ± 12.21	0.080	0.015	0.001
miR-18a-5p	61.15 ± 12.24	46.71 ± 9.15	10.35 ± 2.40	0.145	0.036	0.030
miR-25-3p	12,251.94 ± 1,829.98	7,784.86 ± 1,683.31	3,665.04 ± 1,062.90	0.342	0.166	0.025
miR-92b-3p	12,265.33 ± 4,527.69	6,222.68 ± 1,435.51	3,290.80 ± 2,169.52	0.430	0.368	0.230
miR-363-3p	73.53 ± 15.67	45.49 ± 17.65	4.96 ± 1.50	0.332	0.032	0.024
miR-203-3p	241.67 ± 34.08	39.84 ± 4.75	28.20 ± 11.61	0.017	0.429	0.007
miR-182-5p	78,249.64 ± 13454.85	7,278.75 ± 980.48	2,201.69 ± 874.02	0.023	0.025	0.009
miR-140-5p	379.09 ± 18.83	57.08 ± 3.20	63.10 ± 12.44	0.001	0.711	0.000
miR-148a-3p	55.88 ± 7.15	19.15 ± 3.32	13.56 ± 4.21	0.026	0.445	0.012
miR-148b-3p	87.20 ± 17.47	37.55 ± 8.33	23.43 ± 2.31	0.027	0.282	0.045
miR-152-3p	6.68 ± 0.94	2.93 ± 0.38	3.15 ± 0.62	0.033	0.812	0.063
miR-351-5p	10,342.84 ± 2,340.74	1,714.42 ± 326.23	1,710.35 ± 748.75	0.051	0.997	0.048
miR-7b-5p	149.25 ± 39.73	122.87 ± 25.33	58.33 ± 29.60	0.734	0.247	0.218
miR-223-3p	11.83 ± 0.78	5.46 ± 1.98	2.76 ± 0.43	0.103	0.373	0.001
miR-216b-5p	22.64 ± 7.50	11.45 ± 2.21	4.91 ± 2.39	0.391	0.175	0.156
miR-205-5p	520.52 ± 114.27	5.46 ± 1.67	3.03 ± 0.61	0.031	0.355	0.021
miR-29b-3p	1.03 ± 0.10	3.74 ± 0.77	30.43 ± 6.14	0.046	0.009	0.005
miR-27b-3p	2.25 ± 0.18	1.05 ± 0.10	4.97 ± 0.39	0.005	0.000	0.003
let-7b-5p	2.40 ± 0.49	10.09 ± 2.96	27.59 ± 6.28	0.145	0.093	0.020
let-7c-5p	3.38 ± 0.55	13.84 ± 2.64	22.84 ± 5.03	0.054	0.253	0.023
let-7d-5p	861.38 ± 83.34	1,092.79 ± 37.72	2,086.84 ± 130.25	0.082	0.002	0.001
miR-200c-3p	198.46 ± 21.15	11.48 ± 4.77	15.58 ± 5.79	0.003	0.662	0.002
miR-429-3p	213.01 ± 11.75	35.84 ± 15.62	55.98 ± 21.42	0.000	0.570	0.003
miR-295-3p	2.31 ± 0.28	0.79 ± 0.21	0.48 ± 0.09	0.045	0.368	0.006
miR-322-5p	433.94 ± 61.94	203.92 ± 29.03	162.47 ± 14.18	0.049	0.380	0.025
miR-302d-3p	17.10 ± 2.39	6.81 ± 0.93	0.96 ± 0.09	0.033	0.006	0.004
miR-449a-5p	1,146.47 ± 243.21	467.30 ± 166.38	105.66 ± 25.96	0.235	0.176	0.026
miR-183-5p	23,631.29 ± 4921.11	3,959.05 ± 1306.86	836.84 ± 272.86	0.027	0.146	0.020

In an additional step, the overall relationship of these miRNA candidates was analyzed beyond the already known miR-8, miR-17, miR-25, miR-148 and let-7 gene families, with each family targeting roughly the same set of genes. Of note, miR-96-5p shares most of its seed sequence with miR-92b-3p, a member of the miR-25 family. Also miR-30d-5p and miR-338-3p have seed sequence similarities (appendix, **Figure 31**).

Lastly, the predicted target genes of the evaluated subset of miRNAs overlapping with differential mRNA expression were compared to all so far published deafness genes for autosomal dominant and recessive nonsyndromic hearing loss (https://hereditaryhearingloss.org). The outcome is a list of miRNAs with their possibly targeted deafness genes (**Table 38**). These deafness genes mostly play a role in the cochlea. Deafness genes being among the miRNA target genes in the SOC implicate that these miRNAs could play a role not only in the peripheral but also in the central auditory system. They would therefore represent miRNA components of a shared gene regulatory network. 21 deafness genes were found being among the overlapping differentially expressed genes and target genes of miRNA candidates. Additionally, proposed excitatory and inhibitory synapse-related genes that were found to be predicted targets for miR-96-5p (Jensen and Covault, 2011) were integrated and most of them also turned out to be possibly regulated by many of the miRNA candidates (**Table 38**).

Table 38: Differentially expressed deafness and synapse related genes overlapping with miR candidate´s predicted target genes.
miRNA candidates are now numerically sorted for better overview. Deafness genes were taken from https://hereditaryhearingloss.org. Synaptic related genes were taken from Jensen and Covault, 2011. miRNA families are colour coded: blue, miR-17 family; green, miR-25 family; red, miR-148 family; orange, miR-8 family, violet, let-7 family. DE: differentially expressed.

auditory miRNA candidate	DE deafness genes	DE genes synapse (Jensen and Covault, 2011)	total putatively regulated genes
miR-7b-5p	SLC22A4, CLIC5	CACNB4	3
miR-17-5p	DMXL2, TPRN	SLC1A2, SCN1A, GAD2	5
miR-18a-5p	RDX	SLC1A2, SCN1A, ABAT	4
miR-20a-5p	DMXL2, TPRN	SLC1A2, SCN1A, GAD2	5
miR-20b-5p	DMXL2, TPRN	SLC1A2, SCN1A, GAD2	5
miR-25-3p	EPS8, CLIC5	SLC1A1, SCN1A, ABAT	5
miR-27b-3p	PLS1, GAB1		2
miR-29b-3p	LMX1A, EYA4, COL11A1, REST, ROR1		5
miR-30d-5p	EYA4, MSRB3, GPSM2		3
miR-92b-3p	EPS8, CLIC5	SLC1A1, SCN1A, ABAT	5
miR-96-5p	CLIC5	SLC1A1, SLC1A2, SCN1A, CACNB4, ABAT, GAD2	7
miR-106b-5p	DMXL2, TPRN	SLC1A2, SCN1A, GAD2	5
miR-124-3p	EYA4, COL11A1, MCM2, GAB1		4
miR-130b-3p		ABAT, GAD2	2
miR-139-5p	GAB1		1
miR-140-5p	TJP2, RDX, CLIC5		3
miR-148a-3p	MET		1
miR-148b-3p	MET		1
miR-152-3p	MET		1

miR-182-5p	*MYO6, MET, CLIC5*	*SLC1A1, SLC1A2, SCN1A, CACNB4, ABAT, GAD2*	9
miR-183-5p		*SCN1A, ABAT*	2
miR-200c-3p	*GJB6, EPS8*	*SLC1A2, SCN1A, ABAT, GAD2*	6
miR-203-3p	*DMXL2, MYO6, SLC22A4, EPS8, CLIC5*	*SCN1A, CACNB4, ABAT, GAD2*	9
miR-205-5p	*DMXL2, GJB6, SLC22A4, EPS8*	*SLC1A2*	5
miR-216b-5p	*EPS8*	*SLC1A1, SLC1A2, GAD2*	4
miR-223-3p	*MET*	*SCN1A*	2
miR-295-3p	*DMXL2, ADCY1, MET, EPS8*	*SCN1A, GAD2*	6
miR-302d-3p	*DMXL2, ADCY1, MET, EPS8*	*SCN1A, GAD2*	6
miR-322-5p	*TJP2, MYO6*	*SLC1A1, SCN2A, CACNB4, ABAT*	6
miR-338-3p	*GAB1*		1
miR-351-5p	*MYO6, EPS8*	*SLC1A2, GAD2*	4
miR-363-3p	*EPS8, CLIC5*	*SLC1A1, SCN1A, ABAT*	5
miR-429-3p	*GJB6, EPS8*	*SLC1A2, SCN1A, ABAT, GAD2*	6
miR-449a-5p	*RDX*	*SCN1A, SCN2A, ABAT*	4
let-7b/7c/7d-5p	*LMX1A*		1

The highest number of regulated deafness and synapse-related genes among its predicted target mRNAs was found for miR-182-5p and miR-203-3p with a total of 9 for each miRNA. miR-182-5p contributes 3 deafness genes and 6 synaptic transmission related genes to that number, while miR-203-3p seems to regulate 5 deafness genes. These two microRNAs are followed up by miR-96-5p, regulating 7 relevant genes, 6 of them synapse-related. Possibly regulating synapse-related genes, miR-96-5p shares the top position with miR-182-5p. Regarding only the deafness genes, the highest number of them (5) is putatively regulated by miR-29b-3p and 203-3p. Only two miRNAs from this study, miR-130b-3p and miR-183-5p do not show overlapping regulated targets and deafness genes.

Summarized, 37 putatively important miRNAs for auditory function have been found after analysis of the paired miRNA/mRNA sequencing approach from SOC tissue. Among them, members of the miR-8, miR-17 and miR-25 families seem to be important players in the central auditory system. Most of the candidate miRNAs are involved in the regulation of at least one deafness gene in the auditory periphery. This very much accounts for the importance of these microRNAs to not only central but also peripheral auditory functions, and therefore points towards them being also part of the shared developmental program of the cochlea and SOC.

3.9. Correlation of miR-expression between the peripheral and central auditory system

It is known that the development of the otic placode and the auditory hindbrain is ruled by a shared gene regulatory network, including transcriptions factors and signaling molecules that are of rhombomeric origin and give rise to developmental processes of the peripheral and central auditory system. Here, I ask the question, whether the early shared gene regulatory network also applies to miRNAs in terms of similar regulatory miRNA landscape between both systems and if this extends to later developmental stages. If true, a correlated expression pattern of miRNAs would be expected when comparing the miRNA landscape of the cochlea and the SOC. In order to answer this question, the NGS results for the P0 SOC obtained from this study (**Table 34**) were compared to the P0 cochlea data from Rudnicki et al., 2014a (for miR-27b-3p and 204-5p) and their kindly provided data supplementing their publication (other 10 miRNAs). **Table 39** sums up the results for miRNA expression from both tissues and gives an overview of miRNA expression ratios from the SOC compared to the cochlea.

Table 39: Comparison of miRNA expression from P0 cochlea and SOC.

miRNA	P0 cochlea (CPM)	P0 SOC (CPM)	SOC vs. cochlea (ratio)
miR-let7c-5p	13,818.56	13.84 ± 2.64	0.001
miR-22-3p	17,851.96	14,480.39 ± 2,658.46	0.81
miR-26a-5p	75,034.69	20,713.91 ± 4,443.30	0.28
miR-27b-3p	20,763.806	1.05 ± 0.10	0.00
miR-127-3p	27,721.72	155,199.23 ± 27,968.99	5.6
miR-143-3p	15,959.83	15,869.88 ± 1,129	0.99
miR-181a-5p	132,248.59	172,181.35 ± 37,232.48	1.3
miR-181b-5p	13,300.96	2,639.89 ± 107.80	0.2
miR-181c-5p	16,813.99	12,792.95 ± 960.30	0.76
miR-183-5p	19,409.61	3,959.05 ± 1,306.86	0.2
miR-191-5p	13,494.68	21,312.11 ± 5,855.38	1.58
miR-204-5p	24,237.559	1.35 ± 0.11	0.00

In order to visualize correlated expression levels of miRNAs between tissues, Pearson correlation plots were used. This mathematical approach delivers a tool to determine linear dependence of miRNA expression levels. To draw any conclusions about relatedness of miRNAs to the auditory system, NGS data from a non-auditory tissue, the frontal cortex, was obtained as well and included in this analysis. Each miRNA´s expression level (in CPM) was plotted on the x-axis for the P0 cochlea and on the y-axis for the P0 SOC and the P0 cortex. If a regression line through the datapoints has a slope of 1 (= Pearson correlation coefficient r), the dataset is perfectly correlated in the meaning of linear dependence. **Figure 26** shows the correlation of miRNA expression of P0 SOC and cortex compared to P0 cochlear sensory

epithelium, first for the 12 highest expressed miRNAs in the cochlea (**Figure 26**A) and then for the entire set of expressed 411 miRNAs that were found in all tissues (**Figure 26**B). These correlations were drawn from the 674 miRNAs found in the SOC and 557 miRNAs that were present in the cortex and the cochlea. Graphs are on the $\log_2$ scale to account for the different magnitudes of expression levels of miRNAs.
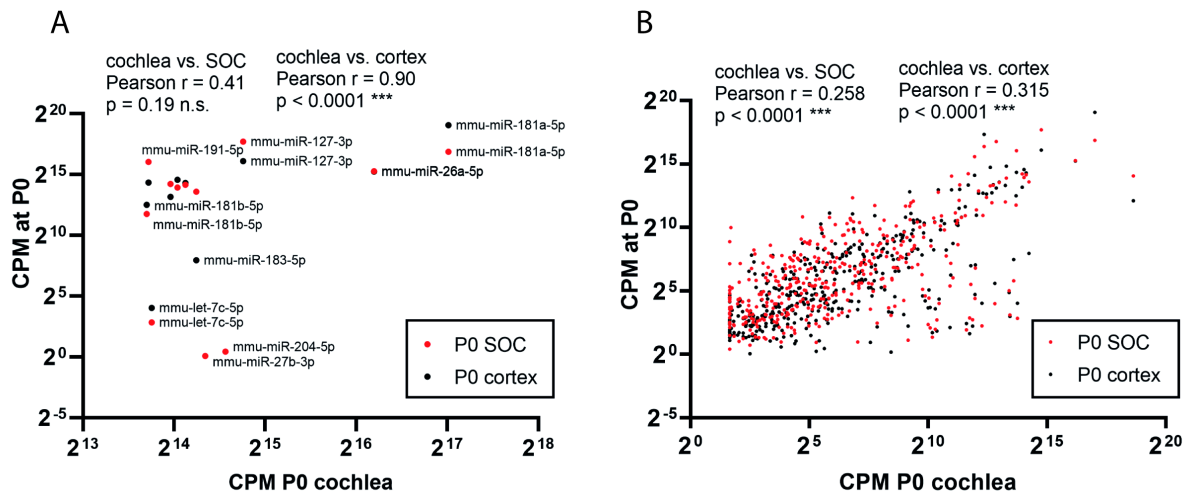
Figure 26: Correlation analysis of miRNA expression between P0 cochlea and SOC/cortex.
A: Datapoints show the 12 most highly expressed miRNAs from the P0 cochlea. Unlabeld points refer to miRNAs-22,-143,-181c and -183. Expression of miRNAs is shown on the $\log_2$ scale. The Pearson correlation coefficient for correlation between miRNA expression of the cochlea and SOC is r = 0.41, p = 0.19. The Pearson correlation coefficient for correlation between miRNA expression of the cochlea and cortex is r = 0.90, p < 0.0001. **B**: Datapoints show the expression of 411 individual miRNAs from P0 cochlea and SOC/cortex on the $\log_2$ scale. The Pearson correlation coefficient for correlation between miRNA expression of the cochlea and SOC is r = 0.258, p < 0.0001. The Pearson correlation coefficient for correlation between miRNA expression of the cochlea and cortex is r = 0.315, p < 0.0001. CPM: counts per million, P: postnatal day, SOC: superior olivary complex, n.s.: not significant; ***: highly significant.

Regarding the 12 highest expressed miRNAs from the cochlea and SOC at P0 (**Figure 26**A), the correlation coefficient r is 0.406, indicating weak positive correlation of miRNA expression. miRNAs let-7c, miR-27b and miR-204-5p are not correlatedly expressed between tissues. The result for this subset of miRNAs is not significant with p = 0.19. miRNA expression of the cochlea and the cortex is almost perfectly correlated with r = 0.90, p < 0.0001. Regarding the entire set of miRNAs that have been found in both cochlea and SOC/cortex at P0, there´s still weak positive correlation of expression of miRNAs between the cochlea and the SOC (r = 0.258, p < 0.0001) and also between the cochlea and the cortex (r = 0.315, p < 0.0001) (**Figure 26**B).

Next, the correlation of miRNA expression between P0 cochlea and SOC and between P0 cochlea and cortex was analyzed for the newly elaborated auditory-related miRNAs from the paired miRNA/mRNA sequencing approach. **Figure 27** shows the Pearson correlation of miRNA expression for 33 of the 37 miRNAs from **Table 36**, **Table 37** and **Figure 24**, **Figure 25**. The missing 4 miRNAs (miRs-7b-5p, 20b-5p, -295-3p, -302d-3p) have not been found among the cochlea data.
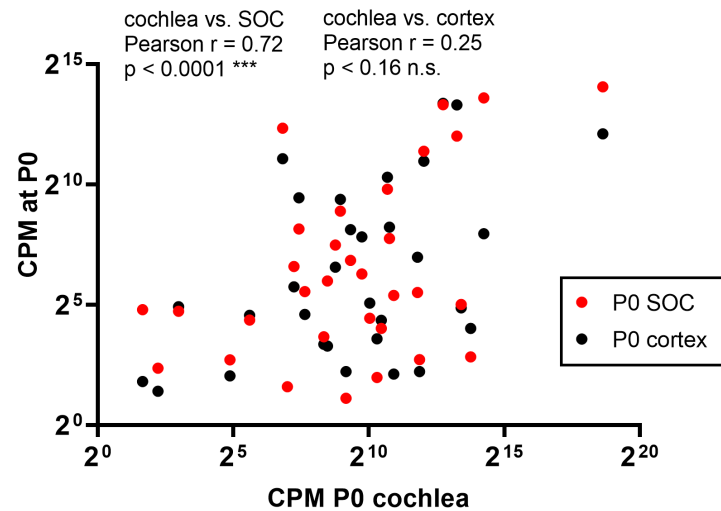
Figure 27: Correlation analysis of miRNA expression from paired miRNA/mRNA analysis between P0 cochlea and SOC/cortex.

Datapoints show the expression of 33 individual miRNAs from P0 cochlea and SOC and cortex on the log2 scale. miRs-7b-5p, 20b-5p, -295-3p, -302d-3p are missing because they were not found in the cochlea data. The Pearson correlation coefficient for correlation between miRNA expression of the cochlea and SOC is r = 0.72, p < 0.0001. The Pearson correlation coefficient for correlation between miRNA expression of the cochlea and cortex is r = 0.25, p = 0.16. CPM: counts per million, P: postnatal day, SOC: superior olivary complex, n.s.: not significant, ***: highly significant. Plot created using the NGS data analyzed by Naama Messika Gold and data from Rudnicki et al, 2014a.

Comparison of miRNA expression between the P0 cochlea and SOC reveals that the subset of miRNAs elaborated in the paired miRNA/mRNA NGS analysis is strongly correlatedly expressed between the two tissues with r = 0.72. Despite this relatively small sample size of 33 miRNAs the result is strongly significant with *p* < 0.0001 (**Figure 27**). There´s no significant correlation for these miRNAs between the P0 cochlea and cortex (r= 0.25, p = 0.16). These results indicate a putative auditory-related function for this subset of miRNAs as their expression levels are strongly correlated in auditory system but not between the auditory periphery and the non-auditory frontal cortex.

Overall, there seems to be a positive correlation between the miRNA landscape of the cochlea and the SOC, meaning the expression levels of microRNAs are similar between the two tissues. This fact supports a shared gene regulatory network of the auditory periphery and central auditory system. However, for the 12 most highly expressed miRNAs from the cochlea and the whole dataset of miRNAs, there´s no indication for exclusively auditory function, because the miRNAs expressed in the non-auditory frontal cortex are also correlatedly expressed with those from the cochlea. Interestingly, the subset of 33 out of the newly proposed 37 miRNAs possibly related to auditory function show high correlation of their expression levels between the cochlea and the SOC but not between the cochlea and cortex. This result strongly argues for the participation in a gene regulatory network governing the development of the peripheral and central auditory system for these miRNAs.

4. Discussion

In this thesis, the central auditory system of the *miR-183/96* ko mouse was characterized for further elaborating the role of miR-96 for development and function of the auditory hindbrain. The results confirmed a critical contribution of this miRNA to auditory brainstem development and function and allowed to distinguish between gain and loss of function effects of the human deafness related miR-96 *Dmdo* mutation. The focus was set on auditory brainstem morphology and molecular and physiological synaptic integrity. Not only morphometric changes in this mouse line were evident, but also (in cooperation) an interesting physiological phenotype. This phenotype was functionally characterized on a molecular level.

Furthermore, light was shed on the general miRNA landscape of the central auditory system and newly obtained data were integrated to already existing data of the peripheral auditory system to answer the question whether miRNAs belong to the shared gene regulatory network underlying the development of both, the peripheral and central auditory system. Furthermore, promising new auditory-related miRNA candidates of this network were presented, that could be analyzed in subsequent research by approaches similar to the ones used to dissect the contribution of mR-96 for the auditory system.

4.1. Volume reduction of auditory brainstem nuclei in *miR-183/96* ko mice

The analysis of auditory brainstem structures in *miR-183/96* ko mice revealed that the aVCN, and parts of the SOC, namely the MNTB and LSO were severely decreased in volume. This phenotype wasn´t observed in nonauditory structures, suggesting it to be auditory specific. The volume reduction is caused by fewer cells in the LSO and MNTB in *miR-183/96* ko. The lack of cells could be discussed to be caused by early cell death or that cells are not born in early embryonic development. Additionally, cells have been smaller in the MNTB showing arrest of cell growth during development. Affected auditory nuclei play a key role in sound source localization, leading to the assumption that the decrease in volume of auditory brainstem nuclei might be due to peripheral deafness and hence missing auditory input to these structures. For discussion of this issue, I will go into some detail of auditory hindbrain development in deaf mice here: Evidence supporting the impact of deafness on the auditory brainstem is delivered by unilateral early (P5) cochlear ablations leading to ipsilateral decrease in the size of the CN being due to loss of cells (Mostafapour et al., 2000). Also electrophysiological and molecular changes have been reported after cochlear ablation experiments (Walmsley et al., 2006). However, cochlear ablation means destroying the whole cochlea and spiral ganglion, the latter representing the direct connection to the auditory nerve and the CNC. In fact, the spiral ganglion with its spontaneous activity from E14 on was identified as key regulator of auditory brainstem formation (Marrs and Spirou, 2012). Naturally occurring deafness in the *dn/dn* mouse model (Deol and Kocher, 1958), harboring a

mutation in the *TMC-1* gene resulting in absence of spontaneous activity in the auditory nerve (Bock et al., 1982) lead to volume reduction of the VCN (Webster, 1985). Another profoundly deaf mouse line lacking the vesicular glutamate transporter VGlut3 in the inner ear also showed volume reduction in the VCN. However, volume reductions have not been reported for the third order auditory nuclei of the SOC (Seal et al., 2008). In this study, the analysis of the peripherally deaf *Cldn14* ko mouse as a control for peripheral deafness, supported the idea of an on-site effect of *miR-183/96* ko at the level of the auditory brainstem by the finding of unchanged volumes of auditory hindbrain structures. In these congenitally deaf mice, hair cells in the cochlea were degenerated by P10-13 and ABRs demonstrated deafness at P15-P17 (Ben-Yosef et al., 2003), similar to the *miR-183/96* ko mouse. Hence, it is plausible that the observed morphological changes in at least the secondary order nuclei of the SOC, the LSO and MNTB, are caused by an on-site role of miR-183/96. This observation was already made in the *Dmdo* mouse (Schlüter et al., 2018) and added miR-96 to the list of deafness genes with a role beyond the cochlea (Willaredt et al., 2014; Michalski and Petit, 2019). Regulation of auditory brainstem development therefore is dependent on miRNAs-183 and -96. This also seems to hold true for other sensory systems and alltogether explains the strong conservation of the miR-183 cluster during evolution.

4.2. Is the *Dmdo* phenotype due to gain or loss of function of microRNA-96?

The *Dmdo* mutation was investigated in the peripheral auditory system (Lewis et al., 2009), the results are summarized in **Figure 28**A. The loss of function of miR-183/96 results found in the auditory periphery (Geng et al., 2018), are summarized in **Figure 28**C. The phenotypes of the *Dmdo* mouse were discussed to be due to gain of function effects of the *Dmdo* mutation, additionally, it was shown by bioinformatics that the gene regulatory networks regulated by miR-96 *Dmdo* and *miR-183/96* ko differ: transcriptomics data exhibit a way larger network with more involved genes and links for the miR-96 *Dmdo* mutation leading to defects even in heterozygotes, where one mutated allele is sufficient to generate an altered phenotype. In the loss of function scenario a knockout of both alleles is necessary to see an effect (Lewis et al., 2019).

Results from the analysis of the *Dmdo* mutation in the auditory brainstem of mice (Schlüter et al., 2018) are summarized in **Figure 28**B. Regarding the morphometry of auditory brainstem nuclei, the similar effect in *miR-183/96* ko mice argues for a loss of function consequence of miR-96, leading to increased cell death during auditory brainstem development. Yet, it is not clear whether this is a direct effect of missing miR-96 regulation. There is the possibility that so far unknown downstream effects of the loss of function of miR-96 cause the volume reduction of auditory brainstem nuclei.

miR-183/96 ko does not affect the immunoreactivity of the potassium channel subunits Kv1.6 and BKβ2, confirming the gain of function effect of decreased expression of Kv1.6 and BKβ2 in *Dmdo* mice which is in agreement with target predictions for the miR-96 *Dmdo* mutation (Schlüter et al., 2018).

Analysis of the presynaptic marker SV2 as previously done in the *Dmdo* mouse revealed no changes in SV2 expression in *miR-183/96* ko mice compared to their wt littermates. This argues for morphologically mature calyces of Held, which was confirmed by analyzing the active zone markers Bassoon and Piccolo and by the electrophysiological data (**Figure 28**D). Regarding these results, the immature calyx in *Dmdo* mice seems to be a gain of function effect of the miR-96 *Dmdo* mutation, too. In total, the *Dmdo* phenotype seems to be more due to a gain of function of the miR-96 *Dmdo* mutation. This leads, also for the auditory brainstem, to a more severe phenotype than the ko condition. This is in agreement with the predictions of a larger network with more involved genes and connections for the *Dmdo* mutation than for the *miR-183/96* ko (Lewis et al., 2019). **Figure 28** sums up the main findings for the *miR-96-Dmdo* mutation and the *miR-96* ko condition that have been elaborated so far for the inner ear and the auditory brainstem.
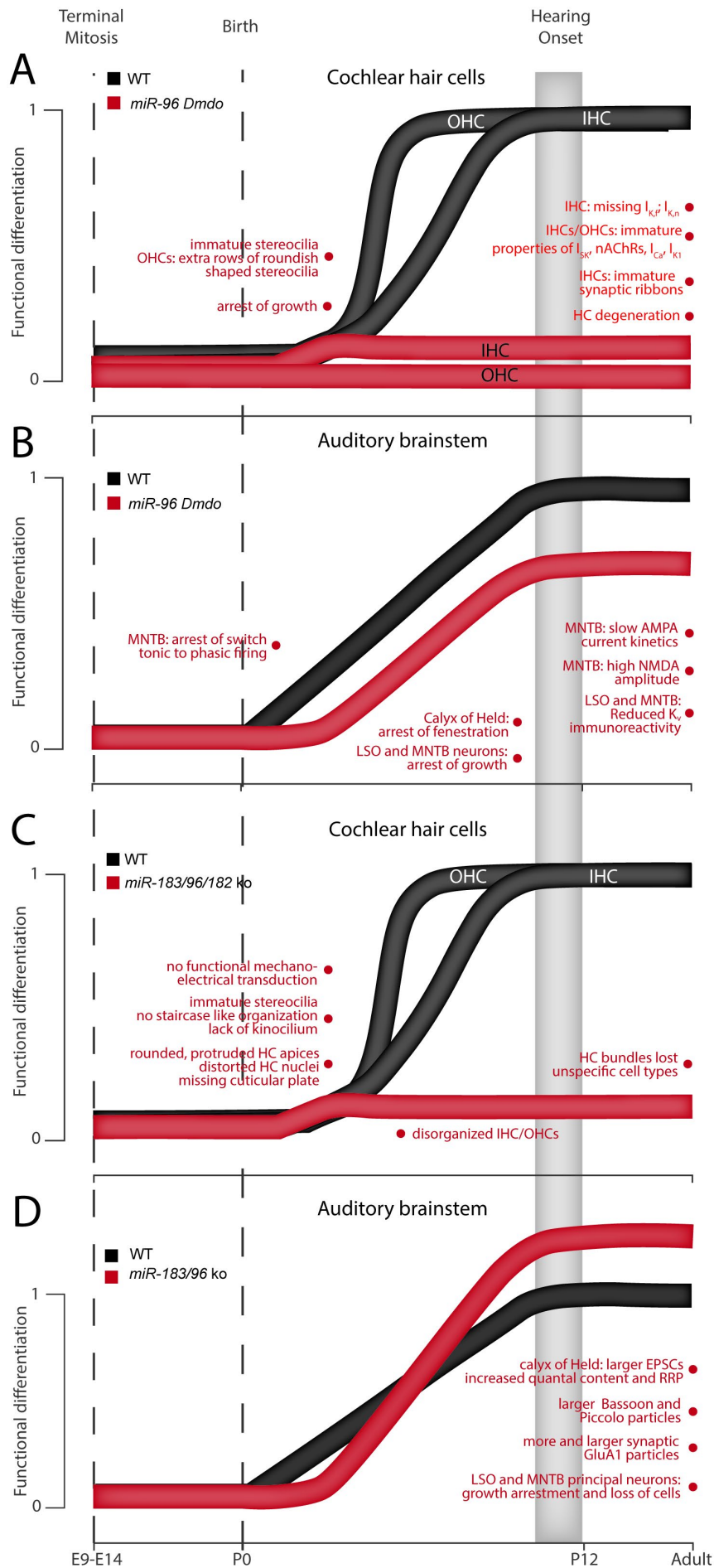
Figure 28: Summary of cochlear and auditory brainstem phenotypes in miR-96 Dmdo and miR-96 ko mice.
Main differences in cochlear hair cell (HC) and central auditory brainstem development between wt and *miR-96 Dmdo* mice (**A, B**) and wt and *miR-96* ko mice (**C, D**). Depicted is the degree of functional differentiation on the y-axis, with 1 indicating fully differentiated functional organs. The x-axis indicates the development of auditory structures from E9 to adult stages. The black curves indicate the development of auditory structures in wt mice while red curves represent the condition of those structures in homozygous transgenic animals. **A:** HC phenotypes and developmentally important membrane currents (I_{Ca}, I_{K1}, $I_{K,f}$, $I_{K,n}$, I_{SK}) and function of membrane proteins (nAChRs) being aberrant or missing in miR-96 *Dmdo* mice. OHC development in miR-96 *Dmdo* mice is arrested at around day of birth, for IHCs at around P3. **B:** Developmental arrest in the auditory brainstem of miR-96 *Dmdo* mice. The growth of LSO and MNTB neurons was arrested. Physiologically, adult miR-96 *Dmdo* mice show slower AMPA current kinetics and higher NMDA amplitudes in MNTB neurons compared with wt mice. The MNTB of miR-96 *Dmdo* mice shows reduced Kv immunoreactivity and no switch from immature to mature firing behavior. The calyx of Held fenestration was developmentally arrested in miR-96 *Dmdo* mice. **C:** HCs of *miR-183/96/182* ko mice don´t show mechanoelectrical transduction at their stereocilia which are disorganized and lack their kinocilium. Hair cell shape is aberrant with roundish protruded HC apices, distorted nuclei and missing cuticular plates. At later stages, IHC/OHC differentiation is not evident and HC bundles are completely lost. **D:** The auditory brainstem of *miR-183/96* ko mice shows growth arrestment of the LSO and MNTB (comparable to the *miR-96 Dmdo* phenotype) but increased synaptic transmission at the calyx of Held displaying presynaptically larger Bassoon and Piccolo particles and postsynaptically more and larger GluA1 particles. E: embryonic day; HC: hair cell, IHC: inner hair cells; I_{Ca}: Ca²⁺ current; I_{K1}: inward rectifier K⁺ current; $I_{K,f}$: large conductance Ca²⁺-activated K⁺ current; $I_{K,n}$: negatively activating K⁺ current; I_{SK}: small conductance Ca²⁺-activated K⁺ current; LSO: lateral superior olive; MNTB: medial nucleus of the trapezoid body; nAChRs: α9α10-nicotinic acetylcholine receptors; OHC: outer hair cells; P: postnatal day; WT: wildtype. Figure modified from Schlüter et al., 2018, summarizing data from Lewis et al., 2009; Kuhn et al., 2011 (**A**); Schlüter et al., 2018 (**B**); Geng et al., 2018 (**C**) and own data (**D**).

Results from the miR-96 *Dmdo* mutation and the miR-183/96 ko condition and their comparison now have shed light on some of the detailed functions of miR-96.

The knowledge of exact consequences of genetic alterations on the molecular level, like raising the gain or loss of function question of the miR-96 *Dmdo* mutation, could contribute to personalized medicine: A gain of negative mRNA regulation by mutations like in miR-96 and therefore decrease in functional protein levels could be medicated by administration of agonists or substitutes for those proteins. In this case the decreased expression of potassium channel subunits could possibly be treated with respective drugs or gene therapeutic approaches. A loss of function of regulation by miR-96 and therefore raised protein levels could be treated with antagonists, where applicable. Additionally, a gene-therapeutic approach delivering artificial miRNA molecules for substitution of the one that lost its function via e.g. viral vectors would be possible nowerdays.

4.3.   A new implication for microRNA-96 function at the calyx of Held

The key finding of our study is that miRs-183/96 are crucially involved in the pre- and postsynaptic regulation of synaptic strength derived from evidence of increased synaptic transmission at the calyx of Held in *miR-183/96* ko mice. These were larger EPSCs, with increased quantal content of SVs and a bigger RRP, larger Bassoon and Piccolo particles at the calyx´s presynapse and more and larger GluA1-particles at the calyx´s postsynaptic side (**Figure 28**D). Investigating auditory synapses in deaf mice always raises the question, whether missing input from the auditory nerve causes most of the functional findings of the downstream synapses, like it was already discussed for the changed morphometry auf auditory brainstem nuclei. Indeed, there

are some examples for that explanation taking the first and second order auditory nuclei into account but not the third order auditory nuclei of the SOC: The endbulb of Held - bushy cell connection in the aVCN was electrophysiologically impaired in DBA mice displaying age related hearing loss (Wang and Manis, 2005). Molecular synaptic changes of the endbulb of Held (fewer SVs and larger postsynaptic densities) have been found in the Shaker-2 mouse displaying dysfunctional cochlear hair cells (Lee et al., 2003). In congenitally deaf *dn/dn* mice (Deol and Kocher, 1958), recordings in the IC in response to electrical stimulation of the auditory nerve delivered evidence of functional central auditory brainstem connections (Bock et al., 1982). However, electrophysiological changes have been reported for the endbulb of Held in the aVCN (Oleskevich and Walmsley, 2002) but not in the calyx of Held in the MNTB (Oleskevich et al., 2004; Youssoufian et al., 2005). Therefore, the here described phenotype at the level of the MNTB is likely to be an on-site effect of loss of miR-183/96 at the auditory brainstem. At the presynapse, an increased RRP size was shown that resulted in an increased quantal content of SVs per EPSC and therefore enlarged EPSCs. Other presynaptic parameters like short term depression and SV replenishment remained unchanged. Moreover, the clusters of the active zone markers Bassoon and Piccolo were larger in *miR-183/96* ko synapses, suggesting an increase in active zone area. Including the *Cldn14* ko mouse as a control for effects arising from peripheral deafness delivered evidence for an on-site effect of miR-183/96 ko since there was no increase in AZ size in the *Cldn14* ko. Since the number of release sites for SVs scales with the area of the active zones (Holderith et al., 2012), the increase in RRP size could be a direct consequence of the increase in active zone size. However, neither Bassoon nor Piccolo have been implicated in the regulation of active zone and RRP size (Gundelfinger et al., 2015; Parthier et al., 2018). Therefore, the increased active zone size is probably caused by the misregulation of a yet unidentified gene. Bassoon or Piccolo are no direct targets of miR-96, consequently this effect has to be discussed as a downstream effect of unidentified misregulation.

On the postsynaptic site, an increase in the quantal amplitude of sEPSCs in *miR-183/96* ko calyces was observed. This effect could be explained by the finding of increased synaptic localization of the AMPAR subunit GluA1. GluA1 is a predicted and validated target of miR-96 (Dambal et al., 2015; Jensen and Covault, 2011). Therefore, ko of miR-96 could possibly result in a lack of downregulation of GluA1 which occurs normally in MNTB principal cells around the onset of hearing at P10-11 (Caicedo and Eybalin, 1999; Koike-Tani et al., 2005). EPSCs at the calyx of Held are vastly mediated by GluA4 (Yang et al., 2011) since this AMPAR subunit shows the fastest kinetics (Mosbacher et al., 1994) and is therefore best suited for the ultrafast synaptic transmission required in the auditory brainstem (Borst and van Soria Hoeve, 2012). An increased abundance of GluA1-subunits at the postsynapse after hearing onset is thus expected to result in slightly slower decay kinetics of EPSCs. Indeed, the results show a slight trend towards such a slowing albeit it only reaches significance in the presence of kynurenic acid. The absence of GluA1 downregulation may therefore interfere with the calyx's ability to transmit sound-induced synaptic signals with sub-millisecond precision.

Of note, a recent study has shown that presynaptic release sites and postsynaptic AMPARs are aligned in so called synaptic nanocolumns and postsynaptic changes are reflected by

rearrangement of the presynaptic release sites (Tang et al., 2016). Thus, the presynaptic changes discussed above could also be a secondary consequence of the increased GluA1 abundance instead of miR-183/96 mediated regulation of a presynaptic gene. Further studies are required to address the molecular mechanism underlying the change in RRP size.

The importance of miR-96 especially for glutamatergic neurons and excitatory synapses was described before (Jensen and Covault, 2011): Target scans for miR-96 revealed potential regulation of the glutamate transporters *SLC1A1* and *SLC1A2* and beyond *GRIA1* three other glutamate receptors, namely *GRIN2B*, *GRID1* and *GRM7*. miR-96 targets also include *RGS2* and *HOMER1*, both coding for proteins that regulate glutamate receptor activity (Kammermeier and Ikeda, 1999; Tu et al., 1998). Furthermore, target predictions for miR-96 name four voltage-gated sodium channel subunits (*SCN1A*, *SCN2A*, *SCN3A* and *SCN9A*) and four voltage-gated calcium channel subunits (*CACNA1C*, *CACNA2D2*, *CACNB1* and *CACNB4*) also being important for excitatory neurotransmission. Of those excitatory synapse-related genes, *SLC1A1*, *SLC1A2*, *GRIA1*, *GRID1*, *GRM7*, *RGS2* and *HOMER1* have been validated in luciferase-assays, while *SLC1A1*, *RGS2* and *HOMER1* were also validated as targets in miR-96 transfected HEK-cells (Jensen and Covault, 2011). This subset of synapse-related genes being potential targets of miR-96 could serve for more in-depth studies of the synaptic phenotype we characterized in the *miR-183/96* ko mouse.

Beyond the role of miR-96 for excitatory neurotransmission, target analysis also revealed inhibitory synapse-related genes like *ABAT* and *GAD2*. These genes are involved in γ-amino butyric acid (GABA) metabolism, which is an inhibitory neurotransmitter being relevant for the auditory system for inhibitory neurons of the LSO. Neurolignin2 (*NLGN2*) and gephyrin (*GPHN*), being involved in inhibitory postsynaptic structure (Essrich et al., 1998; Varoqueaux et al., 2006) were among the miR-96 targets, too, as well as *SLC12A5* coding for the potassium chloride cotransporter KCC2 which is important during development and chloride ion gradient maintenance of inhibitory neurons (Rivera et al., 1999). Of these inhibitory synapse-related genes, *GAD2*, *GPHN*, and *SLC12A5* were validated, *GPHN* even on the protein level (Jensen and Covault, 2011). These findings should give rise to have a closer look at the LSO, where inhibition is essential for detecting interaural level differences for sound source localization.

4.4. Animal model

The animal model that was used lacked both, miR-183 and miR-96 from the polycistronic miR-183 cluster. Deleting miR-96 alone was not possible by the time the mouse line was generated (Prosser et al., 2011) because of only 117 nucleotides of intergenic region between miR-183 and -96. These two miRs share high sequence homology, but still there are small differences within their sequences, resulting in regulation of common and unique target genes (Dambal et al., 2015). As both miRNAs are expressed in the auditory brainstem (data not shown), the observed phenotypes can not exclusively be assigned to either miR-183 or -96.

4.5. miRNA expression in the cochlea and SOC

In this section the question, whether also other miRNAs beyond miR-96 could be part of the shared gene regulatory network underlying development of the inner ear and auditory hindbrain, will be addressed. Therefore, in a first step, 12 miRNAs that were found to be highly expressed in the inner ear (Rudnicki et al., 2014a) were spatially analyzed by *in-situ* hybridization on the auditory brainstem level.

In-situ hybridization resulted in a spatial, qualitative overview of miRNA precursor expression because probes were designed against the precursor miRNA molecule and not the mature miRNAs. The main finding was general abundance of the pre-mir-22, -26a, -27b, -127, -143, -181a, -181b, -181c, -183, -191, -204, and -let-7c in all auditory brainstem nuclei at P4 and in young adult P30 mice. miRNA precursors were also broadly expressed in other neurons of the hindbrain, suggesting a general role of these miRNAs in neuronal development, not necessarily only auditory-related. For most of the miRNA precursors the expression in the LSO was visible in fewer cells in the LSO of the adult stage, compared to their homogeneous expression at P4. For pre-miR-22 and -127 an expression gradient along the tonotopic axis of the adult LSO was shown, although this was not quantified because of lack of whole *in-situ*-hybridization image series of the LSO. Expression of pre-miRNAs seems to be more abundant in cells of the high frequency region of the LSO. The gradient of expression along the tonotopic axis being highest in the high frequency region was also observed in the adult aVCN for pre-mir-26a and -127. If true, a specialized auditory function of these miRNAs important for high frequency tuned neurons is indicated. In the adult stage, miRNA precursor expression always seemed to be refined to distinct neuronal populations with often very prominent expression in the CNC and MNTB, suggesting a role in the maintenance of (auditory) neuronal populations beyond development. Nothing auditory-related has been published yet about these miRNA candidates, therefore especially testing sound source localization at high frequencies in knockout mouse models would be interesting for at least the miRNA candidates showing higher expression in the high frequency regions of the aVCN and LSO.

In order to supplement the spatial information about these 12 miRNAs, a NGS approach was used for quantification of mature miRNA expression in the SOC. These reults were compared to the *in-situ* hybridization results. For miR-let-7c-5p, miR-27b-3p, miR-127-3p, miR-143-3p, and miR-204-5p, a significant increase of mature miRNA expression was found in P16. Contrary, from the P30 *in-situ* hybridization data, less expression would have been expected, assuming low pre-miRNA expression in *in-situ* hybridization data resulting in corresponding low levels of mature miRNA. The discrepancy of *in-situ* hybridization vs. NGS data could be explained by differential regulation of miRNA processing. It is known that high pre-miRNA expression is not mandatorily resulting in high levels of mature miRNAs. Pre-miRNAs being abundant quite ubiquitously throughout the whole brain, like it was observed in the P4 *in-situ* hybridization data, have been shown to be processed to their mature forms in far less cell populations (Obernosterer et al., 2006). This possibly explains, for the juvenile stage, the high abundance of pre-miRNAs in the *in-situ* hybridization images, although they show lower

mature miRNA abundance in the NGS data than the adult specimen. Another explanation is the often very intensive labeling of the adult MNTB in the *in-situ* hybridization images. The MNTB has very large principal cells that, at least measured from the calyx of Held, increase in size until P16 (Morest, 1968) and therefore could contribute to a huge part of the mature miRNA molecules that are higher expressed in P16 vs. P0 in the NGS data. To back up the NGS results a TaqMan qPCR approach was performed for quantification of miRNA-127-3p and -181c-5p. The results validated the NGS data quite well.

4.6.   An approach for identification of new auditory-related miRNAs

Beyond miR-96, some other miRNAs have been proposed in the literature to play a role in the inner ear. However, despite of the assumption that about 60% of protein coding genes is regulated by miRNAs, no other miRNA than miR-96 was analyzed in the central auditory system.

In this study, 37 miRNAs were found to be potentially auditory-relevant (**Table 36**). The choice of miRNAs was based on their differential regulation and significant overlap of their predicted target genes and differentially expressed mRNAs. Among the 37 candidates, I'd like to emphazise the mature miRNAs **miR-18a-5p**, **miR-29b-3p**, **miR-30d-5p**, **miR-96-5p**, **miR-124-3p**, **miR-140-5p**, **miR-182-5p**, **miR-183-5p**, and **miR-200c-3p**. The presence of miRNA-96-5p in this group supports the notion that this type of analysis is able to identify miRNAs important for the auditory system, due to the very well-described auditory function for miR-96.

Assuming the sequence resemblances of miR-30b/d-5p and miR-200b/c-3p (appendix, **Figure 32**) leading to a similar biological function of these miRNAs, in summary the emphasized 9 out of the 37 evaluated candidates have been attributed with auditory relevance before and are likely to also play a role in the central auditory system and thus are interesting candidates for members of a shared gene regulatory network between the peripheral and the central auditory system.

Interestingly, regarding the relationship of found miRNA candidates, some miRNAs with the same target genes and similar sequences are members of gene families and appear accumulated in this analysis, like the miR-17 family. This family includes **miR-17**, **-18a**, -18b, **-20a**, **-20b**, -93, -106a, and -**106b** in mice. Five out of these 8 familiy members (bold letters) were evaluated as miRNA candidates for auditory function. This miRNA family was described to be related to inner ear function as well, hence, the miR-17 family contributes lots of possible miRNA candidates to a possibly shared gene regulatory network and should therefore be kept in mind for analysis in the auditory system. Another miRNA-family that seems to play a more general role, is the miR-25 family. Its members are **miR-25**, -92a-1, -92a-2, and **-92b**. 2 out of these 5 miRs (bold letters) were evaluated as candidates with an auditory function. Members of the miR-148 family, miR-148a-3p, -148b-3p and -152, of the miR-8 family, miR-200c-3p, -429-3p and the let-7 family, let7b/c/d-5p were also part of possibly auditory-related miRNA candidates.

Furthermore, 21 published deafness genes were found being among the predicted targets of miRNAs overlapping with regulated genes from the mRNA analysis. The abundance of these deafness genes among the differentially expressed mRNAs from the SOC implicates a central auditory function for them, in most cases additionally to their known function in the cochlea. This accounts very much for the miRNAs that are regulating those deafness genes being part of a shared gene regulatory network during the development of the peripheral and central auditory system. Regarding the number of deafness and synapse-related genes and the expression level in the SOC, especially miRNAs miR-96-5p, miR-182-5p, miR-200c-3p, miR-203-3p, miR-322-5p, and miR-429-3p could be of high relevance for the auditory system. According to this approach, miR-139-5p, miR-183-5p, miR-223-3p, miR-338-3p, the members of the miR-148 family as well as the let-7 family don´t seem to contribute too much (**Table 38**).

For further ranking of established miRNA candidates in order to choose some of them for e.g. analysis of ko mouse models, following criteria have been chosen that have to be fulfilled by those miRNAs to assure their shared developmental function in the cochlea and SOC: (1) they should show similar expression between cochlea and SOC, (2) they should be differentially expressed between timepoints, (3) they should have shared target genes in the cochlea and SOC, (4) their expression level should be high at E16. To add an evolutionary aspect, miRNAs that are (5) not present in the chicken would be of special interest because they could contribute to the evolutionary newly acquired formation of the mammalian specific central auditory system with its high number of auditory brainstem nuclei. Agreeing with the first criterion, the 37 miRNA candidates show a positive correlation of expression between the cochlea and the SOC that is also highly significant (**Figure 27**). All miRNA candidates fulfill the second criterion being differentially expressed, most of them are downregulated over time with their highest expression at E16 (**Figure 24**; **Figure 25**), being therefore also conform with the fourth criterion. The upregulated ones are lowly expressed at E16 and seem to acquire their function in the SOC later, after embryonic development and maybe around hearing onset. The fifth criterion, not to be present in chicken, was fulfilled by the miRNA candidates miR-25-3p, -92b-3p (both family members of the miR-25 family), -106b-5p, -139-5p, -148b-3p, -152-3p (last two being miR-148 family members), -295-3p, -322-5p, -351-5p, and -200c-3p. Therefore the paired miRNA/mRNA analysis also revealed some miRNAs that could be further investigated from an evolutionary perspective. Of note, also miR-127-3p and miR-181c-5p, which were investigated among the 12 miRNAs by *in-situ* hybridization and are highly expressed in the inner ear as well as in the SOC, are lacking their homologs in chicken. Following table summarizes the evaluated miRNA candidates, regarding their characteristics like expression, gene regulation, accordance with the criteria and earlier appearance in auditory-related studies to give an overview about their possible priority for further studies in knockout mouse models. Criterion (3) "they should have shared target genes in the cochlea and SOC" was regarded as fulfilled when at least one deafness gene was published for respective miRNA. Integrative data from cochlea miRNA and mRNA NGS is still missing to further evaluate this criterion. The priority score was calculated giving one point for each fulfilled criterion and publication and adding the number of regulated deafness/synapse-related genes (**Table 40**).

Table 40: Evaluation of priority for further studies among auditory-related miRNA-candidates.
(1) similar expression between cochlea and SOC; (2) differentially expressed between timepoints; (3) they should have shared target genes in the cochlea and SOC; (4) expression level should be high at E16; (5) no abundance in chicken. miRNA families are colour-coded: blue, miR-17 family; green, miR-25 family; red, miR-148 family; orange, miR-8 family, violet, let-7 family. The priority score was calculated giving one point for each fulfilled criterion and publication and adding the number of regulated deafness/synapse-related genes.

Auditory miRNA candidate	fulfilling criteria					Genes	Published auditory relevance	Priority score
	(1)	(2)	(3)	(4)	(5)			
miR-7b-5p			X	X		3		5
miR-17-5p		X	X			5		7
miR-18a-5p	X	X	X	X		4	(Friedman et al., 2009a)	9
miR-20a-5p	X	X	X	X		5		9
miR-20b-5p		X	X			5		7
miR-25-3p	X	X	X	X		5		9
miR-27b-3p		X	X			2		4
miR-29b-3p	X	X	X			5	(Di Stadio et al., 2018)	9
miR-30d-5p		X				3		4
miR-92b-3p	X		X	X		5		8
miR-96-5p		X	X	X		7	(Lewis et al., 2009; Kuhn et al., 2011; Schlüter et al., 2018)	13
miR-106b-5p	X	X	X	X		5		9
miR-124-3p		X	X			4	(Huyghe et al., 2015; Di Jiang et al., 2016)	8
miR-130b-3p		X		X		2		4
miR-139-5p	X	X	X		X	1		5
miR-140-5p	X	X	X	X		3		7
miR-148a-3p		X	X	X		1		4
miR-148b-3p	X	X	X	X	X	1		6
miR-152-3p		X	X		X	1		4
miR-182-5p		X	X	X		9	(Wang et al., 2012)	13
miR-183-5p	X	X		X		2	(Patel et al., 2013)	6
miR-200c-3p		X	X	X		6		9
miR-203-3p		X	X	X		9		12
miR-205-5p		X	X	X		5		8
miR-216b-5p	X		X			4		6
miR-223-3p	X	X	X			2		5
miR-295-3p		X	X		X	6		9
miR-302d-3p		X	X			6		8
miR-322-5p		X	X	X	X	6		10
miR-338-3p	X	X	X			1		4
miR-351-5p	X	X	X	X	X	4		9
miR-363-3p	X	X	X	X		5		9
miR-429-3p		X	X	X		6		9
miR-449a-5p	X	X	X	X		4		8
let-7b/7c/7d-5p		X	X			1		3

The highest priority score is reached by miR-96-5p and 182-5p, hence, additionally to the *miR-183/96* ko, a *miR-182* ko mouse model would be interesting for the analysis of the auditory brainstem. The next priorized miRNAs should be miR-18a-5p, miR-20a-5p, miR-106b-5p (miR-17 family); miR-25-3p, miR-29b-3p, miR-200c-3p, miR-429-3p (miR-8 family), miR-203-3p, miR-295-3p, miR-322-5p, miR-351-5p, and miR-363-3p.

Limiting the results of this analysis, some candidate miRNAs for a possible auditory role are only lowly expressed throughout the SOC. This fact leads to the question whether these miRNAs could be biologically relevant or not. Answering this question is limited by the method that was used, as the NGS data only give an overview about expression in the whole SOC. They deliver no information about the expression in single cell types. For lowly expressed miRNAs, they could be highly expressed in some cells but appear to be lowly expressed in the whole SOC tissue because of their high dilution by all the other surrounding cells that entered RNA isolation for the analysis. Hence, their biological function in distinct cell types could be of high relevance for the auditory system. Proven biological relevance of miR-96-5p could be used as an estimate of how many miRNA molecules are needed for functional impact. Taken from the NGS data, for miRNA-96 there are (only) around 90 molecules among one million miRNAs at E16, decreasing to around 5 CPM at P16. This shows that biological relevance can be already reached with low levels of miRNA expression. Surely, miRNA function not only depends on number of its molecules, but also on its stability, maybe subcellular compartimentation and target mRNA abundance.

4.7.   Correlated miRNA expression of the cochlea and SOC

Quantitative NGS data were used to determine correlated expression of miRNAs among tissues. For substantiation of evidence for a shared gene regulatory network between the peripheral and the central auditory system, the available P0 cochlea data (Rudnicki et al., 2014a) were compared to the P0 data from the SOC. To draw any conclusions regarding relatedness of miRNAs to the auditory system, a non-auditory control tissue, the frontal cortex, was included. Most of the 12 mature miRNAs that have been the most highly expressed ones from the cochlea, seem to be expressed very strongly also in the SOC, being in line with the findings in the cochlea (Rudnicki et al., 2014a). Trying to answer the question about correlated miRNA expression between the cochlea and the SOC, the expression of only the 12 miRNAs turned out not to be significantly correlated because of the three outliers miR-let-7c-5p, miR-27b-3p, and miR-204-5p. From that result it cannot be concluded that there is a shared gene regulatory network between the SOC and the peripheral auditory system. The relatedness of those 12 miRNAs to exclusively the auditory system could also not be shown, because there was significantly correlated expression between the cochlea and cortex. Nevertheless, within the NGS dataset, not only 12, but in total 411 miRNAs were expressed in the SOC and cortex that were also abundant among the existing P0 cochlea data. This large set of miRNAs showed a positive correlation of expression between the cochlea and both tissues, the SOC and cortex, that was highly significant. Hence, the overall miRNA landscape

from the cochlea and the SOC, but also from the cortex seems to be similar. This substantiates evidence for the hypothesis of a shared gene regulatory network on the miRNA level, but not exclusively for both auditory systems. Here it seems to be a shared network between brain and brain-derived tissues.

After evaluation of the 37 maybe auditory-related miRNAs after integrated analysis of differentialy expressed miRNAs and mRNAs, I would now hypothezise to find the expression of these filtered miRNAs being correlated with the cochlea data. The results exactly show strong linear dependency of the expression of 33 out of these 37 miRNAs between the cochlea and the SOC. This again strengthens the hypothesis for a shared gene regulatory network. In case of this newly elaborated subset of miRNAs, they also seem to be auditory-related because of their weak and not significantly correlated expression between cochlea and cortex. The results from the correlation analysis also authenticate the approach of paired miRNA/mRNA sequencing to find new auditory-related miRNAs. The 4 remaining miRNAs that have not been found among the cochlea data (miRs-7b-5p, 20b-5p, -295-3p, -302d-3p) do therefore not belong to that shared gene regulatory network, but could still play an important role in the central auditory system.

Limiting these results, the P0 cochlea data were obtained from sensory epithelium, containing not only hair cells, but also supporting cells. The SOC data were obtained from tissue not only containing the nuclei of the SOC but also surrounding tissue like glial cells. Therefore, the NGS data deliver no information of miRNA levels from eclusively auditory-related cell types. While the NGS approach of the SOC was done on biological triplicates with high sequencing depth of 20 million reads per sample, the cochlea was sequenced without biological replica at a depth of 10 million reads, excluding the possibility to average the results.

4.8.   Conclusion

Results from the analysis of the *miR-183/96* ko have demonstrated the importance of miR-183/96 for development and function of the auditory hindbrain. Data are pointing towards an essential role of the miR-183 cluster in the gene regulatory network underlying the morphological development of the auditory hindbrain. The importance of this miRNA cluster for sensory systems as reported by the literature and as shown in this study explains the high conservation of this miRNA cluster during evolution. Functional analysis of the *miR-183/96* ko delivered gain and loss of function consequences of the miR-96 *Dmdo* mutation on a molecular level and therefore could contribute to personalized medicine to help those people who are suffering from hearing loss due to mutations in miR-96.

Some of the observed phenoptypes of *miR-183/96* ko are located at the calyx of Held, the well-studied giant central synapse in the central auditory system. Genetic factors driving the morphological and functional maturation of the calyx of Held are yet poorly known. In this study, the miR-183/96 cluster was shown to be involved in the regulation of its synaptic strength, contributing to the understanding of the regulation of key synaptic properties.

Furthermore, a combination of NGS and bioinformatics identified 32 miRNAs as attractive candidates of a shared gene regulatory network between the peripheral and central auditory system, being possibly exclusively auditory-related. They represent thus a set of miRNAs for further analysis in knockout mouse models and could contribute to the gross understanding of genetic regulation underlying development and disease of the auditory system.

4.9. Perspective

To overcome the limitaions of this study, a more comprehensive approach is in progress, extracting hair cells from E16, P0, and P16 cochleae in triplicates and perform the NGS approach with the same requirements as for the SOC. Adding the E16 and P16 stages to the P0 cochlear data will also shed light on differential expression of miRNAs in the cochlea over time. This could be used for the analysis of a possibly shared gene regulatory network on the miRNA level between the peripheral and the central auditory system during development by integrating these data to the SOC data from E16, P0 and P16 animals. miRNAs that play a role in both, the peripheral and the central auditory system will be filtered. They will be analyzed like the miRNA-96 in knockout mouse models and be hypothesized to be another component of the shared gene regulatory network during development of the peripheral and central auditory system.

4.10. Summary

Non-syndromic hearing loss is the most frequent sensory deficit in humans. About 100 genetic loci have been described to contribute to this disease. One deafness gene is *MiR96*, coding for the microRNA miR-96. MicroRNAs are short, single stranded RNA molecules regulating proteinbiosynthesis of about 60% of the proteome and therefore are possibly contributing to all cellular processes. miR-96 is part of a shared gene regulatory network during development of the peripheral and central auditory system. In this thesis, the consequences of a loss of function of miR-96 were analyzed in the mouse auditory brainstem of mice. *miR-183/96* ko lead to deficient morphometry of auditory brainstem nuclei and to molecular and electrophysiological changes at the calyx of Held, a well-studied synapse of the auditory brainstem. At the calyx of Held presynapse, bigger Bassoon and Piccolo particles have been found. These are markers of presynapic active zones and could explain the finding of a larger pool of readily releasable synaptic vesicles. More and larger particles of the postsynaptic glutamate receptor subunit GluA1 could explain the electrophysiological phenotype of increased excitatory postsynaptic currents in *miR-183/96* ko mice. These results were discussed regarding gain and loss of function effects of the mutated form of miR-96 in an earlier analyzed mouse model. The calyx of Held was immature in that miR-96 mutant mouse, while miR-96 ko resulted in increased neurotransmission which causes have been analyzed in this thesis as described above.

Furthermore, general miRNA expression in the auditory brainstem of (wildtype-)mice was analyzed in this thesis. Using an integrative approach of molecular and bioinformatical analysis of miRNA and target mRNA expression at different timepoints, putative regulatory miRNAs of the SOC were identified. These miRNAs may play a role during the development of the central auditory system. A list of 37 miRNA candidates was evaluated, being interesting for further characterization in the auditory system of ko mouse models. This thesis aimed at identification of miRNAs that are possibly part of a shared gene regulatory program between the peripheral and central auditory system. Therefore, correlated expression of miRNAs between both systems was analyzed and revealed strongly correlated expression of 33 ot of the 37 miRNA candidates for auditory function. These candidates possibly could fulfill similar regulatory functions in both systems and therefore be parts of a shared gene reulatory network.

4.11. Zusammenfassung in deutscher Sprache

Nicht-syndromischer Hörverlust ist die häufigste sensorische Erkrankung des Menschen. Über 100 Genorte wurden beschrieben, die hierzu beitragen. Ein Taubheitsgen ist *MiR96*, welches die mikroRNA miR-96 codiert. MikroRNAs sind kurze, einzelsträgige RNA Moleküle, die die Proteinbiosynthese von ca. 60% des Proteoms regulieren, und damit möglicherweise an allen zellulären Prozessen beteiligt sind. miR-96 ist Teil eines geteilten genregulatorischen Netzwerkes während der Entwicklung des periphären und zentralen auditorischen Systems. In dieser Arbeit wurden die Auswirkungen des Entfernens von miR-96 im auditorischen Hirnstamm der Maus untersucht, welches zu veränderter Morphometrie der Hirnstammkerne und zu molekularen und elektrophysiologischen Veränderungen an der Calyx von Held, einer gut untersuchten Synapse des auditorischen Hirnstammes führte. An der Calyx von Held wurden an der Präsynapse größere Bassoon und Piccolo Partikel gefunden, welche Marker für die aktiven Zonen der Präsynapse sind und den elektrophysiologischen Phänotyp eines vergrößerten synaptischen Vesikelvorrats erklären könnten. Mehr und größere Partikel der postsynaptischen Glutamatrezeptoruntereinheit GluA1 erklären den elektrophysiologischen Phänotyp der größeren exzitatorischen postsynaptischen Ströme in *miRNA-183/96* ko Mäusen. Die Ergebnisse wurden vergleichend mit einem Mausmodell, welches eine mutierte Form dieser mikroRNA trägt, im Hinblick auf mögliche Funktionsgewinne oder Verluste der mutierten Form der mikroRNA-96 diskutiert. Die Calyx von Held ist in der mikroRNA-96 Mutante nicht vollständig entwickelt, während bei der Entfernung der mikroRNA-96 eine reife Calyx von Held entsteht, deren gesteigerte Neurotransmission wie oben beschrieben, untersucht wurde.

Desweiteren wurde in dieser Arbeit die generelle mikroRNA Expression im auditorischen Hirnstamm der (Wildtyp-) Maus charakterisiert. Durch einen integrativen Ansatz zur molekularen und bioinformatischen Analyse von mikroRNA und Ziel-mRNA bei verschiedenen Altersstadien wurden potentiell regulatorisch aktive mikroRNAs für den SOC identifiziert, die eine Rolle während der Entwicklung des zentralen auditorischen Systems spielen könnten. Abschließend wird eine Liste von 37 mikroRNA Kandidaten vorgestellt, die für weitere Charakterisierung im auditorischen System im Mausmodell interessant wären, sowie ein

Versuch unternommen, die mikroRNAs ihrer Priorität nach einzuordnen. Ziel war es, mikroRNAs zu identifizieren, die Teil des genregulatorischen Netzwerkes zwischen periphärem und zentralem auditorischen System sein könnten. Um den Bezug zwischen beiden Systemen herzustellen, wurde die Korrelation der Expression dieser mikroRNAs im Innenohr überprüft. 33 der 37 vorgestellten miRNA Kandidaten zeigten stark korrelierte Expression, was darauf hindeutet, dass diese miRNAs ähnliche regulatorische Funktionen in beiden auditorischen Systemen erfüllen und damit Teil eines gemeinsamen genregulatorischen Netzwerkes sein könnten.

5. References

Banks MI, Smith PH (1992) Intracellular recordings from neurobiotin-labeled cells in brain slices of the rat medial nucleus of the trapezoid body. J. Neurosci. 12:2819–2837.

Bartel DP (2009) MicroRNAs: target recognition and regulatory functions. Cell 136:215–233.

Bartel DP (2018) Metazoan MicroRNAs. Cell 173:20–51.

Baskerville S, Bartel DP (2005) Microarray profiling of microRNAs reveals frequent coexpression with neighboring miRNAs and host genes. RNA (New York, N.Y.) 11:241–247.

Benson DA, Karsch-Mizrachi I, Lipman DJ, Ostell J, Sayers EW (2009) GenBank. Nucleic acids research 37:D26-31.

Ben-Yosef T, Belyantseva IA, Saunders TL, Hughes ED, Kawamoto K, Van Itallie CM, Beyer LA, Halsey K, Gardner DJ, Wilcox ER, Rasmussen J, Anderson JM, Dolan DF, Forge A, Raphael Y, Camper SA, Friedman TB (2003) Claudin 14 knockout mice, a model for autosomal recessive deafness DFNB29, are deaf due to cochlear hair cell degeneration. Human molecular genetics 12:2049–2061.

Bernstein E, Caudy AA, Hammond SM, Hannon GJ (2001) Role for a bidentate ribonuclease in the initiation step of RNA interference. Nature 409:363–366.

Bock GR, Frank MP, Steel KP (1982) Preservation of central auditory function in the deafness mouse. Brain Research 239:608–612.

Bohnsack MT, Czaplinski K, Gorlich D (2004) Exportin 5 is a RanGTP-dependent dsRNA-binding protein that mediates nuclear export of pre-miRNAs. RNA (New York, N.Y.) 10:185–191.

Borst JG, Helmchen F, Sakmann B (1995) Pre- and postsynaptic whole-cell recordings in the medial nucleus of the trapezoid body of the rat. The Journal of physiology 489 (Pt 3):825–840.

Borst JGG, van Soria Hoeve J (2012) The calyx of Held synapse: from model synapse to auditory relay. Annual review of physiology 74:199–224.

Brainard MS, Knudsen EI (1993) Experience-dependent plasticity in the inferior colliculus: a site for visual calibration of the neural representation of auditory space in the barn owl. J. Neurosci. 13:4589–4608.

Brawer JR, Morest DK, Kane EC (1974) The neuronal architecture of the cochlear nucleus of the cat. J. Comp. Neurol. 155:251–299.

Caicedo A, Eybalin M (1999) Glutamate receptor phenotypes in the auditory brainstem and mid-brain of the developing rat. The European journal of neuroscience 11:51–74.

Cant NB (1992) The Cochlear Nucleus: Neuronal Types and Their Synaptic Organization. In: The Mammalian Auditory Pathway: Neuroanatomy (Webster DB, ed), pp 66–116. New York: Springer.

Cant NB, Morest DK (1979) The bushy cells in the anteroventral cochlear nucleus of the cat. A study with the electron microscope. Neuroscience 4:1925–1945.

Carpenter EM, Goddard JM, Chisaka O, Manley NR, Capecchi MR (1993) Loss of Hox-A1 (Hox-1.6) function results in the reorganization of the murine hindbrain. Development (Cambridge, England) 118:1063–1075.

Carr CE, Soares D (2002) Evolutionary convergence and shared computational principles in the auditory system. Brain, behavior and evolution 59:294–311.

Chen C-YA, Shyu A-B (2011) Mechanisms of deadenylation-dependent decay. Wiley interdisciplinary reviews. RNA 2:167–183.

Chiang DY, Cuthbertson DW, Ruiz FR, Li N, Pereira FA (2013) A coregulatory network of NR2F1 and microRNA-140. PloS one 8:e83358.

Chu C-y, Rana TM (2006) Translation repression in human cells by microRNA-induced gene silencing requires RCK/p54. PLoS biology 4:e210.

Cordes SP, Barsh GS (1994) The mouse segmentation gene kr encodes a novel basic domain-leucine zipper transcription factor. Cell 79:1025–1034.

Dambal S, Shah M, Mihelich B, Nonn L (2015) The microRNA-183 cluster: the family that plays together stays together. Nucleic acids research 43:7173–7188.

Deol MS, Kocher W (1958) A new gene for deafness in the mouse. Heredity 12:463–466.

Di Jiang, Du J, Zhang X, Zhou W, Zong L, Dong C, Chen K, Chen Y, Chen X, Jiang H (2016) miR-124 promotes the neuronal differentiation of mouse inner ear neural stem cells. International journal of molecular medicine 38:1367–1376.

Di Stadio A, Pegoraro V, Giaretta L, Dipietro L, Marozzo R, Angelini C (2018) Hearing impairment in MELAS: new prospective in clinical use of microRNA, a systematic review. Orphanet journal of rare diseases 13:35.

Ding L, Liu J, Shen H-X, Pan L-P, Liu Q-D, Zhang H-D, Han L, Shuai L-G, Ding E-M, Zhao Q-N, Wang B-S, Zhu B-L (2016) Analysis of plasma microRNA expression profiles in male textile workers with noise-induced hearing loss. Hearing research 333:275–282.

Dodson PD, Barker MC, Forsythe ID (2002) Two Heteromeric Kv1 Potassium Channels Differentially Regulate Action Potential Firing. J. Neurosci. 22:6953–6961.

Doucet JR, Ryugo DK (2006) Structural and functional classes of multipolar cells in the ventral cochlear nucleus. The anatomical record. Part A, Discoveries in molecular, cellular, and evolutionary biology 288:331–344.

Duncan JS, Fritzsch B (2012) Evolution of sound and balance perception: Innovations that aggregate single hair cells into the ear and transform a gravistatic sensor into the organ of corti. Anatomical Record 295:1760–1774.

Ehmann H, Hartwich H, Salzig C, Hartmann N, Clément-Ziza M, Ushakov K, Avraham KB, Bininda-Emonds ORP, Hartmann AK, Lang P, Friauf E, Nothwang HG (2013) Time-dependent gene expression analysis of the developing superior olivary complex. The Journal of biological chemistry 288:25865–25879.

Ehret G (1976) Development of absolute auditory thresholds in the house mouse (Mus musculus). Journal of the American Audiology Society 1:179–184.

Elkan-Miller T, Ulitsky I, Hertzano R, Rudnicki A, Dror AA, Lenz DR, Elkon R, Irmler M, Beckers J, Shamir R, Avraham KB (2011) Integration of transcriptomics, proteomics, and microRNA analyses reveals novel microrna regulation of targets in the mammalian inner ear. PloS one 6.

Essrich C, Lorez M, Benson JA, Fritschy J-M, Lüscher B (1998) Postsynaptic clustering of major GABAA receptor subtypes requires the γ2 subunit and gephyrin. Nature neuroscience 1:563 EP -.

Fan J, Jia L, Li Y, Ebrahim S, May-Simera H, Wood A, Morell RJ, Liu P, Lei J, Kachar B, Belluscio L, Qian H, Li T, Li W, Wistow G, Dong L (2017) Maturation arrest in early postnatal sensory receptors by deletion of the miR-183/96/182 cluster in mouse. Proceedings of the National Academy of Sciences of the United States of America 114:E4271-E4280.

Farago AF, Awatramani RB, Dymecki SM (2006) Assembly of the brainstem cochlear nuclear complex is revealed by intersectional and subtractive genetic fate maps. Neuron 50:205–218.

Forsythe ID, Barnes-Davies M (1993) The binaural auditory pathway: membrane currents limiting multiple action potential generation in the rat medial nucleus of the trapezoid body. Proceedings. Biological sciences 251:143–150.

Friedman LM, Dror AA, Mor E, Tenne T, Toren G, Satoh T, Biesemeier DJ, Shomron N, Fekete DM, Hornstein E, Avraham KB (2009a) MicroRNAs are essential for development and function of inner ear hair cells in vertebrates. Proceedings of the National Academy of Sciences of the United States of America 106:7915–7920.

Friedman RC, Farh KK-H, Burge CB, Bartel DP (2009b) Most mammalian mRNAs are conserved targets of microRNAs. Genome research 19:92–105.

Geiger JRP, Melcher T, Koh D-S, Sakmann B, Seeburg PH, Jonas P, Monyer H (1995) Relative abundance of subunit mRNAs determines gating and Ca2+ permeability of AMPA receptors in principal neurons and interneurons in rat CNS. Neuron 15:193–204.

Geng R, Furness DN, Muraleedharan CK, Zhang J, Dabdoub A, Lin V, Xu S (2018) The microRNA-183/96/182 Cluster is Essential for Stereociliary Bundle Formation and Function of Cochlear Sensory Hair Cells. Scientific reports 8:18022.

Grothe B (2003) New roles for synaptic inhibition in sound localization. Nature reviews. Neuroscience 4:540–550.

Grothe B, Pecka M, McAlpine D (2010) Mechanisms of sound localization in mammals. Physiological reviews 90:983–1012.

Gruters KG, Groh JM (2012) Sounds and beyond: multisensory and other non-auditory signals in the inferior colliculus. Frontiers in neural circuits 6:96.

Gundelfinger ED, Reissner C, Garner CC (2015) Role of Bassoon and Piccolo in Assembly and Molecular Organization of the Active Zone. Frontiers in synaptic neuroscience 7:19.

Guo H, Ingolia NT, Weissman JS, Bartel DP (2010) Mammalian microRNAs predominantly act to decrease target mRNA levels. Nature 466:835–840.

Hatch EP, Noyes CA, Wang X, Wright TJ, Mansour SL (2007) Fgf3 is required for dorsal patterning and morphogenesis of the inner ear epithelium. Development (Cambridge, England) 134:3615–3625.

Held H (2011) Die centrale Gehörleitung: Universitätsbibliothek Johann Christian Senckenberg.

Helfert RH, Schwartz IR (1986) Morphological evidence for the existence of multiple neuronal classes in the cat lateral superior olivary nucleus. The Journal of comparative neurology 244:533–549.

Hertzano R, Elkon R, Kurima K, Morrisson A, Chan S-L, Sallin M, Biedlingmaier A, Darling DS, Griffith AJ, Eisenman DJ, Strome SE (2011) Cell type-specific transcriptome analysis reveals a major role for Zeb1 and miR-200b in mouse inner ear morphogenesis. PLoS genetics 7:e1002309.

Holderith N, Lorincz A, Katona G, Rózsa B, Kulik A, Watanabe M, Nusser Z (2012) Release probability of hippocampal glutamatergic terminals scales with the size of the active zone. Nature neuroscience 15:988–997.

Huang Q, Ou Y, Xiong H, Yang H, Zhang Z, Chen S, Ye Y, Zheng Y (2017) The miR-34a/Bcl-2 Pathway Contributes to Auditory Cortex Neuron Apoptosis in Age-Related Hearing Loss. Audiology & neuro-otology 22:96–103.

Hutvágner G, Zamore PD (2002) A microRNA in a multiple-turnover RNAi enzyme complex. Science (New York, N.Y.) 297:2056–2060.

Huyghe A, van den Ackerveken P, Sacheli R, Prévot P-P, Thelen N, Renauld J, Thiry M, Delacroix L, Nguyen L, Malgrange B (2015) MicroRNA-124 Regulates Cell Specification in the Cochlea through Modulation of Sfrp4/5. Cell reports 13:31–42.

Jensen KP, Covault J (2011) Human miR-1271 is a miR-96 paralog with distinct non-conserved brain expression pattern. Nucleic acids research 39:701–711.

Jonas S, Izaurralde E (2015) Towards a molecular understanding of microRNA-mediated gene silencing. Nature reviews. Genetics 16:421–433.

Kadner A, Kulesza RJ, Berrebi AS (2006) Neurons in the medial nucleus of the trapezoid body and superior paraolivary nucleus of the rat may play a role in sound duration coding. Journal of neurophysiology 95:1499–1508.

Kammermeier PJ, Ikeda SR (1999) Expression of RGS2 Alters the Coupling of Metabotropic Glutamate Receptor 1a to M-Type K+ and N-Type Ca2+ Channels. Neuron 22:819–829.

Kawamata T, Tomari Y (2010) Making RISC. Trends in biochemical sciences 35:368–376.

Koike-Tani M, Saitoh N, Takahashi T (2005) Mechanisms underlying developmental speeding in AMPA-EPSC decay time at the calyx of Held. The Journal of neuroscience : the official journal of the Society for Neuroscience 25:199–207.

Kopp-Scheinpflug C, Tozer AJB, Robinson SW, Tempel BL, Hennig MH, Forsythe ID (2011) The sound of silence: ionic mechanisms encoding sound termination. Neuron 71:911–925.

Körber C, Horstmann H, Venkataramani V, Herrmannsdörfer F, Kremer T, Kaiser M, Schwenger DB, Ahmed S, Dean C, Dresbach T, Kuner T (2015) Modulation of Presynaptic Release Probability by the Vertebrate-Specific Protein Mover. Neuron 87:521–533.

Kuhn S, Johnson SL, Furness DN, Chen J, Ingham N, Hilton JM, Steffes G, Lewis MA, Zampini V, Hackney CM, Masetto S, Holley MC, Steel KP, Marcotti W (2011) miR-96 regulates the progression of differentiation in mammalian cochlear inner and outer hair cells. Proceedings of the National Academy of Sciences of the United States of America 108:2355–2360.

Lagos-Quintana M, Rauhut R, Meyer J, Borkhardt A, Tuschl T (2003) New microRNAs from mouse and human. RNA (New York, N.Y.) 9:175–179.

Lee DJ, Cahill HB, Ryugo DK (2003) Effects of congenital deafness in the cochlear nuclei of Shaker-2 mice: an ultrastructural analysis of synapse morphology in the endbulbs of Held. Journal of neurocytology 32:229–243.

Lee Y, Kim M, Han J, Yeom K-H, Lee S, Baek SH, Kim VN (2004) MicroRNA genes are transcribed by RNA polymerase II. The EMBO journal 23:4051–4060.

Lewis MA, Buniello A, Hilton JM, Zhu F, Zhang WI, Evans S, van Dongen S, Enright AJ, Steel KP (2016) Exploring regulatory networks of miR-96 in the developing inner ear. Scientific reports 6:23363.

Lewis MA, Di Domenico F, Ingham NJ, Prosser HM, Steel KP (2019) Hearing impairment due to Mir183/96/182 mutations suggests both loss and gain of function effects. bioRxiv doi: 10.1101/579003.

Lewis MA, Quint E, Glazier AM, Fuchs H, Angelis MH de, Langford C, van Dongen S, Abreu-Goodger C, Piipari M, Redshaw N, Dalmay T, Moreno-Pelayo MA, Enright AJ, Steel KP (2009) An ENU-induced mutation of miR-96 associated with progressive hearing loss in mice. Nature genetics 41:614–618.

Li H, Kloosterman W, Fekete DM (2010) MicroRNA-183 family members regulate sensorineural fates in the inner ear. The Journal of neuroscience : the official journal of the Society for Neuroscience 30:3254–3263.

Li HS, Borg E (1991) Age-related loss of auditory sensitivity in two mouse genotypes. Acta oto-laryngologica 111:827–834.

Li Q, Peng X, Huang H, Li J, Wang F, Wang J (2017) RNA sequencing uncovers the key microRNAs potentially contributing to sudden sensorineural hearing loss. Medicine 96:e8837.

Li Y, Peng A, Ge S, Wang Q, Liu J (2014) miR-204 suppresses cochlear spiral ganglion neuron survival in vitro by targeting TMPRSS3. Hearing research 314:60–64.

Lim LP, Glasner ME, Yekta S, Burge CB, Bartel DP (2003) Vertebrate microRNA genes. Science (New York, N.Y.) 299:1540.

Lufkin T, Dierich A, LeMeur M, Mark M, Chambon P (1991) Disruption of the Hox-1.6 homeobox gene results in defects in a region corresponding to its rostral domain of expression. Cell 66:1105–1119.

Lumayag S, Haldin CE, Corbett NJ, Wahlin KJ, Cowan C, Turturro S, Larsen PE, Kovacs B, Witmer PD, Valle D, Zack DJ, Nicholson DA, Xu S (2013) Inactivation of the microRNA-183/96/182 cluster results in syndromic retinal degeneration. Proceedings of the National Academy of Sciences of the United States of America 110:E507-16.

Lund E, Güttinger S, Calado A, Dahlberg JE, Kutay U (2004) Nuclear export of microRNA precursors. Science (New York, N.Y.) 303:95–98.

Maricich SM, Xia A, Mathes EL, Wang VY, Oghalai JS, Fritzsch B, Zoghbi HY (2009) Atoh1-lineal neurons are required for hearing and for the survival of neurons in the spiral ganglion and

brainstem accessory auditory nuclei. The Journal of neuroscience : the official journal of the Society for Neuroscience 29:11123–11133.

Marrs GS, Morgan WJ, Howell DM, Spirou GA, Mathers PH (2013) Embryonic origins of the mouse superior olivary complex. Developmental neurobiology 73:384–398.

Marrs GS, Spirou GA (2012) Embryonic assembly of auditory circuits: spiral ganglion and brainstem. The Journal of physiology 590:2391–2408.

McKay IJ, Lewis J, Lumsden A (1996) The role of FGF-3 in early inner ear development: an analysis in normal and kreisler mutant mice. Developmental biology 174:370–378.

Mencía A, Modamio-Høybjør S, Redshaw N, Morín M, Mayo-Merino F, Olavarrieta L, Aguirre LA, del Castillo I, Steel KP, Dalmay T, Moreno F, Moreno-Pelayo MA (2009) Mutations in the seed region of human miR-96 are responsible for nonsyndromic progressive hearing loss. Nature genetics 41:609–613.

Michalski N, Petit C (2019) Genes Involved in the Development and Physiology of Both the Peripheral and Central Auditory Systems. Annual review of neuroscience.

Moore DR (1991) Anatomy and Physiology of Binaural Hearing. Int J Audiol 30:125–134.

Morest DK (1968) The growth of synaptic endings in the mammalian brain: a study of the calyces of the trapezoid body. Zeitschrift fur Anatomie und Entwicklungsgeschichte 127:201–220.

Mosbacher J, Schoepfer R, Monyer H, Burnashev N, Seeburg PH, Ruppersberg JP (1994) A molecular determinant for submillisecond desensitization in glutamate receptors. Science (New York, N.Y.) 266:1059–1062.

Mostafapour SP, Cochran SL, Del Puerto NM, Rubel EW (2000) Patterns of cell death in mouse anteroventral cochlear nucleus neurons after unilateral cochlea removal. The Journal of comparative neurology 426:561–571.

Mourelatos Z, Dostie J, Paushkin S, Sharma A, Charroux B, Abel L, Rappsilber J, Mann M, Dreyfuss G (2002) miRNPs: a novel class of ribonucleoproteins containing numerous microRNAs. Genes & development 16:720–728.

Musicant AD, Chan JCK, Hind JE (1990) Direction-dependent spectral properties of cat external ear: New data and cross-species comparisons. The Journal of the Acoustical Society of America 87:757–781.

Noben-Trauth K, Zheng QY, Johnson KR (2003) Association of cadherin 23 with polygenic inheritance and genetic modification of sensorineural hearing loss. Nature genetics 35:21–23.

Nothwang HG (2016) Evolution of mammalian sound localization circuits: A developmental perspective. Progress in neurobiology 141:1–24.

Obernosterer G, Leuschner PJF, Alenius M, Martinez J (2006) Post-transcriptional regulation of microRNA expression. RNA (New York, N.Y.) 12:1161–1167.

Okamura K, Hagen JW, Duan H, Tyler DM, Lai EC (2007) The mirtron pathway generates microRNA-class regulatory RNAs in Drosophila. Cell 130:89–100.

Oleskevich S, Walmsley B (2002) Synaptic transmission in the auditory brainstem of normal and congenitally deaf mice. The Journal of physiology 540:447–455.

Oleskevich S, Youssoufian M, Walmsley B (2004) Presynaptic plasticity at two giant auditory synapses in normal and deaf mice. The Journal of physiology 560:709–719.

Pang J, Xiong H, Yang H, Ou Y, Xu Y, Huang Q, Lai L, Chen S, Zhang Z, Cai Y, Zheng Y (2016) Circulating miR-34a levels correlate with age-related hearing loss in mice and humans. Experimental gerontology 76:58–67.

Parks TN (2000) The AMPA receptors of auditory neurons. Hearing research 147:77–91.

Parthier D, Kuner T, Körber C (2018) The presynaptic scaffolding protein Piccolo organizes the readily releasable pool at the calyx of Held. The Journal of physiology 596:1485–1499.

Patel M, Cai Q, Ding D, Salvi R, Hu Z, Hu BH (2013) The miR-183/Taok1 target pair is implicated in cochlear responses to acoustic trauma. PloS one 8:e58471.

Pawlik B, Schlüter T, Hartwich H, Breuel S, Heepmann L, Nothwang HG (2016) Comparative Analysis of Gene Regulatory Network Components in the Auditory Hindbrain of Mice and Chicken. Brain, behavior and evolution 88:161–176.

Pecka M, Zahn TP, Saunier-Rebori B, Siveke I, Felmy F, Wiegrebe L, Klug A, Pollak GD, Grothe B (2007) Inhibiting the inhibition: a neuronal network for sound localization in reverberant environments. The Journal of neuroscience : the official journal of the Society for Neuroscience 27:1782–1790.

Petralia RS, Wenthold RJ (1992) Light and electron immunocytochemical localization of AMPA-selective glutamate receptors in the rat brain. J. Comp. Neurol. 318:329–354.

Pfaffl MW (2001) A new mathematical model for relative quantification in real-time RT-PCR. Nucleic acids research 29:45e-45.

Pierce ML, Weston MD, Fritzsch B, Gabel HW, Ruvkun G, Soukup GA (2008) MicroRNA-183 family conservation and ciliated neurosensory organ expression. Evolution & development 10:106–113.

Prochnik SE, Rokhsar DS, Aboobaker AA (2007) Evidence for a microRNA expansion in the bilaterian ancestor. Development genes and evolution 217:73–77.

Prosser HM, Koike-Yusa H, Cooper JD, Law FC, Bradley A (2011) A resource of vectors and ES cells for targeted deletion of microRNAs in mice. Nature biotechnology 29:840–845.

Riccardi S, Bergling S, Sigoillot F, Beibel M, Werner A, Leighton-Davies J, Knehr J, Bouwmeester T, Parker CN, Roma G, Kinzel B (2016) MiR-210 promotes sensory hair cell formation in the organ of corti. BMC genomics 17:309.

Rivera C, Voipio J, Payne JA, Ruusuvuori E, Lahtinen H, Lamsa K, Pirvola U, Saarma M, Kaila K (1999) The K+/Cl- co-transporter KCC2 renders GABA hyperpolarizing during neuronal maturation. Nature 397:251–255.

Robinson MD, Oshlack A (2010) A scaling normalization method for differential expression analysis of RNA-seq data. Genome biology 11:R25.

Rosengauer E, Hartwich H, Hartmann AM, Rudnicki A, Satheesh SV, Avraham KB, Nothwang HG (2012) Egr2::cre mediated conditional ablation of dicer disrupts histogenesis of mammalian central auditory nuclei. PloS one 7:e49503.

Ruby JG, Jan CH, Bartel DP (2007) Intronic microRNA precursors that bypass Drosha processing. Nature 448:83–86.

Rudnicki A, Isakov O, Ushakov K, Shivatzki S, Weiss I, Friedman LM, Shomron N, Avraham KB (2014a) Next-generation sequencing of small RNAs from inner ear sensory epithelium identifies microRNAs and defines regulatory pathways. BMC genomics 15:484.

Rudnicki A, Shivatzki S, Beyer LA, Takada Y, Raphael Y, Avraham KB (2014b) Microrna-224 regulates pentraxin 3, a component of the humoral arm of innate immunity, in inner ear inflammation. Human molecular genetics 23:3138–3146.

Sacheli R, Nguyen L, Borgs L, Vandenbosch R, Bodson M, Lefebvre P, Malgrange B (2009) Expression patterns of miR-96, miR-182 and miR-183 in the development inner ear. Gene expression patterns : GEP 9:364–370.

Sayers EW et al. (2018) Database resources of the National Center for Biotechnology Information. Nucleic acids research 47:D23-8.

Schlüter T, Berger C, Rosengauer E, Fieth P, Krohs C, Ushakov K, Steel KP, Avraham KB, Hartmann AK, Felmy F, Nothwang HG (2018) miR-96 is required for normal development of the auditory hindbrain. Human molecular genetics 27:860–874.

Schneggenburger R, Meyer AC, Neher E (1999) Released Fraction and Total Size of a Pool of Immediately Available Transmitter Quanta at a Calyx Synapse. Neuron 23:399–409.

Seal RP, Akil O, Yi E, Weber CM, Grant L, Yoo J, Clause A, Kandler K, Noebels JL, Glowatzki E, Lustig LR, Edwards RH (2008) Sensorineural Deafness and Seizures in Mice Lacking Vesicular Glutamate Transporter 3. Neuron 57:263–275.

Shepherd GM (2004) The Synaptic Organization of the Brain: Oxford University Press.

Sivakumaran TA, Resendes BL, Robertson NG, Giersch ABS, Morton CC (2006) Characterization of an abundant COL9A1 transcript in the cochlea with a novel 3' UTR: Expression studies and detection of miRNA target sequence. Journal of the Association for Research in Otolaryngology : JARO 7:160–172.

Soldà G, Robusto M, Primignani P, Castorina P, Benzoni E, Cesarani A, Ambrosetti U, Asselta R, Duga S (2012) A novel mutation within the MIR96 gene causes non-syndromic inherited hearing loss in an Italian family by altering pre-miRNA processing. Human molecular genetics 21:577–585.

Sommer I, Lingenhhl K, Friauf E (1993) Principal cells of the rat medial nucleus of the trapezoid body: an intracellular in vivo study of their physiology and morphology. Exp Brain Res 95.

Sonntag M, Englitz B, Kopp-Scheinpflug C, Rübsamen R (2009) Early postnatal development of spontaneous and acoustically evoked discharge activity of principal cells of the medial nucleus of the trapezoid body: an in vivo study in mice. The Journal of neuroscience : the official journal of the Society for Neuroscience 29:9510–9520.

Soukup GA, Fritzsch B, Pierce ML, Weston MD, Jahan I, McManus MT, Harfe BD (2009) Residual microRNA expression dictates the extent of inner ear development in conditional Dicer knockout mice. Developmental biology 328:328–341.

Spirou GA, Young ED (1991) Organization of dorsal cochlear nucleus type IV unit response maps and their relationship to activation by bandlimited noise. Journal of neurophysiology 66:1750–1768.

Steinert JR, Postlethwaite M, Jordan MD, Chernova T, Robinson SW, Forsythe ID (2010) NMDAR-mediated EPSCs are maintained and accelerate in time course during maturation of mouse and rat auditory brainstem in vitro. The Journal of physiology 588:447–463.

Tang A-H, Chen H, Li TP, Metzbower SR, MacGillavry HD, Blanpied TA (2016) A trans-synaptic nanocolumn aligns neurotransmitter release to receptors. Nature 536:210–214.

Taschenberger H, Gersdorff H von (2000) Fine-tuning an auditory synapse for speed and fidelity: developmental changes in presynaptic waveform, EPSC kinetics, and synaptic plasticity. The Journal of neuroscience : the official journal of the Society for Neuroscience 20:9162–9173.

Taschenberger H, Leão RM, Rowland KC, Spirou GA, Gersdorff H von (2002) Optimizing Synaptic Architecture and Efficiency for High-Frequency Transmission. Neuron 36:1127–1143.

Thompson AM, Schofield BR (2000) Afferent projections of the superior olivary complex. Microsc. Res. Tech. 51:330–354.

Tolbert LP, Morest DK (1982) The neuronal architecture of the anteroventral cochlear nucleus of the cat in the region of the cochlear nerve root: Golgi and Nissl methods. Neuroscience 7:3013–3030.

Tollin DJ (2003) The lateral superior olive: a functional role in sound source localization. The Neuroscientist : a review journal bringing neurobiology, neurology and psychiatry 9:127–143.

Tu JC, Xiao B, Yuan JP, Lanahan AA, Leoffert K, Li M, Linden DJ, Worley PF (1998) Homer Binds a Novel Proline-Rich Motif and Links Group 1 Metabotropic Glutamate Receptors with IP3 Receptors. Neuron 21:717–726.

Urness LD, Paxton CN, Wang X, Schoenwolf GC, Mansour SL (2010) FGF signaling regulates otic placode induction and refinement by controlling both ectodermal target genes and hindbrain Wnt8a. Developmental biology 340:595–604.

Varoqueaux F, Aramuni G, Rawson RL, Mohrmann R, Missler M, Gottmann K, Zhang W, Südhof TC, Brose N (2006) Neuroligins determine synapse maturation and function. Neuron 51:741–754.

Vendrell V, Vázquez-Echeverría C, López-Hernández I, Alonso BD, Martinez S, Pujades C, Schimmang T (2013) Roles of Wnt8a during formation and patterning of the mouse inner ear. Mechanisms of development 130:160–168.

Walmsley B, Berntson A, Leao RN, Fyffe REW (2006) Activity-dependent regulation of synaptic strength and neuronal excitability in central auditory pathways. The Journal of physiology 572:313–321.

Wang X-R, Zhang X-M, Du J, Jiang H (2012) MicroRNA-182 regulates otocyst-derived cell differentiation and targets T-box1 gene. Hearing research 286:55–63.

Wang Y, Manis PB (2005) Synaptic transmission at the cochlear nucleus endbulb synapse during age-related hearing loss in mice. Journal of neurophysiology 94:1814–1824.

Webster DB (1985) The spiral ganglion and cochlear nuclei of deafness mice. Hearing research 18:19–27.

Weedman DL, Pongstaporn T, Ryugo DK (1996) Ultrastructural study of the granule cell domain of the cochlear nucleus in rats: Mossy fiber endings and their targets. J. Comp. Neurol. 369:345–360.

Weston MD, Pierce ML, Jensen-Smith HC, Fritzsch B, Rocha-Sanchez S, Beisel KW, Soukup GA (2011) MicroRNA-183 family expression in hair cell development and requirement of microRNAs for hair cell maintenance and survival. Developmental dynamics : an official publication of the American Association of Anatomists 240:808–819.

Weston MD, Pierce ML, Rocha-Sanchez S, Beisel KW, Soukup GA (2006) MicroRNA gene expression in the mouse inner ear. Brain Research 1111:95–104.

Weston MD, Tarang S, Pierce ML, Pyakurel U, Rocha-Sanchez SM, McGee J, Walsh EJ, Soukup GA (2018) A mouse model of miR-96, miR-182 and miR-183 misexpression implicates miRNAs in cochlear cell fate and homeostasis. Scientific reports 8:3569.

Wienholds E, Kloosterman WP, Miska E, Alvarez-Saavedra E, Berezikov E, Bruijn E de, Horvitz HR, Kauppinen S, Plasterk RHA (2005) MicroRNA expression in zebrafish embryonic development. Science (New York, N.Y.) 309:310–311.

Willaredt MA, Ebbers L, Nothwang HG (2014) Central auditory function of deafness genes. Hearing research 312:9–20.

Wright TJ, Mansour SL (2003) Fgf3 and Fgf10 are required for mouse otic placode induction. Development (Cambridge, England) 130:3379–3390.

Wu K-C, Chen X-J, Jin G-H, Wang X-Y, Yang D-D, Li Y-P, Xiang L, Zhang B-W, Zhou G-H, Zhang C-J, Jin Z-B (2019) Deletion of miR-182 Leads to Retinal Dysfunction in Mice. Investigative ophthalmology & visual science 60:1265–1274.

Xu S, Witmer PD, Lumayag S, Kovacs B, Valle D (2007) MicroRNA (miRNA) transcriptome of mouse retina and identification of a sensory organ-specific miRNA cluster. The Journal of biological chemistry 282:25053–25066.

Yan D, Xing Y, Ouyang X, Zhu J, Chen Z-Y, Lang H, Liu XZ (2012) Analysis of miR-376 RNA cluster members in the mouse inner ear. International journal of experimental pathology 93:450–457.

Yang Y-M, Aitoubah J, Lauer AM, Nuriya M, Takamiya K, Jia Z, May BJ, Huganir RL, Wang L-Y (2011) GluA4 is indispensable for driving fast neurotransmission across a high-fidelity central synapse. The Journal of physiology 589:4209–4227.

Yi R, Qin Y, Macara IG, Cullen BR (2003) Exportin-5 mediates the nuclear export of pre-microRNAs and short hairpin RNAs. Genes & development 17:3011–3016.

Youssoufian M, Oleskevich S, Walmsley B (2005) Development of a robust central auditory synapse in congenital deafness. Journal of neurophysiology 94:3168–3180.

Zeng Y, Yi R, Cullen BR (2005) Recognition and cleavage of primary microRNA precursors by the nuclear processing enzyme Drosha. The EMBO journal 24:138–148.

Zhang KD, Stoller ML, Fekete DM (2015) Expression and Misexpression of the miR-183 Family in the Developing Hearing Organ of the Chicken. PloS one 10.

Erklärung

Hiermit erkläre ich, dass ich die vorliegende Arbeit selbstständig verfasst habe und keine als die angegebenen Quellen und Hilfsmittel verwendet habe. Ich versichere, dass diese Arbeit weder in ihrer Gesamtheit noch in Teilen einer anderen Hochschule zur Begutachtung in einem Promotionsverfahren vorliegt oder vorgelegen hat und dass ich die Leitlinien guter wissenschaftlicher Praxis der Carl von Ossietzky Universität Oldenburg befolgt habe. Weiterhin versichere ich, dass im Zusammenhang mit dem Promotionsvorhaben keine kommerziellen Vermittlungs- oder Beratungsdienste (Promotionsberatung) in Anspruch genommen worden sind.

___Gstadt, 25.02.2020_____ (Ort, Datum) _____C. Krohs_____(Constanze Krohs)

6. Appendix
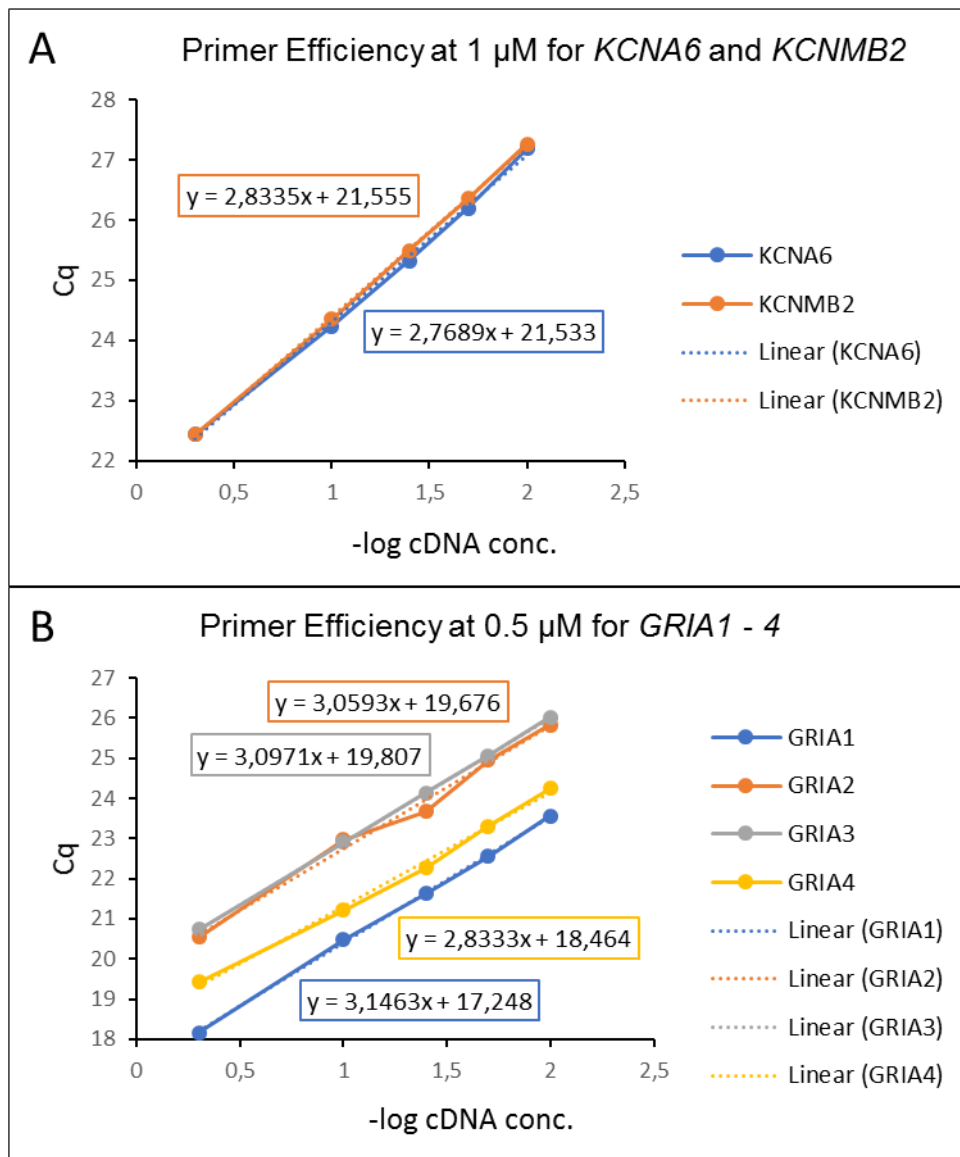
Figure 29: Primer efficiency tests for qPCR primers.
Diagrams show the -log of cDNA concentration used in efficiency tests on the x-axis and the quantification cycle when the signal was detected above background fluorescence on the y-axis (Cq). For each gene the dotted line represents the linear regression of original data. Linear equations of regression lines are shown in the colour-coded boxes for each gene. The slope of regression lines was used to calculate the primer efficiency, see table 39. **A:** Primer efficiency diagram for primers for the genes *KCNA6* and *KCNMB2*, tested successfully at 1 µM primer concentration. **B:** Primer efficiency diagram for primers for the genes *GRIA1-4*, tested successfully at 0.5 µM primer concentration.

Table 41: Primer efficiency tests for qPCR primers.

-log cDNA conc.	mean Cq *KCNA6*	mean Cq *KCNMB2*	mean Cq *GRIA1*	mean Cq *GRIA2*	mean Cq *GRIA3*	mean Cq *GRIA4*
0.3	22.44	22.44	18.16	20.55	20.74	19.42
1	24.24	24.355	20.48	22.965	22.905	21.21
1.4	25.32	25.49	21.625	23.67	24.14	22.26
1.7	26.195	26.355	22.55	24.945	25.055	23.31
2	27.185	27.265	23.555	25.825	26.01	24.245
slope	2,77	2,83	3,15	3,06	3,10	2,83
1/slope	0,36	0,35	0,32	0,33	0,32	0,35
Primer efficiency	2,30	2,25	2,08	2,12	2,10	2,25

Table 42: Properties of calyx of Held synapses recorded in normal ACSF.

Parameter	wt	*miR-183/96* ko	p-value
sEPSC			
n	9	6	
Amplitude (pA)	56.2 ± 3.2	73.0 ± 5.7	0.0299
Rise time (µs)	120 ± 5	105 ± 5	0.0577
τ_{decay} (ms)	0.302 ± 0.015	0.312 ± 0.020	0.6244
Frequency (Hz)	2.87 ± 0.57	4.06 ± 0.57	0.1809
eEPSC			
n	10	12	
Amplitude (nA)	16.81 ± 2.32	36.10 ± 3.41	0.0002
Rise time (µs)	322 ± 15	327 ± 9	0.777
τ_{decay} (ms)	0.363 ± 0.026	0.315 ± 0.018	0.1409
Quantal content (SVs)	272 ± 39	507 ± 57	0.0041
STD (100 Hz)			
n	10	11	
τ (ms)	22.3 ± 4.3	19.3 ± 2.1	0.5182
Depression (%)	90.2 ± 1.5	90.9 ± 0.9	0.6887
PPR	0.57 ± 0.07	0.57 ± 0.05	0.9728
steady-state EPSC (nA)	1.70 ± 0.25	3.11 ± 0.43	0.0037
RRP			
n	10	11	
RRP size (nA)	53.49 ± 6.89	100.60 ± 11.86	0.0034
RRP size (SVs)	899 ± 79	1386 ± 156	0.0142
Replenishment rate (nA/ms)	0.177 ± 0.026	0.329 ± 0.035	0.0029
norm. repl. rate (ms^{-1})	0.012 ± 0.002	0.010 ± 0.001	0.3221
P_r	0.322 ± 0.034	0.367 ± 0.030	0.3436

Table 43: Properties of calyx of Held synapses recorded in ACSF supplemented with 1 mM kynurenic acid.

Parameter	wt	*miR-183/96* ko	p-value
eEPSC			
n	15	17	
Amplitude (nA)	1.92 ± 0.21	3.33 ± 0.38	0.0037
Rise time (µs)	271 ± 5	285 ± 6	0.072
τ_{decay} (ms)	0.308 ± 0.008	0.341 ± 0.012	0.0377
Quantal content (SVs)	289 ± 32	494 ± 56	0.0046
STD (100 Hz)			
n	15	18	
τ (ms)	22.1 ± 3.5	27.9 ± 2.7	0.1966
Depression (%)	92.4 ± 0.9	91.9 ± 1.0	0.6764
PPR	0.62 ± 0.06	0.72 ± 0.05	0.1775
steady-state EPSC (pA)	209 ± 25	285 ± 0.31	0.0742
RRP			
n	15	18	
RRP size (nA)	8.47 ± 0.89	13.39 ± 1.17	0.0029
RRP size (SVs)	1278 ± 134	1987 ± 174	0.0038
Replenishment rate (nA/ms)	0.022 ± 0.003	0.032 ± 0.004	0.0526
norm. repl. rate (ms^{-1})	0.012 ± 0.001	0.011 ± 0.001	0.3147
P_r	0.230 ± 0.012	0.241 ± 0.016	0.6007
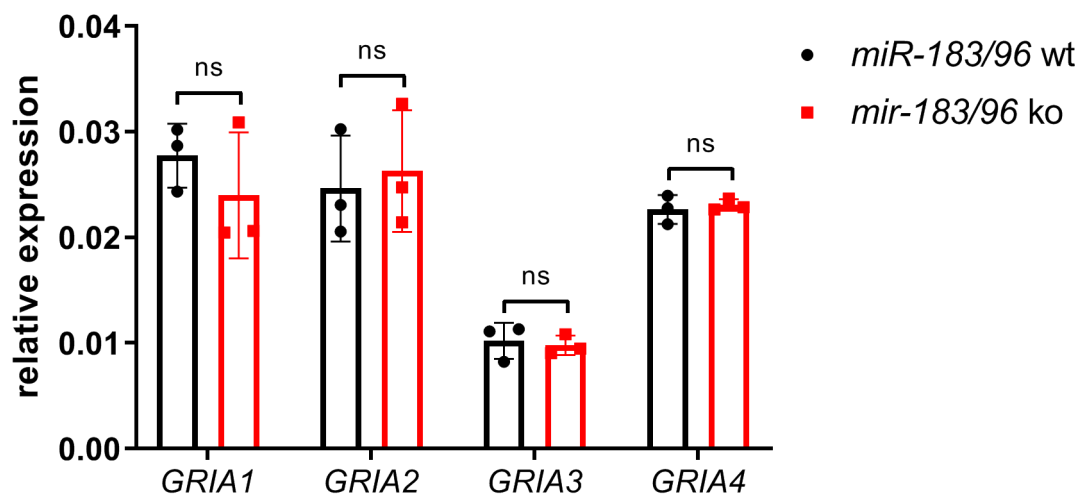
Figure 30: Quantitative PCR for GRIA1-4 in miR-183/96 wt and ko mice.
No changes were observed in the mRNA levels of the AMPA receptor subunits *GRIA1-4* in the SOC of P30 *miR-183/96* ko mice compared to their wt littermates. Barplots represent the relative expression of respective genes compared to the expression of *RPL3*. Single data points represent each n, the error bars show the standard deviation among samples. N = 3 per genotype. Statistical significance of differences between groups was tested using ANOVA. Ns = not significant.

A


```
mmu-let-7b-5p 0.02337
mmu-let-7c-5p 0.02209
mmu-let-7d-5p 0.10892
mmu-miR-124-3p 0.26199
mmu-miR-216b-5p 0.29356
mmu-miR-200c-3p 0.13281
mmu-miR-429-3p 0.09446
mmu-miR-106b-5p 0.07277
mmu-miR-17-5p 0.04409
mmu-miR-20b-5p 0.04287
mmu-miR-20a-5p 0.02998
mmu-miR-18a-5p 0.13292
mmu-miR-148a-3p 0.04868
mmu-miR-148b-3p 0.04223
mmu-miR-152-3p 0.05581
mmu-miR-130b-3p 0.27094
mmu-miR-295-3p 0.14571
mmu-miR-302d-3p 0.11516
mmu-miR-322-5p 0.34501
mmu-miR-25-3p 0.13985
mmu-miR-92b-3p 0.13287
mmu-miR-363-3p 0.30279
mmu-miR-139-5p 0.28479
mmu-miR-205-5p 0.21631
mmu-miR-351-5p 0.21226
mmu-miR-140-5p 0.29856
mmu-miR-203-3p 0.35144
mmu-miR-30d-5p 0.30451
mmu-miR-182-5p 0.15328
mmu-miR-183-5p 0.11945
mmu-miR-96-5p 0.19276
mmu-miR-27b-3p 0.27414
mmu-miR-338-3p 0.30671
mmu-miR-223-3p 0.30414
mmu-miR-29b-3p 0.26729
mmu-miR-449a-5p 0.22415
mmu-miR-7b-5p 0.18494
```

B

```
mmu-miR-106b-5p    UAAAGUGCUGACAGUGCAGA--U
mmu-miR-17-5p      CAAAGUGCUUACAGUGCAGGUAG
mmu-miR-20a-5p     UAAAGUGCUUAUAGUGCAGGUAG
mmu-miR-20b-5p     CAAAGUGCUCAUAGUGCAGGUAG
                   ******** * *******
```

C

```
mmu-miR-25-3p      CAUUGCACUUGUCUCGGUCUG-A
mmu-miR-363-3p     AAUUGCACG-GUAUCCAUCUGUA
mmu-miR-92b-3p     UAUUGCACUCGUCCCGGCCUC-C
                   ******* ** *   **
```

```
mmu-miR-92b-3p     UAUUGCACUCGUCCCGGCCU-CC
mmu-miR-96-5p      UUUGGCACUAGCACAUUUUUGCU
                   * * ***** * *     * *
```

D

```
mmu-miR-148a-3p    UCAGUGCACUACAGAACUUUGU
mmu-miR-148b-3p    UCAGUGCAUCACAGAACUUUGU
mmu-miR-152-3p     UCAGUGCAUGACAGAACUUG-G
                   *******  ********
```

E

```
mmu-miR-200c-3p    UAAUACUGCCGGGUAAUGAUGGA
mmu-miR-429-3p     UAAUACUGUCUGGUAAUGCCG-U
                   ******** * *******  *
```

F

```
mmu-let-7b-5p      UGAGGUAGUAGGUUGUGUGGUU
mmu-let-7c-5p      UGAGGUAGUAGGUUGUAUGGUU
mmu-let-7d-5p      AGAGGUAGUAGGUUGCAUAGUU
                   *************  * ***
```

Figure 31: Relationship of miRNAs possibly playing a role in the central auditory system.
A: Cladogram of mature miRNAs based on their sequences. Numbers behind the miR names represent the consistency index among miRNA sequences. Members of the miR-17 family (miR-106b-5p, miR-17-5p, miR-18a-5p, miR-20a-5p, miR-20b-5p) and the miR-25 family (miR-25-3p, miR-363-3p, miR-92b-3p) are clustering together. miR-96-5p is also clustering with the miR-25 family. **B**: Multiple sequence alignment of members of the miR-17 family showing most nucleotides of their stem sequences being identical. **C**: Multiple sequence alignment of members of the miR-25 family showing their seed sequences (nucleotides 2-8) being identical. Multiple sequence alignment of miR-92b-3p and miR-96-5p shows similarities in their seed sequences. **D**: Multiple sequence alignment of the miR-148 family. **E**: Multiple sequence alignment of the miR-8 family. **F**: Multiple sequence alignment of the let-7 family. Multiple sequence alignments were done with the EMBL-EBI T-Coffee tool (https://www.ebi.ac.uk/Tools/msa/tcoffee/) choosing ClustalW output format.

```
mmu-miR-30b-5p   UGUAAACAUCCUACACUCAGCU
mmu-miR-30d-5p   UGUAAACAUCCCCGACUGGAAG
                 **********   ***


 mmu-miR-200b-3p  UAAUACUGCCUGGUAAUGAUG-A
 mmu-miR-200c-3p  UAAUACUGCCGGGUAAUGAUGGA
                  ********** ********* *
```

Figure 32: Comparison of auditory-related miRs from the literature and miRNA candidates from paired miRNA/mRNA analysis.
Multiple sequence alignment of miR-30b-5p/-30d-5p and miR-200b-3p/200c-3p showing identical seed sequences for miR-30b and -d and almost identical stem sequence for miR-200b and -c. Multiple sequence alignments were done with the EMBL-EBI T-Coffee tool (https://www.ebi.ac.uk/Tools/msa/tcoffee/) choosing ClustalW output format.

Table 44: Upregulated miRNAs from E16, P0 and P16 SOC NGS data.

Upregulated miRNAs are sorted by their log$_2$FC values P16 vs. E16, showing total increase of expression over time on the log$_2$ scale. CPM: counts per million, E: embryonic day, FC: fold change, P: postnatal day; TMM: trimmed mean of M-values.

miRNA	regulation	TMM normalized log$_2$CPM values of samples											Adj. F-p-value	log$_2$FC P0 vs. E16	log$_2$FC P16 vs. P0	log$_2$FC P16 vs. E16
		E16_1	E16_2	E16_3	E16_4	P0_1	P0_2	P0_3	P0_4	P16_1	P16_2	P16_3				
mmu-miR-7080-3p	up	-1,97	-1,97	-1,97	-1,27	-1,49	-1,14	-1,56	-2,10	2,11	2,69	2,17	1,36E-02	1,81	4,85	6,66
mmu-miR-7032-3p	up	-1,58	-1,97	-1,90	-1,69	-1,54	-0,08	-1,65	-1,22	2,07	2,34	2,57	2,11E-02	1,73	4,76	6,49
mmu-miR-1199-5p	up	-2,14	-1,15	-2,14	-1,93	-1,88	-2,14	-2,14	-1,93	3,86	2,21	2,09	2,52E-02	-0,97	6,90	5,93
mmu-miR-338-5p	up	4,51	4,28	4,32	5,45	5,95	5,20	6,36	4,76	9,88	9,53	10,53	2,09E-04	1,20	4,34	5,55
mmu-miR-34a-5p	up	4,49	5,42	5,55	5,63	5,93	7,24	7,45	6,39	11,38	10,32	10,50	4,83E-03	1,75	3,60	5,35
mmu-miR-3547-3p	up	-0,42	-0,59	-0,17	0,55	2,14	1,78	1,57	0,88	3,33	4,03	3,54	8,00E-04	2,75	2,40	5,15
mmu-miR-138-1-3p	up	0,14	0,26	-1,01	0,70	1,45	1,02	1,88	0,55	4,46	4,14	4,10	2,05E-03	1,83	3,18	5,02
mmu-miR-29b-3p	up	0,31	-0,12	-0,39	0,26	2,67	1,33	1,64	1,56	5,51	4,50	4,53	1,01E-02	1,95	2,99	4,94
mmu-miR-3087-3p	up	-1,44	-1,75	-1,75	-1,84	-0,10	0,42	-1,34	-0,14	-0,05	1,59	0,91	1,67E-02	3,17	1,42	4,59
mmu-miR-338-3p	up	5,43	4,81	5,60	5,64	6,99	6,56	6,20	6,22	11,74	9,53	10,00	2,94E-04	1,24	3,29	4,53
mmu-miR-7047-3p	up	0,29	-0,20	1,00	0,00	0,83	1,90	1,66	1,83	3,00	4,70	4,29	4,96E-03	1,57	2,84	4,41
mmu-miR-1224-5p	up	4,30	5,30	5,27	5,59	6,70	7,89	8,23	6,96	7,71	9,17	8,65	6,76E-03	2,63	1,39	4,02
mmu-miR-3065-3p	up	3,05	3,01	3,52	3,30	4,41	3,64	3,61	3,78	7,13	7,01	7,14	2,80E-04	0,53	3,28	3,82
mmu-miR-770-5p	up	3,47	2,54	2,54	2,79	5,20	4,22	4,73	4,78	5,27	6,69	6,62	2,17E-04	1,90	1,89	3,79
mmu-miR-448-5p	up	1,23	1,91	1,98	1,08	3,16	2,60	2,93	3,53	4,13	5,76	5,38	1,81E-03	1,16	2,60	3,76
mmu-let-7b-5p	up	1,41	1,88	1,23	-0,10	3,00	2,64	2,55	4,34	3,36	5,03	5,31	6,15E-03	1,54	1,98	3,52
mmu-miR-3071-5p	up	2,60	2,50	2,26	1,13	4,14	3,57	3,30	4,99	3,48	5,97	6,38	6,77E-03	1,34	2,15	3,49
mmu-miR-1188-5p	up	1,42	2,00	2,10	1,52	2,70	3,05	4,11	3,61	3,06	5,58	5,00	7,34E-03	1,50	1,91	3,41
mmu-miR-871-3p	up	2,53	2,66	2,54	2,99	3,75	4,54	4,85	3,97	5,80	5,92	5,61	1,51E-04	1,92	1,48	3,40
mmu-miR-470-5p	up	1,22	0,95	0,97	1,86	1,53	2,45	2,86	1,47	4,89	3,99	3,79	4,68E-03	1,43	1,94	3,37
mmu-miR-1249-3p	up	7,89	8,15	8,46	7,79	9,13	9,69	10,01	9,98	9,93	11,63	11,45	1,56E-04	1,53	1,84	3,37
mmu-miR-212-5p	up	3,97	4,46	4,10	3,86	5,10	5,75	5,95	5,92	6,78	7,57	7,46	1,44E-04	1,53	1,82	3,35
mmu-miR-7653-3p	up	-1,07	-0,65	-0,94	0,03	0,68	1,43	0,73	0,03	2,52	1,43	1,38	7,42E-03	2,28	1,06	3,34
mmu-miR-219b-5p	up	4,56	4,11	3,62	4,62	3,49	3,88	3,21	3,01	8,19	7,20	7,38	1,10E-03	-0,44	3,73	3,29
mmu-miR-150-3p	up	-0,26	-0,71	0,70	0,95	1,56	2,09	2,67	1,06	2,90	2,24	2,42	4,15E-03	2,55	0,73	3,28
mmu-miR-219a-2-3p	up	8,14	8,19	8,11	9,04	7,64	7,83	7,86	6,88	12,71	11,36	11,39	2,09E-04	-0,45	3,70	3,25
mmu-miR-146b-5p	up	-0,29	0,84	0,67	1,30	2,18	2,48	2,60	1,52	3,97	3,12	3,12	1,14E-03	1,92	1,31	3,24
mmu-miR-146a-5p	up	-0,44	1,11	1,27	2,17	0,92	2,38	2,73	0,48	4,14	3,12	2,98	4,67E-02	1,33	1,81	3,14
mmu-miR-3552	up	2,03	2,23	1,59	1,49	3,96	2,24	2,94	3,51	4,55	5,25	5,10	8,77E-03	0,93	2,16	3,09
mmu-miR-150-5p	up	6,18	6,22	6,41	6,43	7,28	7,81	7,40	7,33	9,46	9,24	9,22	1,20E-06	1,30	1,72	3,02
mmu-miR-881-3p	up	-1,27	-1,02	-0,02	-0,08	0,27	0,44	1,10	-0,08	1,26	1,54	1,46	4,60E-02	1,55	1,39	2,94
mmu-miR-344b-3p	up	1,89	2,44	2,51	3,63	3,85	4,22	4,03	2,68	7,05	4,82	4,51	2,78E-03	1,65	1,17	2,82
mmu-let-7c-5p	up	2,15	1,48	2,14	0,89	3,55	2,93	3,80	4,47	3,26	4,64	5,09	6,55E-03	1,72	1,09	2,81
mmu-miR-1298-3p	up	5,91	6,78	6,77	6,08	7,86	8,01	8,13	8,41	8,95	9,36	9,37	2,11E-04	1,44	1,36	2,80
mmu-miR-874-5p	up	1,87	1,44	0,63	0,91	2,43	2,67	2,82	3,04	3,08	4,02	3,91	3,34E-03	1,64	1,13	2,78
mmu-miR-700-5p	up	4,21	5,34	5,61	5,10	5,04	6,76	6,67	6,11	7,04	7,80	7,58	7,33E-03	1,22	1,48	2,70
mmu-miR-770-3p	up	7,07	7,44	7,33	7,14	8,62	9,29	9,73	9,35	7,96	10,08	9,89	1,56E-04	2,02	0,68	2,70
mmu-miR-138-5p	up	11,78	10,54	10,73	10,87	12,55	12,02	12,19	12,40	12,96	13,63	13,69	8,00E-04	1,36	1,32	2,68
mmu-miR-666-3p	up	7,48	6,75	6,47	6,97	8,23	7,30	7,68	7,67	8,90	9,67	9,50	2,78E-03	0,80	1,86	2,66
mmu-miR-383-3p	up	1,20	1,25	1,39	0,33	2,26	1,99	2,14	3,08	1,85	4,11	3,81	2,88E-02	1,04	1,61	2,64
mmu-miR-3102-5p.2-5p	up	2,34	2,54	1,57	1,72	2,62	2,92	3,32	3,38	2,97	4,92	4,50	2,03E-02	1,01	1,60	2,61
mmu-miR-212-3p	up	4,15	3,83	3,61	4,16	5,18	4,69	5,05	4,68	6,91	6,58	6,28	1,52E-03	1,05	1,55	2,60
mmu-miR-132-3p	up	7,41	7,89	7,93	7,57	8,91	8,83	9,11	9,13	10,47	10,43	10,33	2,94E-04	1,12	1,47	2,59
mmu-miR-497a-5p	up	7,03	6,10	6,39	5,71	7,59	7,03	6,94	7,98	7,96	8,98	9,23	4,83E-03	0,83	1,75	2,58
mmu-miR-330-5p	up	5,80	5,11	5,54	6,10	6,56	6,09	6,28	5,69	9,13	8,02	7,97	4,08E-03	0,75	1,80	2,55
mmu-miR-330-3p	up	3,83	4,24	4,44	5,23	4,25	4,96	5,25	3,76	8,40	6,67	6,53	2,03E-02	0,57	1,97	2,54
mmu-miR-668-5p	up	-0,66	-0,41	-0,46	0,15	0,23	0,88	1,62	0,25	1,47	1,60	1,08	4,02E-02	1,73	0,77	2,51
mmu-miR-132-5p	up	1,43	2,29	1,62	1,38	2,83	2,59	3,27	3,30	3,91	4,37	4,29	1,22E-02	1,05	1,43	2,48
mmu-miR-3093-3p	up	1,54	1,20	1,41	1,95	2,19	2,97	3,52	2,32	2,99	3,44	3,64	3,75E-03	1,69	0,74	2,43
mmu-miR-204-3p	up	2,63	1,80	1,95	1,44	2,86	2,69	2,02	3,20	2,92	4,34	4,69	3,40E-02	0,68	1,76	2,43
mmu-miR-412-5p	up	5,82	5,35	5,39	6,12	6,46	6,30	6,48	5,82	8,04	7,90	7,90	1,66E-03	0,87	1,54	2,41
mmu-miR-877-3p	up	2,19	2,31	2,50	1,96	2,38	1,97	1,58	2,35	3,93	4,99	4,44	1,22E-02	-0,41	2,82	2,41
mmu-miR-370-5p	up	1,04	1,70	2,08	1,00	1,63	3,52	3,09	3,36	2,45	3,94	3,87	2,03E-02	1,51	0,87	2,38
mmu-miR-666-5p	up	9,70	9,67	9,46	10,08	10,11	10,66	10,94	10,10	11,79	12,06	11,67	1,81E-03	1,02	1,29	2,32
mmu-miR-1843b-5p	up	4,99	4,48	3,94	5,46	5,73	5,08	5,02	4,28	7,97	6,72	6,56	2,60E-02	0,69	1,55	2,25
mmu-miR-328-3p	up	8,37	8,91	8,90	8,53	8,88	9,37	9,79	9,54	10,00	11,02	10,94	5,71E-03	0,64	1,59	2,23
mmu-miR-490-3p	up	3,22	3,56	3,81	4,05	4,70	4,98	5,01	4,38	6,56	5,79	5,48	1,85E-03	1,29	0,91	2,20
mmu-miR-874-3p	up	4,58	4,56	4,72	4,69	5,78	6,35	6,40	6,11	6,61	6,97	6,49	2,97E-04	1,65	0,54	2,20
mmu-miR-490-5p	up	1,12	3,61	3,25	3,27	2,81	5,15	5,23	3,79	4,62	5,09	4,19	4,64E-02	1,74	0,42	2,16
mmu-miR-375-3p	up	9,03	8,97	8,53	9,28	7,67	8,02	8,43	7,61	8,16	10,33	11,93	4,59E-02	-0,76	2,89	2,13
mmu-miR-1197-3p	up	4,92	4,37	4,63	3,92	5,61	4,73	4,95	5,81	4,83	6,76	6,88	4,21E-02	0,47	1,61	2,08
mmu-miR-6412	up	4,10	4,00	3,93	3,63	5,48	4,71	4,19	5,18	5,41	6,12	6,06	1,73E-02	0,73	1,28	2,02
mmu-miR-664-3p	up	1,28	2,23	1,52	3,76	2,68	3,46	3,75	1,21	7,37	2,95	2,75	4,90E-02	1,53	0,47	2,00
mmu-miR-124-3p	up	11,33	11,97	11,55	10,39	12,30	12,97	12,95	13,97	11,56	13,61	13,57	7,46E-03	1,33	0,67	2,00
mmu-miR-3061-3p	up	3,99	3,52	3,78	3,82	4,85	4,76	4,68	4,70	5,46	5,53	5,93	4,15E-03	1,05	0,93	1,98
mmu-miR-323-5p	up	2,82	3,24	2,99	3,43	4,35	4,02	4,86	4,00	4,80	5,22	4,77	8,77E-03	1,23	0,73	1,96
mmu-miR-1843a-5p	up	5,17	5,15	4,75	5,66	5,79	5,78	5,81	5,16	7,92	6,90	6,82	1,31E-02	0,73	1,17	1,90
mmu-miR-1981-5p	up	5,14	4,60	4,99	5,03	5,68	5,69	5,96	5,65	6,36	6,74	6,81	4,83E-03	0,92	0,97	1,89
mmu-miR-7688-5p	up	3,03	2,71	3,05	2,22	3,44	3,34	3,52	4,14	3,45	4,62	5,04	4,88E-02	0,65	1,22	1,86
mmu-miR-3059-5p	up	6,33	6,76	6,31	7,15	7,66	7,89	8,00	7,17	8,80	8,66	7,82	6,05E-05	1,30	0,54	1,84
mmu-miR-700-3p	up	5,12	6,09	5,36	5,31	5,45	6,50	6,85	6,48	6,56	7,37	7,19	3,24E-02	0,85	0,94	1,79
mmu-miR-3061-5p	up	3,86	3,45	3,30	3,24	4,67	3,98	4,19	4,57	4,50	5,40	5,30	2,27E-02	0,76	1,03	1,79
mmu-miR-324-5p	up	7,88	8,22	8,56	7,82	8,29	9,04	8,98	9,17	9,16	10,01	9,95	1,56E-02	0,67	1,12	1,78
mmu-miR-433-3p	up	9,22	9,49	9,35	10,41	10,15	10,54	11,00	9,51	11,76	11,29	10,99	7,77E-03	1,10	0,68	1,78
mmu-miR-380-3p	up	9,81	9,55	9,45	8,83	9,90	9,70	9,67	10,53	9,66	11,26	11,42	4,64E-02	0,26	1,45	1,71
mmu-miR-181d-5p	up	3,40	3,21	3,14	2,91	4,40	4,56	4,48	4,81	3,91	5,09	4,78	2,50E-02	1,36	0,35	1,71
mmu-miR-139-5p	up	5,02	4,98	4,72	4,42	4,95	5,29	5,33	5,67	5,19	6,61	6,44	4,59E-02	0,44	1,21	1,65
mmu-let-7b-3p	up	6,29	6,00	6,30	6,81	6,91	6,88	6,79	6,25	8,32	7,89	7,71	2,03E-02	0,61	1,02	1,64
mmu-miR-3068-3p	up	4,20	3,22	3,84	3,95	5,57	4,55	4,46	4,67	5,76	5,30	5,41	2,27E-02	1,03	0,57	1,60
mmu-miR-151-5p	up	11,54	11,55	11,31	11,33	11,10	11,44	11,54	11,50	12,86	13,04	12,97	2,33E-02	-0,01	1,59	1,58

miRNA	regulation	TMM normalized log$_2$CPM values of samples											Adj. F-p-value	log$_2$FC P0 vs. E16	log$_2$FC P16 vs. P0	log$_2$FC P16 vs. E16
		E16_1	E16_2	E16_3	E16_4	P0_1	P0_2	P0_3	P0_4	P16_1	P16_2	P16_3				
mmu-miR-27b-3p	up	1,33	1,25	0,72	1,29	0,47	0,01	-0,21	-0,10	2,07	2,60	2,22	4,37E-02	-1,14	2,66	1,51
mmu-miR-187-3p	up	5,64	5,19	5,25	5,59	6,28	6,01	6,35	5,98	6,46	6,83	6,82	1,13E-02	0,84	0,62	1,47
mmu-let-7d-5p	up	10,15	9,63	9,44	9,67	10,17	9,91	10,13	10,14	10,75	11,12	11,18	4,67E-02	0,39	1,03	1,42
mmu-miR-21a-3p	up	6,03	5,85	5,44	5,06	5,51	5,16	4,74	5,85	6,74	6,97	7,12	2,95E-02	-0,55	1,85	1,30
mmu-miR-1839-5p	up	7,77	7,69	7,52	8,28	8,44	8,18	8,22	7,66	9,23	8,96	8,90	4,71E-02	0,51	0,75	1,26
mmu-miR-129-5p	up	7,39	7,97	8,02	9,12	9,54	10,15	10,43	8,71	10,80	8,98	8,88	7,52E-04	2,09	-0,88	1,21
mmu-miR-326-3p	up	7,19	7,07	7,09	7,20	7,47	7,60	8,00	7,61	8,10	8,42	8,13	4,63E-02	0,60	0,59	1,19
mmu-miR-670-3p	up	4,75	4,69	5,66	4,36	5,69	6,24	5,73	6,56	5,96	6,01	6,34	4,67E-02	0,99	0,14	1,14
mmu-miR-592-5p	up	7,17	7,15	7,28	6,69	8,19	8,27	8,19	8,72	7,03	8,10	8,49	8,42E-03	1,09	-0,05	1,04
mmu-miR-323-3p	up	9,27	9,56	8,92	9,53	10,17	10,14	10,45	9,98	9,40	10,36	10,25	1,92E-02	0,95	0,06	1,01
mmu-miR-487b-3p	up	9,48	8,88	8,67	8,92	10,48	9,76	9,91	10,13	9,05	10,04	10,01	1,31E-02	1,02	-0,04	0,98
mmu-miR-30d-5p	up	1,47	0,87	0,16	2,08	1,87	2,37	2,37	0,97	3,54	1,14	0,93	3,22E-02	1,58	-0,71	0,86
mmu-miR-383-5p	up	7,21	6,42	6,75	7,30	8,86	7,85	7,94	7,71	7,56	7,56	7,43	6,33E-03	1,28	-0,61	0,66
mmu-miR-873a-5p	up	5,26	5,07	4,80	6,39	6,50	6,17	6,19	4,94	7,78	5,74	5,40	4,67E-02	1,09	-0,43	0,66
mmu-miR-551b-5p	up	0,56	0,34	-0,34	0,57	1,48	2,18	1,37	1,30	0,91	0,22	0,03	1,40E-02	1,84	-1,61	0,23
mmu-miR-6390	up	-0,79	-0,22	-0,05	-0,56	0,71	1,54	1,88	1,59	-1,03	0,45	-0,79	2,36E-02	2,12	-1,93	0,19

Table 45: Downregulated miRNAs from E16, P0 and P16 SOC NGS data.

Downregulated miRNAs are sorted by their log$_2$FC values P16 vs. E16, showing total decrease of expression over time on the log$_2$ scale. CPM: counts per million, E: embryonic day, FC: fold change, P: postnatal day; TMM: trimmed mean of M-values.

miRNA	regulation	TMM normalized log$_2$CPM values of samples											Adj. F-p-value	log$_2$FC P0 vs. E16	log$_2$FC P16 vs. P0	log$_2$FC P16 vs. E16
		E16_1	E16_2	E16_3	E16_4	P0_1	P0_2	P0_3	P0_4	P16_1	P16_2	P16_3				
mmu-miR-183-3p	down	5,46	4,94	4,38	6,33	2,55	2,33	2,40	1,02	1,39	-2,25	-0,91	5,23E-05	-2,66	-5,54	-8,20
mmu-miR-205-5p	down	9,31	8,80	7,58	9,66	1,89	2,13	3,48	1,41	2,24	0,95	1,27	6,26E-07	-6,00	-2,06	-8,06
mmu-miR-199a-5p	down	4,60	3,45	3,27	3,73	0,03	-1,62	-1,21	-0,89	-2,45	-1,91	-1,98	1,78E-05	-6,52	-0,52	-7,04
mmu-miR-205-3p	down	4,41	2,43	1,81	2,88	-1,07	-2,43	-1,44	-1,64	-1,64	-1,64	-1,64	4,68E-04	-6,12	-0,50	-6,62
mmu-miR-214-3p	down	10,79	10,59	10,13	9,93	5,12	5,51	6,19	6,18	2,15	4,28	4,53	3,76E-07	-4,70	-1,40	-6,11
mmu-miR-675-3p	down	3,63	4,36	3,71	4,21	0,76	0,90	1,46	0,73	-0,63	-0,73	-1,50	2,36E-05	-3,09	-2,89	-5,99
mmu-miR-182-5p	down	15,84	16,13	15,84	16,92	12,86	13,23	12,95	12,03	12,05	9,27	10,77	1,14E-04	-3,01	-2,89	-5,90
mmu-miR-3063-3p	down	1,50	1,21	1,02	1,44	-0,09	-1,36	0,02	-0,67	-2,24	-2,24	-2,24	8,10E-04	-2,57	-3,29	-5,86
mmu-miR-206-3p	down	8,25	7,54	6,78	7,43	2,22	2,24	2,70	2,48	2,51	1,89	1,39	3,91E-07	-5,02	-0,81	-5,82
mmu-miR-214-5p	down	9,23	9,82	9,52	8,28	3,97	5,06	4,06	5,61	1,83	3,48	3,78	3,91E-07	-4,87	-0,88	-5,75
mmu-miR-183-5p	down	12,70	14,78	14,85	14,88	9,75	12,78	12,55	10,92	10,63	8,26	9,27	1,92E-05	-2,30	-2,92	-5,22
mmu-miR-335-3p	down	8,78	9,90	9,62	12,05	8,15	9,14	9,16	6,20	9,82	4,05	4,47	6,05E-04	-0,94	-4,26	-5,20
mmu-miR-208b-3p	down	5,06	4,10	3,93	5,09	1,31	1,23	-0,17	0,06	1,95	-0,57	0,51	9,84E-05	-3,58	-1,60	-5,18
mmu-miR-483-3p	down	1,21	1,94	1,36	2,39	-0,91	0,70	-1,43	-1,44	-1,91	-1,91	-1,45	8,77E-03	-2,39	-2,75	-5,14
mmu-miR-135a-1-3p	down	6,66	7,74	7,33	8,44	5,79	7,25	7,37	5,60	4,17	2,44	1,81	6,54E-04	-0,46	-4,66	-5,12
mmu-miR-148a-5p	down	8,02	7,93	7,18	9,92	6,82	6,36	6,39	4,32	7,05	2,90	2,57	1,38E-03	-1,45	-3,63	-5,08
mmu-miR-18b-3p	down	0,72	1,53	1,03	1,94	-0,65	0,55	0,10	-0,85	-0,58	-1,68	-1,68	1,11E-02	-1,23	-3,60	-4,82
mmu-miR-96-5p	down	5,81	6,32	7,15	6,40	3,14	4,24	3,62	3,70	2,80	1,21	2,55	9,84E-05	-2,69	-2,08	-4,77
mmu-miR-302d-3p	down	3,23	4,19	4,49	4,20	2,46	3,32	2,56	2,55	0,24	-0,40	-0,10	7,98E-04	-1,25	-3,50	-4,75
mmu-miR-351-3p	down	2,41	2,53	3,20	4,62	-0,12	1,51	1,55	-0,92	2,85	-0,47	-0,93	1,04E-02	-1,71	-2,85	-4,56
mmu-miR-322-3p	down	7,18	7,09	6,54	8,66	5,29	5,09	5,12	3,44	5,74	2,72	2,29	2,97E-04	-1,96	-2,59	-4,55
mmu-miR-20b-5p	down	1,03	1,54	2,11	1,60	-0,73	-0,30	0,45	-0,24	-1,60	-1,06	-1,60	5,30E-03	-2,04	-2,37	-4,41
mmu-miR-295-3p	down	1,00	1,65	0,70	1,30	0,60	-0,94	-1,09	-0,66	-0,44	-1,78	-1,31	8,42E-03	-2,30	-2,07	-4,37
mmu-miR-494-3p	down	0,74	1,15	1,11	1,39	-0,55	0,83	0,55	-0,11	0,25	-1,47	-1,47	3,13E-02	-0,66	-3,64	-4,30
mmu-miR-376c-3p	down	5,17	4,80	5,09	6,23	5,22	4,58	4,42	3,53	3,07	0,87	1,41	1,11E-03	-0,48	-3,66	-4,14
mmu-miR-203-3p	down	8,02	7,93	7,10	8,36	5,75	5,24	5,34	4,77	5,81	3,37	4,16	1,14E-04	-2,34	-1,65	-3,99
mmu-miR-296-3p	down	6,50	6,95	6,52	8,81	5,67	6,13	6,43	3,93	6,28	3,02	2,42	7,82E-03	-0,80	-3,16	-3,96
mmu-miR-615-3p	down	3,89	4,93	4,08	5,54	4,49	4,47	4,75	3,33	4,48	0,92	0,10	5,37E-03	-0,01	-3,92	-3,93
mmu-miR-19b-1-5p	down	1,11	1,44	1,64	1,41	-0,13	0,90	-0,91	-0,03	-0,26	-1,59	-0,78	4,02E-02	-1,44	-2,48	-3,92
mmu-miR-449a-3p	down	2,14	2,43	1,51	0,26	-0,04	-0,11	-0,75	1,46	-1,92	-0,99	-1,92	9,79E-03	-2,41	-1,50	-3,91
mmu-miR-503-5p	down	5,40	5,75	5,63	5,12	2,63	3,36	2,55	3,32	0,40	1,59	1,82	1,78E-05	-2,63	-1,26	-3,89
mmu-miR-363-3p	down	6,92	6,28	5,88	5,17	5,58	5,08	4,55	6,26	1,12	2,10	3,07	2,48E-03	-1,07	-2,72	-3,79
mmu-miR-450b-5p	down	5,55	5,05	4,82	4,79	2,64	1,89	1,19	2,26	1,32	1,46	1,57	1,34E-05	-3,27	-0,37	-3,63
mmu-miR-135b-3p	down	2,16	1,52	1,89	2,66	2,37	2,00	0,92	0,96	-0,74	-1,02	-0,74	3,13E-02	-0,13	-3,50	-3,63
mmu-miR-335-5p	down	10,18	9,36	9,98	9,57	9,76	8,87	8,36	9,27	6,01	6,08	6,46	6,54E-04	-0,88	-2,75	-3,63
mmu-miR-130a-5p	down	2,01	0,93	1,62	2,38	0,88	0,45	0,07	-0,39	-0,93	-1,21	-0,93	2,22E-02	-1,16	-2,46	-3,62
mmu-miR-381-3p	down	12,78	12,12	11,93	13,71	12,48	11,81	11,51	10,50	11,41	8,76	8,57	5,92E-03	-0,53	-3,02	-3,55
mmu-miR-374b-5p	down	4,72	5,35	5,25	6,40	4,31	4,60	4,53	3,19	4,12	1,73	1,80	2,42E-03	-0,82	-2,69	-3,51
mmu-miR-301a-5p	down	3,27	3,41	2,94	3,69	2,99	2,64	2,25	2,14	2,22	0,73	-0,64	1,08E-02	-0,69	-2,80	-3,50
mmu-miR-152-5p	down	8,24	7,68	7,66	8,19	6,75	6,07	5,70	5,85	5,60	4,20	4,64	1,14E-04	-1,75	-1,73	-3,48
mmu-miR-216b-5p	down	3,90	3,62	3,88	5,60	3,69	3,96	3,74	2,00	3,54	0,41	0,79	1,73E-02	-0,08	-3,38	-3,46
mmu-miR-351-5p	down	13,74	12,40	12,58	13,98	11,41	10,67	10,64	9,83	11,90	9,39	9,31	6,79E-04	-2,06	-1,37	-3,42
mmu-miR-92b-3p	down	13,12	12,51	12,67	14,76	13,25	12,51	12,86	10,87	13,07	9,38	9,23	2,28E-02	-0,21	-3,21	-3,42
mmu-miR-141-5p	down	4,02	3,21	2,79	2,21	-0,83	-0,45	-0,09	0,68	-2,26	-0,56	0,00	5,49E-04	-3,91	0,52	-3,39
mmu-miR-301b-5p	down	2,32	0,73	0,74	1,53	1,31	-0,20	-0,04	0,10	-2,31	-1,08	-1,50	4,87E-02	-1,13	-2,22	-3,35
mmu-miR-449a-5p	down	10,53	10,66	10,13	8,51	8,27	8,28	7,72	10,02	5,06	7,03	7,25	8,00E-04	-2,08	-1,26	-3,34
mmu-miR-200c-3p	down	7,04	7,90	7,59	7,85	1,64	4,79	3,02	2,81	2,61	3,49	4,88	2,95E-04	-3,93	0,59	-3,34
mmu-miR-450a-5p	down	6,82	6,59	6,70	6,76	5,01	4,66	4,66	4,72	3,80	3,44	3,60	1,35E-05	-1,97	-1,26	-3,23
mmu-miR-690	down	4,29	4,86	4,56	6,13	4,94	4,46	3,86	2,86	0,47	1,69	1,52	5,47E-03	-0,58	-2,63	-3,21
mmu-miR-483-5p	down	5,56	5,57	5,13	5,45	3,80	3,16	4,02	3,63	1,54	2,32	2,49	1,79E-04	-1,89	-1,25	-3,14
mmu-miR-140-5p	down	8,52	8,34	8,72	8,65	5,82	6,08	5,67	5,73	6,61	5,31	5,70	9,33E-06	-2,63	-0,37	-3,00
mmu-miR-219a-1-3p	down	4,74	4,90	4,80	5,05	3,96	4,37	4,34	3,99	2,03	1,77	2,08	9,90E-04	-0,57	-2,38	-2,95
mmu-miR-455-5p	down	8,77	8,93	8,66	7,52	5,15	5,39	5,14	6,50	3,67	5,61	6,02	1,34E-05	-3,36	0,45	-2,90
mmu-miR-15b-3p	down	3,34	4,22	4,31	5,08	3,80	3,20	3,01	2,21	4,12	1,13	1,60	1,11E-02	-1,02	-1,87	-2,89
mmu-miR-10b-3p	down	1,71	2,16	1,79	1,16	1,64	2,30	4,06	3,39	0,22	-0,27	-0,83	2,65E-02	0,93	-3,72	-2,79
mmu-miR-503-3p	down	4,60	4,69	4,09	5,24	2,23	2,32	2,58	1,60	3,37	2,08	1,61	2,97E-04	-2,19	-0,59	-2,78
mmu-miR-148a-3p	down	5,95	5,62	5,21	6,24	4,92	4,05	4,05	3,70	4,67	2,87	2,98	1,38E-03	-1,41	-1,36	-2,77
mmu-miR-140-3p	down	8,39	8,38	7,71	7,56	5,39	5,10	4,86	5,72	3,77	5,36	5,54	1,35E-05	-2,97	0,26	-2,71
mmu-miR-7b-5p	down	6,84	6,62	6,61	8,16	7,60	7,04	6,84	5,69	7,15	3,97	4,11	1,58E-02	0,24	-2,88	-2,64
mmu-miR-6715-5p	down	0,43	3,84	3,20	0,73	-2,20	-1,36	-1,21	0,17	-1,88	-0,95	-0,54	1,01E-04	-5,40	2,77	-2,63
mmu-miR-20a-3p	down	2,29	2,11	2,62	1,41	1,42	1,98	1,58	2,59	-0,72	-0,20	-0,11	2,91E-02	-0,48	-2,15	-2,62
mmu-miR-223-3p	down	3,44	3,37	3,56	3,84	3,62	1,83	1,27	1,85	1,78	0,63	1,73	1,05E-02	-1,61	-1,01	-2,62
mmu-miR-485-3p	down	2,18	2,41	2,50	3,43	1,89	2,45	2,43	1,19	0,66	0,24	-0,11	4,07E-02	-0,18	-2,37	-2,55
mmu-miR-7a-1-3p	down	5,31	6,06	6,42	6,36	5,41	5,97	5,62	5,23	4,32	3,51	3,41	9,56E-03	-0,36	-2,15	-2,50
mmu-miR-542-3p	down	6,38	6,62	6,10	5,90	4,70	4,78	4,01	4,96	3,00	3,68	4,12	4,62E-04	-1,79	-0,68	-2,47
mmu-miR-130b-5p	down	7,92	7,42	7,22	7,47	6,76	6,65	6,44	6,66	4,63	5,03	5,06	1,38E-03	-0,81	-1,64	-2,45
mmu-miR-345-3p	down	6,61	6,57	6,87	7,70	5,74	6,76	6,80	5,42	6,67	4,05	4,37	3,60E-02	-0,18	-2,19	-2,37
mmu-miR-18a-5p	down	5,62	5,95	6,64	5,08	4,30	5,66	5,51	6,15	2,19	3,35	4,03	4,59E-02	-0,64	-1,71	-2,35
mmu-miR-376b-3p	down	7,86	7,48	6,92	7,54	7,16	6,97	6,62	6,80	4,82	5,04	5,06	6,33E-03	-0,43	-1,91	-2,35
mmu-miR-130b-3p	down	6,17	5,81	5,84	5,00	5,12	5,08	5,21	6,07	1,08	3,80	3,65	2,55E-02	-0,63	-1,60	-2,23
mmu-miR-431-5p	down	11,68	11,76	11,29	10,95	9,82	10,42	10,58	10,90	7,67	9,32	9,33	4,15E-03	-1,09	-1,14	-2,23
mmu-miR-10a-3p	down	2,83	4,06	3,42	2,81	3,94	4,82	5,29	5,31	1,19	1,46	1,23	1,38E-03	1,34	-3,52	-2,18
mmu-miR-28a-3p	down	7,01	7,18	7,23	7,87	6,04	6,69	6,90	5,82	6,44	4,91	4,92	1,30E-02	-0,60	-1,57	-2,17
mmu-miR-200a-5p	down	5,15	4,73	3,87	3,63	1,31	2,55	0,14	2,28	-1,30	1,22	3,40	3,11E-02	-2,92	0,75	-2,17
mmu-miR-493-3p	down	5,67	4,29	4,26	4,50	2,70	2,39	2,69	2,84	1,36	2,85	2,22	1,90E-03	-1,98	-0,15	-2,13
mmu-miR-673-3p	down	8,53	8,65	8,60	9,79	7,81	8,27	8,31	6,93	8,79	6,67	6,11	4,63E-02	-0,54	-1,58	-2,11
mmu-miR-10a-5p	down	1,31	2,75	2,40	1,36	3,14	4,11	4,29	4,64	0,65	0,45	0,25	8,09E-02	1,79	-3,90	-2,11
mmu-miR-455-3p	down	6,11	4,92	5,24	5,37	3,14	2,30	2,39	2,66	3,13	3,16	3,57	8,59E-05	-2,83	0,74	-2,09
mmu-miR-1193-3p	down	3,80	5,46	5,34	4,91	2,89	4,11	4,02	3,63	1,83	3,30	2,54	2,63E-02	-1,26	-0,76	-2,02
mmu-miR-9-3p	down	8,07	8,52	9,11	9,90	9,45	9,07	8,84	7,79	8,98	6,64	6,61	4,91E-02	0,18	-2,19	-2,01

miRNA	regulation	TMM normalized log$_2$CPM values of samples											Adj. F-p-value	log$_2$FC P0 vs. E16	log$_2$FC P16 vs. P0	log$_2$FC P16 vs. E16
		E16_1	E16_2	E16_3	E16_4	P0_1	P0_2	P0_3	P0_4	P16_1	P16_2	P16_3				
mmu-miR-154-3p	down	3,55	4,32	4,44	4,18	3,28	4,17	4,00	3,74	1,61	2,15	2,21	4,67E-02	-0,27	-1,73	-2,00
mmu-miR-17-3p	down	5,29	5,19	5,09	4,95	4,55	4,57	4,66	4,84	2,50	3,07	3,45	1,18E-02	-0,54	-1,42	-1,96
mmu-miR-872-5p	down	10,33	9,21	9,40	9,32	9,72	8,17	7,94	8,94	7,22	7,56	8,03	1,97E-02	-1,10	-0,85	-1,95
mmu-miR-149-3p	down	2,28	2,86	2,70	3,47	2,99	3,32	3,67	2,47	1,11	0,92	0,62	1,66E-02	0,59	-2,52	-1,93
mmu-miR-148b-3p	down	5,23	7,00	6,78	6,19	3,59	5,53	5,83	5,13	4,72	4,08	4,75	4,59E-02	-1,27	-0,64	-1,91
mmu-miR-7a-2-3p	down	5,70	5,99	6,17	6,29	5,89	5,97	6,04	5,63	4,27	4,13	4,04	1,05E-02	-0,08	-1,83	-1,91
mmu-miR-544-5p	down	0,69	0,21	1,05	2,78	2,09	1,93	1,95	-0,14	2,42	-0,98	-0,51	4,02E-02	1,30	-3,19	-1,89
mmu-miR-135a-2-3p	down	5,88	5,46	5,31	5,15	5,37	4,97	5,18	5,57	2,54	3,74	3,66	2,35E-02	-0,32	-1,55	-1,87
mmu-miR-106b-5p	down	7,94	8,10	7,98	7,49	7,28	7,06	6,74	7,54	4,94	6,09	6,33	5,76E-03	-0,97	-0,88	-1,85
mmu-miR-16-2-3p	down	2,18	2,23	2,35	2,58	1,93	1,16	0,72	0,94	1,59	0,59	0,82	2,31E-02	-1,22	-0,58	-1,80
mmu-miR-10b-5p	down	1,62	2,90	2,96	1,29	2,79	4,16	4,62	5,07	1,18	1,22	0,83	6,97E-03	1,54	-3,28	-1,74
mmu-miR-370-3p	down	9,26	8,45	8,17	9,63	9,91	8,98	9,18	8,35	8,11	7,05	6,75	2,11E-02	0,58	-2,30	-1,72
mmu-miR-181a-2-3p	down	11,94	11,30	11,00	10,83	10,89	10,52	10,40	11,19	8,60	9,71	9,80	3,22E-02	-0,67	-0,98	-1,65
mmu-miR-18a-3p	down	3,87	4,14	3,81	3,81	1,92	2,42	2,54	2,42	1,97	2,45	2,19	1,45E-02	-1,62	0,01	-1,61
mmu-miR-25-3p	down	13,72	13,95	13,72	12,58	12,32	12,71	12,50	13,72	10,18	12,07	12,44	2,52E-02	-1,08	-0,51	-1,59
mmu-miR-429-3p	down	7,59	7,96	7,57	7,78	4,06	6,48	3,62	4,65	3,85	5,27	6,84	3,70E-02	-2,51	0,93	-1,59
mmu-miR-20a-5p	down	9,07	9,03	9,35	9,15	8,35	8,53	8,10	8,32	7,56	7,48	7,63	8,10E-03	-0,79	-0,79	-1,59
mmu-miR-299a-5p	down	6,27	7,15	7,50	6,32	5,67	6,33	5,83	6,59	3,84	5,32	5,61	3,55E-02	-0,99	-0,57	-1,56
mmu-miR-200b-5p	down	2,79	3,15	2,89	2,30	-0,49	1,79	-1,01	0,74	-1,87	0,62	2,12	3,98E-02	-2,83	1,30	-1,53
mmu-miR-673-5p	down	8,50	8,35	7,93	7,72	7,06	7,04	7,33	7,69	5,40	6,79	6,67	1,04E-02	-1,00	-0,52	-1,52
mmu-miR-1a-3p	down	4,92	4,45	3,49	5,84	3,84	2,58	2,89	1,55	4,65	2,92	3,36	4,09E-02	-1,45	0,02	-1,43
mmu-miR-322-5p	down	9,30	8,39	8,81	8,32	8,03	7,49	6,91	7,99	7,08	7,23	7,66	8,42E-03	-1,25	-0,12	-1,38
mmu-miR-106b-3p	down	7,28	7,92	8,00	8,10	6,39	7,35	7,28	6,65	6,66	6,40	6,39	4,52E-02	-0,71	-0,61	-1,32
mmu-miR-574-5p	down	6,65	6,95	6,72	6,27	4,59	5,33	5,36	5,59	3,74	5,39	5,48	2,32E-02	-1,52	0,21	-1,31
mmu-miR-299a-3p	down	7,01	6,60	6,29	6,27	5,31	5,37	5,42	5,73	5,03	5,22	5,45	5,67E-03	-1,12	-0,13	-1,25
mmu-miR-362-3p	down	3,67	3,19	3,78	3,33	3,10	2,26	2,30	2,77	2,26	2,24	2,64	3,13E-02	-1,10	-0,08	-1,17
mmu-miR-17-5p	down	1,61	2,10	2,13	1,81	1,23	1,12	0,60	1,12	0,76	0,86	0,93	4,91E-02	-1,11	-0,04	-1,15
mmu-miR-345-5p	down	7,03	6,93	7,01	7,46	5,95	6,49	6,16	5,73	6,77	5,93	5,60	4,89E-02	-0,72	-0,41	-1,13
mmu-miR-12191-3p	down	4,53	3,56	2,95	4,11	0,75	1,10	-1,35	-0,27	2,91	3,20	2,63	2,42E-03	-3,80	2,82	-0,98
mmu-miR-99b-3p	down	6,33	6,66	6,40	6,64	5,26	5,62	6,00	5,44	5,24	5,42	5,63	2,88E-02	-0,84	-0,12	-0,96
mmu-miR-124-5p	down	5,33	5,85	5,82	5,78	6,01	6,60	6,84	6,37	4,85	4,57	4,86	1,01E-02	0,82	-1,78	-0,95
mmu-miR-144-5p	down	4,95	3,84	4,12	4,54	2,86	2,08	2,08	2,81	3,79	3,26	3,68	3,75E-02	-1,35	0,44	-0,92
mmu-miR-574-3p	down	7,02	7,40	7,15	6,93	5,22	6,01	6,41	6,15	4,93	6,14	6,49	1,40E-02	-1,19	0,31	-0,88
mmu-miR-152-3p	down	2,27	3,25	2,86	2,36	0,72	1,62	1,80	1,81	0,52	1,91	2,09	2,44E-02	-1,42	0,64	-0,78
mmu-miR-128-2-5p	down	4,53	4,97	5,56	5,07	5,55	7,19	7,07	6,55	4,58	4,43	4,20	1,32E-03	1,78	-2,36	-0,57
mmu-miR-542-5p	down	5,82	5,58	5,25	4,60	4,11	3,84	4,16	4,99	2,90	4,69	5,46	3,27E-02	-1,38	0,87	-0,50
mmu-miR-410-5p	down	2,34	2,67	3,14	3,32	3,26	4,84	4,96	3,75	2,65	2,46	1,98	3,63E-03	1,81	-2,07	-0,26
mmu-miR-142a-3p	down	3,53	2,96	3,58	2,79	3,07	1,82	2,15	2,91	3,10	3,01	3,22	4,59E-02	-1,14	0,91	-0,23

Table 46: NGS data from SOC of the most highly expressed miRNAs from the cochlea.
CPM: counts per million, E: embryonic day, P: postnatal day; FC: fold change, P: postnatal day; TMM: trimmed mean of M-values.

miRNA	regulation	TMM normalized log₂CPM values of samples											Adj. F-p-value	log₂FC P0 vs. E16	log₂FC P16 vs. P0	log₂FC P16 vs. E16
		E16_1	E16_2	E16_3	E16_4	P0_1	P0_2	P0_3	P0_4	P16_1	P16_2	P16_3				
mmu-let-7c-5p	up	2,15	1,48	2,14	0,89	3,55	2,93	3,80	4,47	3,26	4,64	5,09	6,55E-03	1,72	1,09	2,81
mmu-miR-22-3p	ns	14,24	13,15	13,22	14,19	14,52	13,53	13,66	13,25	15,75	14,30	14,36	4,85E-01	0,27	0,53	0,80
mmu-miR-26a-5p	ns	15,61	14,61	14,60	15,75	15,12	14,11	14,05	13,61	15,67	13,63	13,75	1,76E-01	-0,64	-0,58	-1,22
mmu-miR-27b-3p	up	1,33	1,25	0,72	1,29	0,47	0,01	-0,21	-0,10	2,07	2,60	2,22	4,37E-02	-1,14	2,66	1,51
mmu-miR-127-3p	ns	17,31	17,50	17,31	17,80	16,46	17,48	17,83	16,82	18,83	18,42	18,08	3,43E-01	0,00	0,99	0,99
mmu-miR-143-3p	ns	14,21	14,58	13,76	14,30	14,26	13,74	13,91	13,85	14,37	14,28	14,62	5,04E-01	-0,34	0,52	0,18
mmu-miR-191-5p	ns	14,35	14,94	14,93	16,62	13,70	14,91	15,08	12,68	17,53	12,81	12,61	3,25E-01	-0,32	-1,55	-1,86
mmu-miR-204-5p	ns	-0,23	1,15	0,71	0,40	0,06	0,71	0,35	0,52	0,89	1,48	1,67	5,26E-01	-0,27	1,38	1,11
mmu-miR-181a-5p	ns	18,24	17,03	16,72	16,81	18,09	16,55	16,74	17,65	17,52	17,39	17,63	8,30E-01	-0,22	0,36	0,14
mmu-miR-181b-5p	ns	12,24	12,04	12,10	12,22	11,20	11,46	11,49	11,29	12,18	11,37	11,52	6,54E-02	-0,68	0,04	-0,63
mmu-miR-181c-5p	ns	13,52	13,13	13,00	13,11	13,93	13,52	13,35	13,71	13,32	13,36	13,35	3,70E-01	0,40	-0,26	0,14
mmu-miR-183-5p	down	12,70	14,78	14,85	14,88	9,75	12,78	12,55	10,92	10,63	8,26	9,27	1,92E-03	-2,30	-2,92	-5,22

Table 47: NGS data of evaluated miRNA candidates with a possible role in auditory brainstem functional development.
CPM: counts per million, E: embryonic day, FC: fold change, P: postnatal day; TMM: trimmed mean of M-values.

miRNA	regulation	TMM normalized log₂CPM values of samples											Adj. F-p-value	log₂FC P0 vs. E16	log₂FC P16 vs. P0	log₂FC P16 vs. E16
		E16_1	E16_2	E16_3	E16_4	P0_1	P0_2	P0_3	P0_4	P16_1	P16_2	P16_3				
mmu-miR-124-3p	up	11,33	11,97	11,55	10,39	12,30	12,97	12,95	13,97	11,56	13,61	13,57	7,46E-03	1,33	0,67	2,00
mmu-miR-30d-5p	up	1,47	0,87	0,16	2,08	1,87	2,37	2,37	0,97	3,54	1,14	0,93	3,22E-02	1,58	-0,71	0,86
mmu-miR-338-3p	up	5,43	4,81	5,60	5,64	6,99	6,56	6,20	6,22	11,74	9,53	10,00	2,94E-04	1,24	3,29	4,53
mmu-miR-139-5p	up	5,02	4,98	4,72	4,42	4,95	5,29	5,33	5,67	5,19	6,61	6,44	4,59E-02	0,44	1,21	1,65
mmu-miR-96-5p	down	5,81	6,32	7,15	6,40	3,14	4,24	3,62	3,70	2,80	1,21	2,55	9,84E-05	-2,69	-2,08	-4,77
mmu-miR-130b-3p	down	6,17	5,81	5,84	5,00	5,12	5,08	5,21	6,07	1,08	3,80	3,65	2,55E-02	-0,63	-1,60	-2,23
mmu-miR-17-5p	down	1,61	2,10	2,13	1,81	1,23	1,12	0,60	1,12	0,76	0,86	0,93	4,91E-02	-1,11	-0,04	-1,15
mmu-miR-20a-5p	down	9,07	9,03	9,35	9,15	8,35	8,53	8,10	8,32	7,56	7,48	7,63	8,10E-03	-0,79	-0,79	-1,59
mmu-miR-20b-5p	down	1,03	1,54	2,11	1,60	-0,73	-0,30	0,45	-0,24	-1,60	-1,06	-1,60	5,30E-03	-2,04	-2,37	-4,41
mmu-miR-106b-5p	down	7,94	8,10	7,98	7,49	7,28	7,06	6,74	7,54	4,94	6,09	6,33	5,76E-03	-0,97	-0,88	-1,85
mmu-miR-18a-5p	down	5,62	5,95	6,64	5,08	4,30	5,66	5,51	6,15	2,19	3,35	4,03	4,59E-02	-0,64	-1,71	-2,35
mmu-miR-25-3p	down	13,72	13,95	13,72	12,58	12,32	12,71	12,50	13,72	10,18	12,07	12,44	2,52E-02	-1,08	-0,51	-1,59
mmu-miR-92b-3p	down	13,12	12,51	12,67	14,76	13,25	12,51	12,86	10,87	13,07	9,38	9,23	2,28E-02	-0,21	-3,21	-3,42
mmu-miR-363-3p	down	6,92	6,28	5,88	5,17	5,58	5,08	4,55	6,26	1,12	2,10	3,07	2,48E-03	-1,07	-2,72	-3,79
mmu-miR-203-3p	down	8,02	7,93	7,10	8,36	5,75	5,24	5,34	4,77	5,81	3,37	4,16	1,14E-04	-2,34	-1,65	-3,99
mmu-miR-182-5p	down	15,84	16,13	15,84	16,92	12,86	13,23	12,95	12,03	12,05	9,27	10,77	1,14E-04	-3,01	-2,89	-5,90
mmu-miR-140-5p	down	8,52	8,34	8,72	8,65	5,82	6,08	5,67	5,73	6,61	5,31	5,70	9,33E-06	-2,63	-0,37	-3,00
mmu-miR-148a-3p	down	5,95	5,62	5,21	6,24	4,92	4,05	4,05	3,70	4,67	2,87	2,98	1,38E-03	-1,41	-1,36	-2,77
mmu-miR-148b-3p	down	5,23	7,00	6,78	6,19	3,59	5,53	5,83	5,13	4,72	4,08	4,75	4,59E-02	-1,27	-0,64	-1,91
mmu-miR-152-3p	down	2,27	3,25	2,86	2,36	0,72	1,62	1,80	1,81	0,52	1,91	2,09	2,44E-02	-1,42	0,64	-0,78
mmu-miR-351-5p	down	13,74	12,40	12,58	13,98	11,41	10,67	10,64	9,83	11,90	9,39	9,31	6,79E-04	-2,06	-1,37	-3,42
mmu-miR-7b-5p	down	6,84	6,62	6,61	8,16	7,60	7,04	6,84	5,69	7,15	3,97	4,11	1,58E-02	0,24	-2,88	-2,64
mmu-miR-223-3p	down	3,44	3,37	3,56	3,84	3,62	1,83	1,27	1,85	1,78	0,63	1,73	1,05E-02	-1,61	-1,01	-2,62
mmu-miR-216b-5p	down	3,90	3,62	3,88	5,60	3,69	3,96	3,74	2,00	3,54	0,41	0,79	1,73E-02	-0,08	-3,38	-3,46
mmu-miR-205-5p	down	9,31	8,80	7,58	9,66	1,89	2,13	3,48	1,41	2,24	0,95	1,27	6,26E-07	-6,00	-2,06	-8,06
mmu-miR-29b-3p	up	0,31	-0,12	-0,39	0,26	2,67	1,33	1,64	1,56	5,51	4,50	4,53	1,01E-03	1,95	2,99	4,94
mmu-miR-27b-3p	up	1,33	1,25	0,72	1,29	0,47	0,01	-0,21	-0,10	2,07	2,60	2,22	4,37E-02	-1,14	2,66	1,51
mmu-let-7b-5p	up	1,41	1,88	1,23	-0,10	3,00	2,64	2,55	4,34	3,36	5,03	5,31	6,15E-03	1,54	1,98	3,52
mmu-let-7c-5p	up	2,15	1,48	2,14	0,89	3,55	2,93	3,80	4,47	3,26	4,64	5,09	6,55E-03	1,72	1,09	2,81
mmu-let-7d-5p	up	10,15	9,63	9,44	9,67	10,17	9,91	10,13	10,14	10,75	11,12	11,18	4,67E-02	0,39	1,03	1,42
mmu-miR-200c-3p	down	7,04	7,90	7,59	7,85	1,64	4,79	3,02	2,81	2,61	3,49	4,88	2,95E-04	-3,93	0,59	-3,34
mmu-miR-429-3p	down	7,59	7,96	7,57	7,78	4,06	6,48	3,62	4,65	3,85	5,27	6,84	3,70E-02	-2,51	0,93	-1,59
mmu-miR-295-3p	down	1,00	1,65	0,70	1,30	0,60	-0,94	-1,09	-0,66	-0,44	-1,78	-1,31	8,42E-03	-2,30	-2,07	-4,37
mmu-miR-322-5p	down	9,30	8,39	8,81	8,32	8,03	7,49	6,91	7,99	7,08	7,23	7,66	8,42E-03	-1,25	-0,12	-1,38
mmu-miR-302d-3p	down	3,23	4,19	4,49	4,20	2,46	3,32	2,56	2,55	0,24	-0,40	-0,10	7,98E-04	-1,25	-3,50	-4,75
mmu-miR-449a-5p	down	10,53	10,66	10,13	8,51	8,27	8,28	7,72	10,02	5,06	7,03	7,25	8,00E-04	-2,08	-1,26	-3,34
mmu-miR-183-5p	down	12,70	14,78	14,85	14,88	9,75	12,78	12,55	10,92	10,63	8,26	9,27	1,92E-03	-2,30	-2,92	-5,22